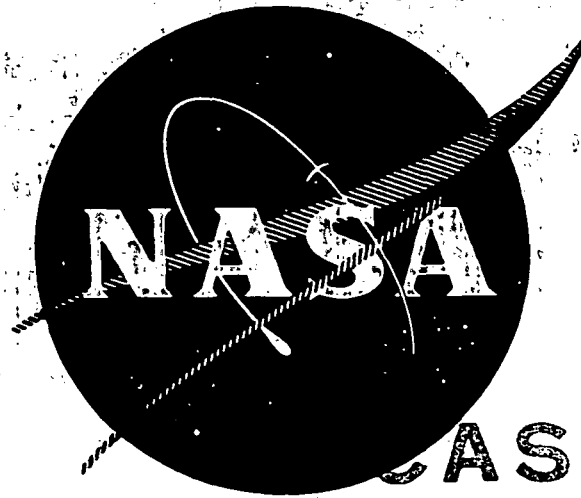


NASA-CR-120825
WANL-PR(WWW)-11
NOVEMBER 1971



CASE FILE
COPY

FINAL REPORT
AFTERHEAT DISTRIBUTION
OF A
MOBILE NUCLEAR POWER PLANT

By

W.G. Parker, L.E. VanBibber and Y.S. Tang

Westinghouse Electric Corporation
Astronuclear Laboratory
P.O. Box 10864
Pittsburgh, Pennsylvania 15236

Prepared For

National Aeronautics and Space Administration

November 1971

Contract NAS 3-14405

NASA Lewis Research Center
Cleveland, Ohio

Richard Puthoff, Project Manager

NOTICE

This report was prepared as an account of Government-sponsored work. Neither the United States, nor the National Aeronautics and Space Administration (NASA), nor any person acting on behalf of NASA:

- A.) Makes any warranty or representation, expressed or implied, with respect to the accuracy, completeness, or usefulness of the information contained in this report, or that the use of any information, apparatus, method, or process disclosed in this report may not infringe privately-owned rights; or
- B.) Assumes any liabilities with respect to the use of, or for damages resulting from the use of, any information, apparatus, method or process disclosed in this report.

As used above, "person acting on behalf of NASA" includes any employee or contractor of NASA, or employee of such contractor, to the extent that such employee or contractor of NASA or employee of such contractor prepares, disseminates, or provides access to any information pursuant to his employment or contract with NASA, or his employment with such contractor.

Requests for copies of this report should be referred to

National Aeronautics and Space Administration
Scientific and Technical Information Facility
P.O. Box 33
College Park, Md. 20740

FINAL REPORT

AFTERHEAT DISTRIBUTION OF A MOBILE
NUCLEAR POWER PLANT

By

W. G. Parker, L. E. VanBibber and Y. S. Tang

Westinghouse Electric Corporation
Astronuclear Laboratory
P. O. Box 10864
Pittsburgh, Pennsylvania 15236

Prepared For

National Aeronautics and Space Administration

November 1971

Contract NAS 3-14405

NASA Lewis Research Center
Cleveland, Ohio

Richard Puthoff, Project Manager

FOREWORD

This is the final report for the project entitled "Afterheat Distribution of a Mobile Nuclear Power Plant". The work was performed under NASA Contract NAS 3-14405.

The Program Manager for Westinghouse was Mr. A. R. Jones. Dr. Y. S. Tang was the Principal Investigator for the first task. Mr. W. G. Parker replaced Dr. Tang for the second and third tasks. The contributors to this study included Dr. Y. S. Tang, Mr. W. G. Parker and Mr. L. E. VanBibber.

TABLE OF CONTENTS

	<u>Page</u>
FOREWARD	iii
ABSTRACT	xiii
SUMMARY	xv
1.0 INTRODUCTION	1-1
2.0 TASK I - ESATA PROGRAM DEVELOPMENT	2-1
2.1 Program Description	2-1
2.1.1 General Description of Code	2-1
2.1.2 Computational Procedure of Code	2-4
2.1.3 Internal Node Generators	2-6
2.1.4 Features and Limitations	2-10
2.1.5 Input and Output Options	2-15
2.2 Subroutine Description	2-16
2.2.1 Program Control and Call Subroutines	2-16
2.2.2 TAP-A Functional Subroutines	2-17
2.2.3 HTM Generation Subroutines	2-19
2.2.4 Heat Generation Subroutines	2-20
2.2.5 Property Data Subroutines	2-24
2.2.6 Core-Shield Melt and Displace Subroutine	2-26
2.2.7 Pressure and Stress Subroutine	2-29
3.0 TASK II - HEAT TRANSFER CALCULATIONS	3-1
3.1 Helium Gas Cooled Thermal Reactor Power Plant	3-1
3.2 HTM Description	3-1
3.3 HTM Results	3-4
3.3.1 HTM, LiH/VO ₂ Shield Option Checkout Problem	3-4
3.3.2 HTM-2 Results	3-8
3.3.3 HTM-3 Results	3-18
3.3.4 HTM-4 Results	3-29
3.3.5 HTM-5 Results	3-30

TABLE OF CONTENTS (Continued)

	<u>Page</u>	
3.3.6	HTM-6 Results	3-34
3.3.7	HTM-7 Results	3-44
3.3.8	HTM-8 Results	3-47
3.3.9	Comparison of Containment Vessel Temperatures and Pressures	3-56
4.0	TASK III - DISCUSSION OF RESULTS	4-1
4.1	Contractural Questions and Discussion	4-1
4.2	General Discussion	4-5
4.2.1	Model Options	4-5
4.2.2	Shield Options	4-6
4.2.3	Heat Pipe Operation	4-7
4.2.4	Soil Burial	4-8
4.2.5	Fission Product Decay and Redistribution	4-8
4.2.6	Metal-Water Reaction	4-9
4.2.7	Component Melting and Displacement	4-10
4.2.8	Pressure and Stress	4-11
5.0	CONCLUSIONS AND DESIGN RECOMMENDATIONS	5-1
6.0	RECOMMENDATIONS FOR FUTURE WORK	6-1
APPENDIX A	HTM GENERATION SUBROUTINES	A-1
APPENDIX B	HEAT GENERATION SUBROUTINES	B-1
APPENDIX C	PROPERTY DATA SUBROUTINES	C-1
APPENDIX D	CORE & SHIELD MELT AND DISPLACE SUBROUTINES	D-1
APPENDIX E	PRESSURE AND STRESS SUBROUTINES	E-1

TABLE OF CONTENTS (Continued)

		<u>Page</u>
APPENDIX F	SYMBOLS	F-1
APPENDIX G	REFERENCES	G-1

LIST OF ILLUSTRATIONS

<u>Figure</u>		<u>Page</u>
2-1	Schematic Drawing of a Nuclear Aircraft Power Plant	2-2
2-2	ESATA Code Package Schematic Flow Chart	2-3
2-3	Nodal Model for Undeformed HTM	2-7
2-4	Nodal Model for Deformed HTM	2-9
2-5	Nodal Model for In-Pile Test Model	2-11
2-6	Reactor Shield Designs	2-12
2-7	Fission Product Decay Curves	2-22
3-1	Nodal Model for Undeformed HTM	3-6
3-2	HTM-2 Model Description	3-9/10
3-3	Temperature History for HTM-2	3-11
3-4	Core Displacement for HTM-2	3-13/14
3-5	Containment Vessel Circumferential Temperature Profile for HTM-2	3-16
3-6	Fission Product Redistribution for HTM-2	3-17
3-7	HTM-3 Model Description	3-19/20
3-8	Temperature History for HTM-3	3-21
3-9	Core Displacement for HTM-3	3-23/24
3-10	Final Core Displacement for HTM-3	3-25/26
3-11	Fission Product Redistribution for HTM-3	3-27
3-12	Containment Vessel Circumferential Temperature Profile for HTM-3	3-28
3-13	HTM-4 Model Description	3-31/32
3-14	Temperature History for HTM-4	3-33
3-15	Core and Shield Displacement for HTM-4	3-35/36
3-16	Containment Vessel Circumferential Temperature Profile for HTM-4	3-37
3-17	Fission Product Redistribution for HTM-4	3-38
3-18	Model Description for HTM-5 and HTM-7	3-39/40
3-19	Temperature History for HTM-5	3-41

LIST OF ILLUSTRATIONS (Continued)

<u>Figure</u>	<u>Page</u>
3-20 Fission Product Redistribution for HTM-5	3-42
3-21 Containment Vessel Circumferential Temperature Profile for HTM-5	3-43
3-22 Temperature History for HTM-6	3-45
3-23 Temperature History for HTM-7	3-46
3-24 Containment Vessel Circumferential Temperature Profile for HTM-7	3-48
3-25 Fission Product Redistribution for HTM-7	3-49
3-26 HTM-8 Model Description	3-51/52
3-27 Temperature History for HTM-8	3-53
3-28 Containment Vessel Circumferential Temperature Profile for HTM-8	3-54
3-29 Fission Product Redistribution for HTM-8	3-55
3-30 Comparison of Peak Containment Vessel Temperatures	3-57
3-31 Comparison of Internal Pressure and Containment Vessel Stresses	3-58
A-1 Summary Flow Diagram for HTMGEN Subroutine	A-2
A-2 Nodal Model for Undeformed HTM	A-5
A-3 Nodal Model for Deformed HTM	A-6
A-4 Nodal Model for In-Pile Test Model	A-7
A-5 VCAL1 Subroutine	A-9
A-6 VCAL2 Subroutine	A-12
A-7 VCAL3 Subroutine	A-13
A-8 VCAL5 Subroutine	A-14
A-9 Dimensions for Representative Nodes in An Undeformed HTM	A-16
B-1 The Effect of Liquid Depth on Iodine Release from Molten Uranium	B-4
B-2 Temperature Effect on Release of Fission Products	B-6
B-3 Normalized Temperature Effect on Fission Product Release	B-7
B-4 Estimated Fission Product Release From UO ₂ Fuel	B-9

LIST OF ILLUSTRATIONS (Continued)

<u>Figure</u>		<u>Page</u>
B-5	Fission Product Decay Curves	B-11
B-6	Fission Product Decay Heat Curves Due to Gamma Fission After 1 Year Operation	B-13
B-7	Fission Product Decay Heat Curves Due to Beta Ray Emission	B-14
B-8	FISSON Subroutine	B-18
B-9	Linear Rate Constants for the Molybdenum-Steam Reaction (1370-1970°K)	B-21
B-10	Arrhenius X_{plot} for the Tungsten-Steam Reaction	B-22
B-11	REACT Subroutine	B-28
C-1	Logic for Heat Pipe Simulation	C-2
C-2	Maximum Heat Flux Versus Heat Pipe Evaporator Temperature	C-4
D-1	Subroutine TMPICAL	D-2
D-2	Subroutine CSMELT	D-7
E-1	Larson-Miller Curve for SS-316	E-4

LIST OF TABLES

<u>Table</u>		<u>Page</u>
2-1	Yields and Characteristics of Important Fission Product Elements	2-21
2-2	Deposition Patterns in Thermal Gradient Tube	2-23
3-1	Reactor Characteristics	3-2
3-2	Materials of Construction	3-2
3-3	Heat Transfer Models	3-3
3-4	Initial Temperatures and Pressures	3-5
3-5	Core Mass and Area	3-5
3-6	Key Radii and Thicknesses	3-7
3-7	Tabulation of HTM-1 UO ₂ Detachment	3-7
A-1	HTMGEN Nomenclature	A-3
B-1	Yields and Characteristics of Important Fission Product Elements	B-3
B-2	Fraction of Fission Product Release	B-5
B-3	Deposition Patterns in Thermal Gradient Tube	B-8
B-4	Normalized Gamma Energy Yield	B-10
B-5	Fission Product Group Decay Gammas Calculation	B-12
B-6	Heat and Free Energy of Formation of Mo O ₃	B-25
B-7	Heat and Free Energy of Formation of Fe ₃ O ₄	B-26
C-1	Heat Pipe Nomenclature	C-3
C-2	Soil Samples	C-16
C-3	The Derived Thermal Conductivity of the Nine Types of Soil	C-17
C-4	Specific Heats of Various Substances	C-18
D-1	Nomenclature for the TMPCAL Subroutine	D-3

ABSTRACT

A computer program (ESATA) was developed to analyze the transient afterheat temperature and pressure response of a mobile gas cooled reactor power plant following impact. This program considers (in addition to the standard modes of heat transfer) fission product decay and transport, metal-water reactions, core and shield melting and displacement, and pressure and containment vessel stress response. Analyses were performed for eight cases (both deformed and undeformed models) to verify operability of the program options. The results indicated that for a 350 psi (241 n/cm^2) initial internal pressure, the containment vessel can survive over 100,000 seconds following impact before creep rupture occurs. Recommendations were developed as to directions for redesign to extend containment vessel life.

SUMMARY

A multi-dimensional transient heat transfer analysis computer program (ESATA - Executive Subroutines for Afterheat Temperature Analysis) was developed to analyze the afterheat temperature response of a mobile gas cooled nuclear reactor power plant following impact. The ESATA program considers phenomena such as fission product decay and transport, metal-water reactions, core and shield melting and displacement (including heat of fusion), pressure and containment vessel stress buildup and soil property variations. It was developed from a generalized heat transfer code, TAP-A.

The ESATA code was tailored to analyze both undeformed and deformed reactor models with five shield options, alternate heat pipe operation and alternate degrees of ground burial. Six heat transfer models (HTM's) representing alternative power plant designs were chosen for analysis. The analysis both insured operation of the code and established preliminary thermal and stress information of the power plants following impact. Two additional HTM's were analyzed. One demonstrated a technique to handle temperature sensitive containment insulation. The second represented a planned in-pile experiment. The results of analysis of all eight HTM's were as follows:

- Time before rupture of the containment vessel ranged from 10,000 seconds for a deformed model to 170,000 seconds for an undeformed model with an initial internal pressure of 350 psi (241 n/cm^2). The internal pressure at rupture varied from 1000 psi (689 n/cm^2) to 1600 psi (1103 n/cm^2), and the peak containment vessel temperature varied from 1500°R (833°K) to 1900°R (1056°K) at rupture.
- Time to rupture of the vessel should be significantly increased by lowering the initial pressure through the addition of a means of removing helium prior to impact.

- The use of LiH as a thermal capacitance material placed between heavy metal shield layers increased the life time of the containment vessel. A representative increase from 12,000 to 100,000 seconds in the time to rupture for the undeformed model was indicated.
- Deformation of the reactor with a tungsten/lithium-hydride/uranium oxide (W/LiH/ UO_2) shield shortened the time to failure from 100,000 to 10,000 seconds. Similar results are expected for the W/water/ UO_2 shield, W/water, and W/LiH shields.
- Partial earth burials of 33 percent and 50 percent for the undeformed model indicated a negligible effect (about 6000 seconds) on the containment vessel temperature response and the time to failure.
- The presence of 5 percent of the moderator water (160 lbm (72.6 kgm)) is sufficient to increase the internal pressure by 50 (35.5 n/cm^2) to 160 psi (110 n/cm^2) by hydrogen release from metal-water reactions. This release occurs within the first 200 seconds of the transient.

1.0 INTRODUCTION

The use of mobile nuclear reactors has been considered over several years for a variety of future applications. In general reactors for these applications can be classified in two ways: first, those that supply power to large low speed earth surface vehicles and second, those that supply power to high speed, high altitude vehicles. Examples of the first category are ships, submarines and air cushion vehicles. Airplanes and launch vehicles would be in the second category.

In all mobile reactors, fission products must be contained with the same level of confidence as in stationary power plants. This is true not only in their normal modes of operation but in the event of a crash impact where loss of coolant and structural failure will occur.

One method for containing fission products under these severe conditions is to put the reactor in a containment vessel and design the containment vessel and its contents to absorb the impact energy without rupturing. After impact the heat from the decay of fission products is dissipated through the containment vessel wall and radiated into the surrounding environment.

The heat transfer analysis of this containment system is complex. In addition to conduction, radiation and convection, the core melts, thus introducing the heats of fusion and vaporization. Also, fission products within the containment vessel that are generating the heat are being transported radially outward and condensing on cooler surfaces resulting in mobile and multiple heat sources. The resultant effect is to have a reactor core that initially heats up, melts, slumps downward into the shield material, and finally resolidifies. The resolidification is due to both the reduced level of heat generation of the fission products and the redistribution of these fission products toward the containment vessel.

A three-task effort was conducted to provide the capability and perform preliminary calculations of the reactor afterheat temperature response of a mobile gas cooled nuclear power plant following impact. The first task of this program was to generate a multi-dimensional transient heat transfer analysis computer program entitled, "Executive Sub-routines for Afterheat Temperature Analysis (ESATA)" tailored to solve this problem. Unique features included in this program were fission product decay and transport, metal-water reactions, core/shield melting and displacement (including heat of fusion), and soil property changes. The second task was to perform preliminary calculations for eight heat transfer models (HTM's). The third task was to analyze the results and respond to nine contractual questions related to design and impact conditions.

The remainder of this report describes the results of this contract. A brief description of the ESATA program including features and limitations, generalized heat transfer models, the program logic, and a summary of each subroutine is presented in Section 2.0. Section 3.0 describes the results of the 8 HTM's. Section 4.0 discusses the trends observed from the results, modeling considerations, and responses to the nine contractual questions. Sections 5.0 and 6.0 present the conclusions and recommendations. Detailed descriptions of the ESATA subroutines, data, and supporting equations are presented in Appendices A to E. A User's Manual for the ESATA program is given in Reference 1.

2.0 TASK I - ESATA PROGRAM DEVELOPMENT

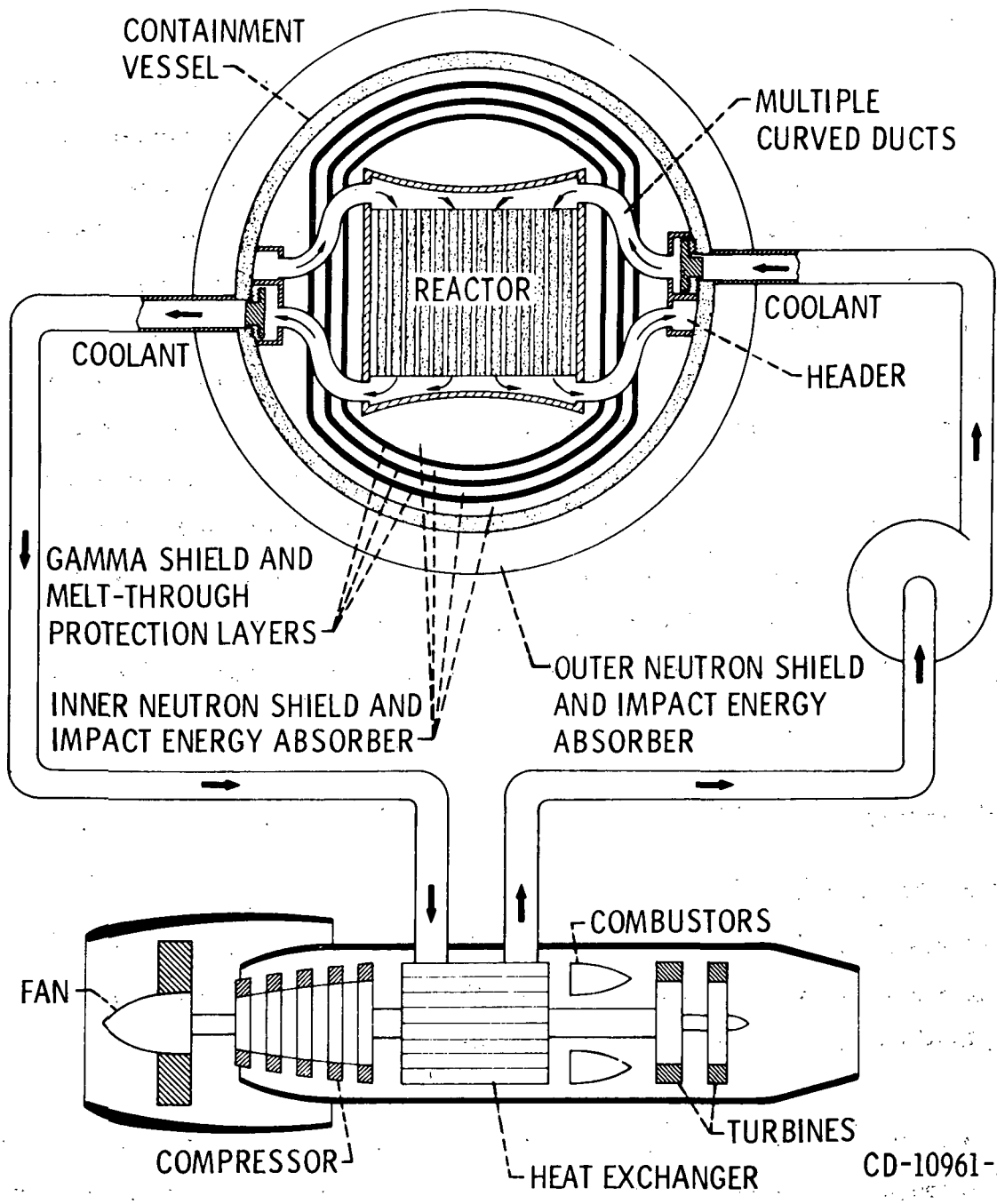
The ESATA program was developed to analyze the thermal safety aspects of post impacted mobile nuclear power plants. Specifically, the program calculates the transient temperature and pressure response for a gas-cooled thermal reactor power plant (Figure 2-1) following impact. The analysis is based on a closed system (containing trapped helium gas) where the nuclear afterheat must be dissipated by conduction through the containment wall. Phenomena, such as core and shield melting and displacement, fission product time/temperature release followed by condensation and subsequent reevaporation, metal-water, chemical reactions, and pressure buildup due to increased temperatures of the trapped helium gas and volatile products are simulated. This program was developed to handle a specific geometry with or without physical deformation of the system and with a variable degree of burial. Flexibility was built into the program to consider variable reactor core, shield, and containment vessel dimensions, variable weight and temperatures and several shield options. A stress analysis is performed to estimate the creep rupture of the containment vessel.

2.1 PROGRAM DESCRIPTION

2.1.1 General Description of Code

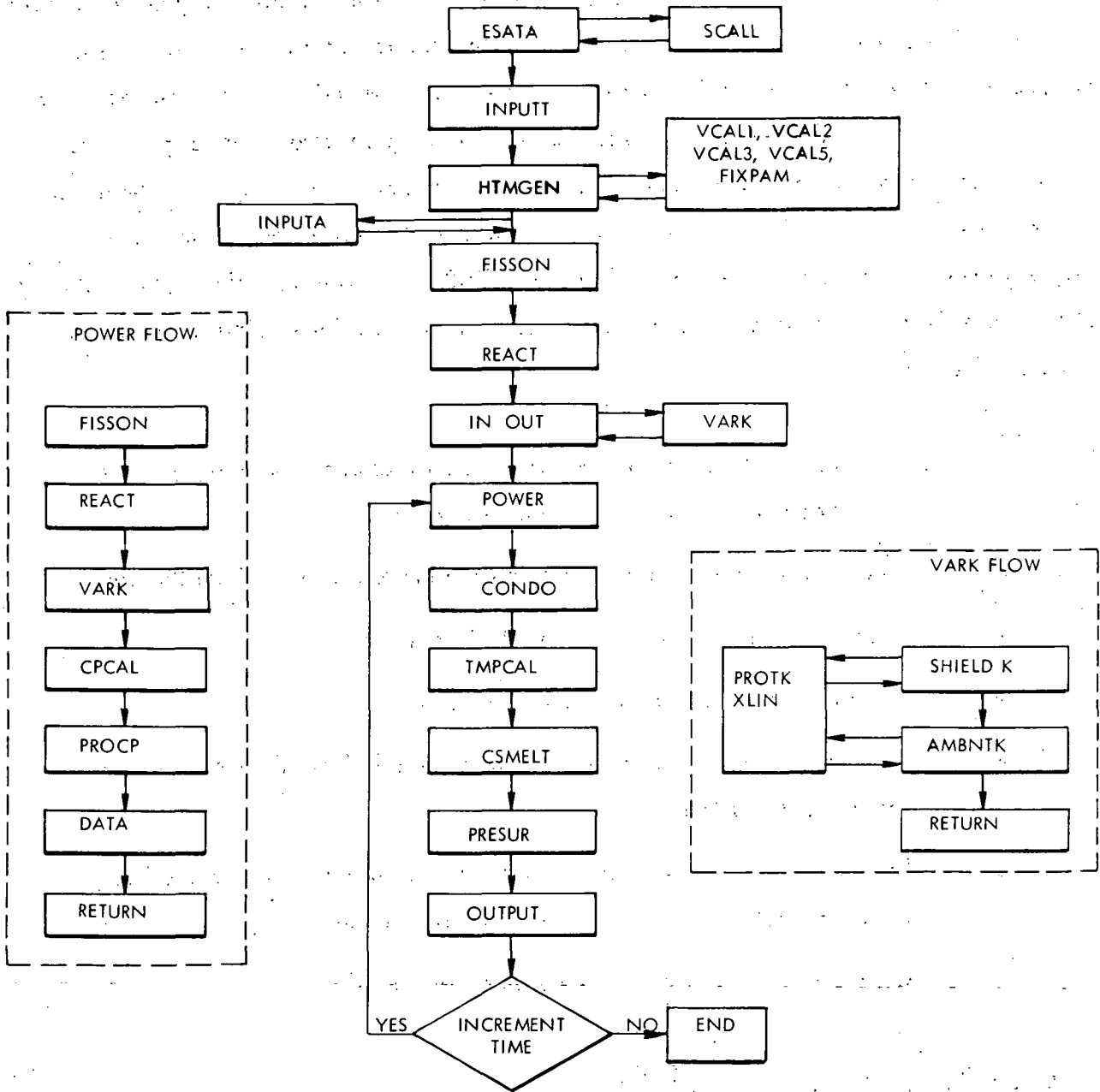
Figure 2-2 presents a schematic flow chart of the ESATA code package. Each of the subroutines contained in the ESATA code are identified in the figure including the general sequence in which they are executed by the program.

The ESATA program uses the existing TAP-A computer program ⁽²⁾ developed by Westinghouse. The TAP-A computer program (written in FORTRAN-IV) was developed to solve problems involving transient and steady-state heat transfer in multi-dimensional systems having arbitrary geometric configurations, boundary conditions, initial conditions, and physical



CD-10961-22

Figure 2-1. Schematic Drawing of a Nuclear Aircraft Power Plant



613628-17B

Figure 2-2. ESATA Code Package Schematic Flow Chart

properties. The program already had the capability to consider the following modes of heat transfer and boundary conditions: internal conduction and radiation, free and forced convection, radiation at external surfaces, specified time dependent surface temperatures, and specified time dependent surface heat fluxes. The program also handles space and temperature dependent thermal conductivity and heat capacity and space/time dependent internal heat generation rates. In addition, the external boundary (environmental) temperatures can be functions of time. The use of TAP-A, therefore, offered the advantage of having an existing fully operational computerized procedure for solving complex heat transfer problems.

The ESATA program was developed by adding new subroutines and modifying existing TAP-A subroutines to account for the following phenomena:

- Heat source redistribution due to fission product release from the core.
- Metal/water chemical reactions within the core.
- Melting of the reactor core and shield.
- Displacement of the core relative to the shield/containment vessel due to core/shield melting.
- Pressure buildup within the containment vessel due to vaporized fission products, metal/water reactions, and cover gases.
- Creep rupture analysis of the containment vessel.

2.1.2 Calculational Procedure of Code

The ESATA subroutines were arranged to allow for overlays such that more problem data space could be utilized within core storage limits for the IBM 7094 II/7044 computer system. The overlay structure is defined in Section 3.1.2 of Reference 1. The calculational procedure in ESATA is summarized as follows:

- Step 1 Input data is read by the main program routine ESATA and by subroutine INPUTT.
- Step 2 The input data is processed and nodal structure representations for the reactor power plants are set up in subroutines HTMGEN, FIXPAM, VCAL1, VCAL2, VCAL3, and VCAL5.
- Step 3 The initial heating rate distributions are established in subroutines FISSION and REACT from the input data.
- Step 4 The input data, the geometry setup, the initial heating rate distributions, and initial temperatures are output by subroutine INOUT.
- Step 5 Time is incremented by a predefined amount.
- Step 6 Heat source distributions due to fission products and chemical reactions and temperature dependent material properties to be held constant during the time interval are established by subroutine POWER. Note that subroutine POWER calls other subroutines as indicated in Figure 2-2 during the process of establishing these data.
- Step 7 Temperatures for all system components are computed in subroutines CONDO and STCALC.
- Step 8 Melting and displacement of the reactor core and shield based on the computer temperatures are established in subroutines TMPCAL and CSMELT.
- Step 9 Internal pressure buildup and the corresponding containment vessel stress level is computed in subroutine PRESUR.
- Step 10 Temperature distributions, pressure, heat source distributions, the amount of core/shield that is molten and the location of the core relative to the shield/containment vessel is output by subroutine OUTPUT.

Step 11. Time is again incremented and Steps 6 through 10 repeated. The calculation is terminated when the run time specified as part of the input is exceeded.

2.1.3 Internal Node Generators

Three generalized heat transfer models were developed and stored in the ESATA program to minimize input data requirements. Two of the models represent the undeformed and deformed configurations of the gas-cooled thermal reactor concept. The third is an in-pile test model being developed for testing in the NASA Plum Brook Test Facility.

The undeformed HTM is shown in Figure 2-3. This model contains 218 internal nodes. The following basic modeling assumptions were made:

1. Two-dimensional analysis with line of symmetry perpendicular to soil and coexistent with core centerline.
2. No internal deformation with structure intact.
3. Neglect piping and structural support (Their mass is lumped in the core mass for proper capacitance.).

The homogenized core (having specific materials properties defined) and inner shield region are divided into 38 cylindrical and interfacing nodes (nodes 1 through 38). Of the 38 nodes, those representing the core are established based on the core height and radius specified as part of the input to the program. The interfacing nodes (for example, node 1) are used to mathematically couple the cylindrical nodes representing the core/inner shield to spherical nodes representing the remainder of the system. In the spherical node regions, each shield layer (for example, nodes 38 through 50) and the gaps between the shield layers (for example, nodes 51 through 62) are discretely modeled. The gaps between the layers can either

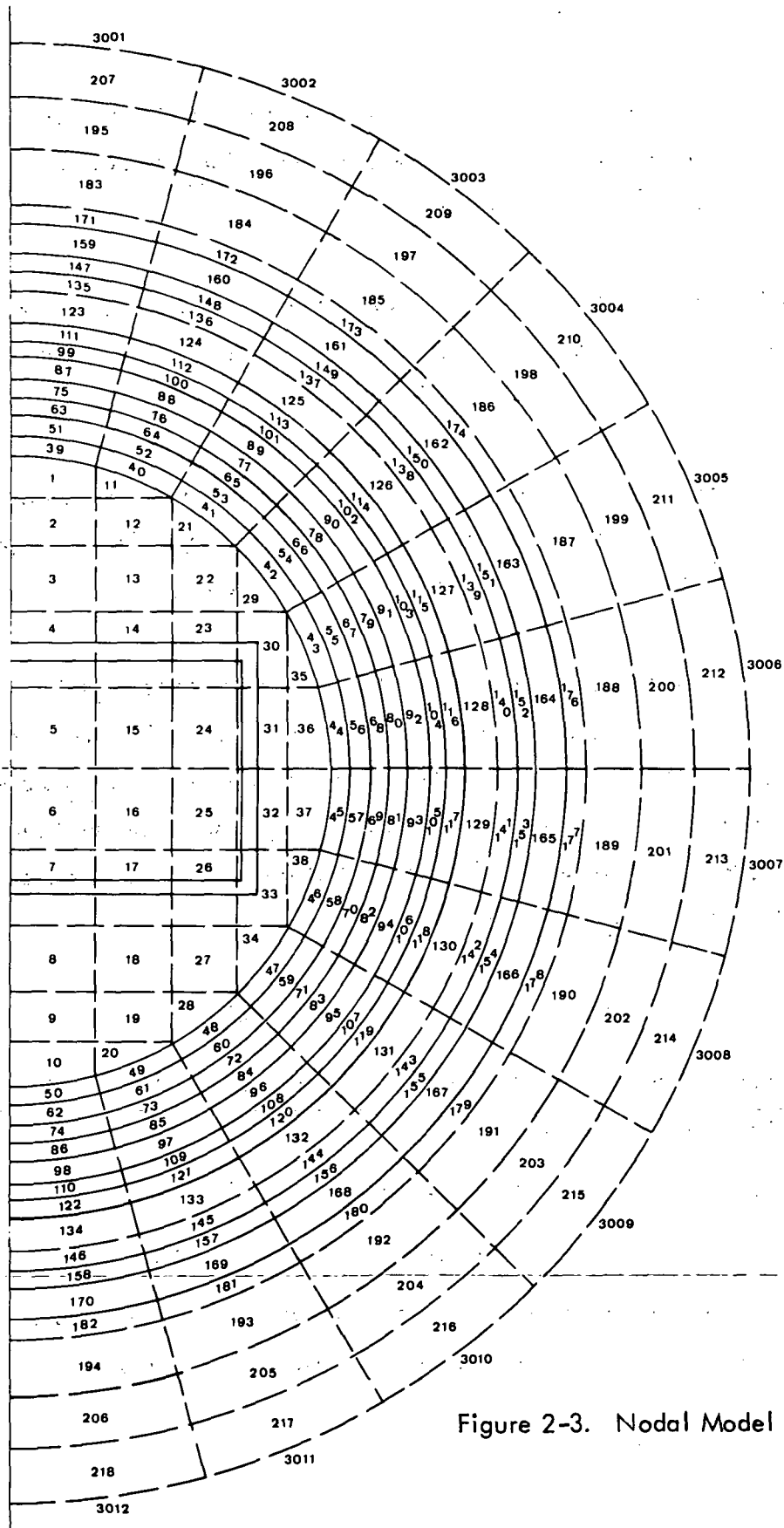


Figure 2-3. Nodal Model for Undeformed HTM

represent void (helium) or LiH or composite material depending on the shield option specified. Also, nodes 135 through 146 represent depleted UO_2 insulation, void, composite material, or LiH dependent on the input option specified.

Nodes 147 to 158 represent the sodium heat pipes. The use of these nodes as heat pipes is dependent on the input option specified, no heat pipes, 50 percent of the heat pipes working, or 100 percent working.

Nodes 159 through 170 represent the containment vessel. The remaining nodes represent soil or air dependent on the percent burial defined for the problem. The minimum percent burial for this model is 33 percent, and the maximum is 100 percent.

The deformed model, Figure 2-4 is arranged similar to the undeformed model in the top half of the model. The layers represented in that region are the same. The lower half of the model is comprised entirely of cylindrical nodes. The layers represented discretely in the top portion are also represented in the lower portion. To provide a continuity in the division of nodes between the upper and lower halves of the model, the number of nodes (293) is considerably greater than the undeformed model.

Modeling assumptions applicable to the deformed model include:

1. Two-dimensional analysis with line of symmetry perpendicular to soil and coexistent with core centerline.
2. Deformation of vessel and core in lower half only.
3. Degree of diametral deformation is fixed at 30 percent.
4. For those shield designs having LiH, the LiH in the deformed region is assumed compressed to a thickness of one inch between each tungsten shield layer.

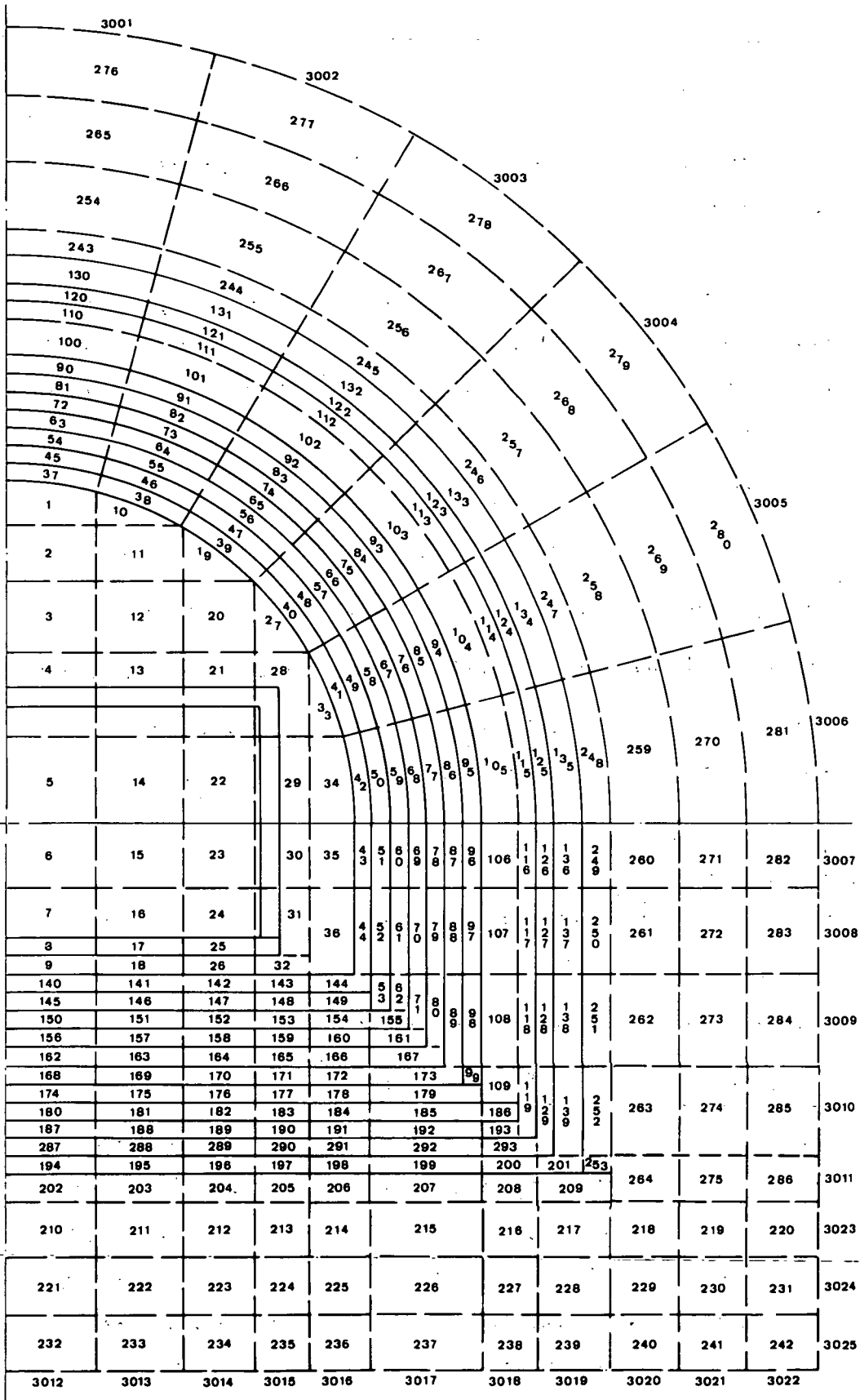


Figure 2-4. Nodal Model for Deformed HTM

5. For those shields without LiH, all layers in the deformed region of the model are assumed to be in perfect contact.

The Plum Brook in-pile test model is shown in Figure 2-5. Nodes 1 to 40 are cylindrical nodes representing the core interfacing nodes which encompass the core region. Nodes 41 to 112 represent depleted UO_2 . Nodes 113 to 124 represent the containment shell. Basic assumptions for this model are:

1. Two-dimensional analysis with axi-symmetrical flux distribution.
2. Thermocouples and thermocouple insulation port are neglected.
3. Core consists of enriched UO_2 with representative material properties.
4. Containment wall dissipates heat by radiation and convection to surroundings.
5. Radial power factor simulating the resulting flux distribution due to the location of the test model in the Plum Brook reactor is included.

2.1.4 Features and Limitations

The ESATA program contains the following calculational and modeling features and limitations:

1. Reactor concept - gas cooled thermal reactor concept.
2. Reactor core - homogeneous, uniform temperature core.
3. Five shield configurations (Figure 2-6). Design 1 consists of 4 heavy metal (W) shield layers separated by trapped helium with water having been removed. Referring to Figure 2-3, the four shield layers would be represented by nodes 39-50, 63-74, 87-98, and 111-122. Nodes adjacent to these layers represent radiation gaps. Design 2 consists of the 4 heavy metal shield layers separated by LiH. The same nodes that are in Design 1 would represent the

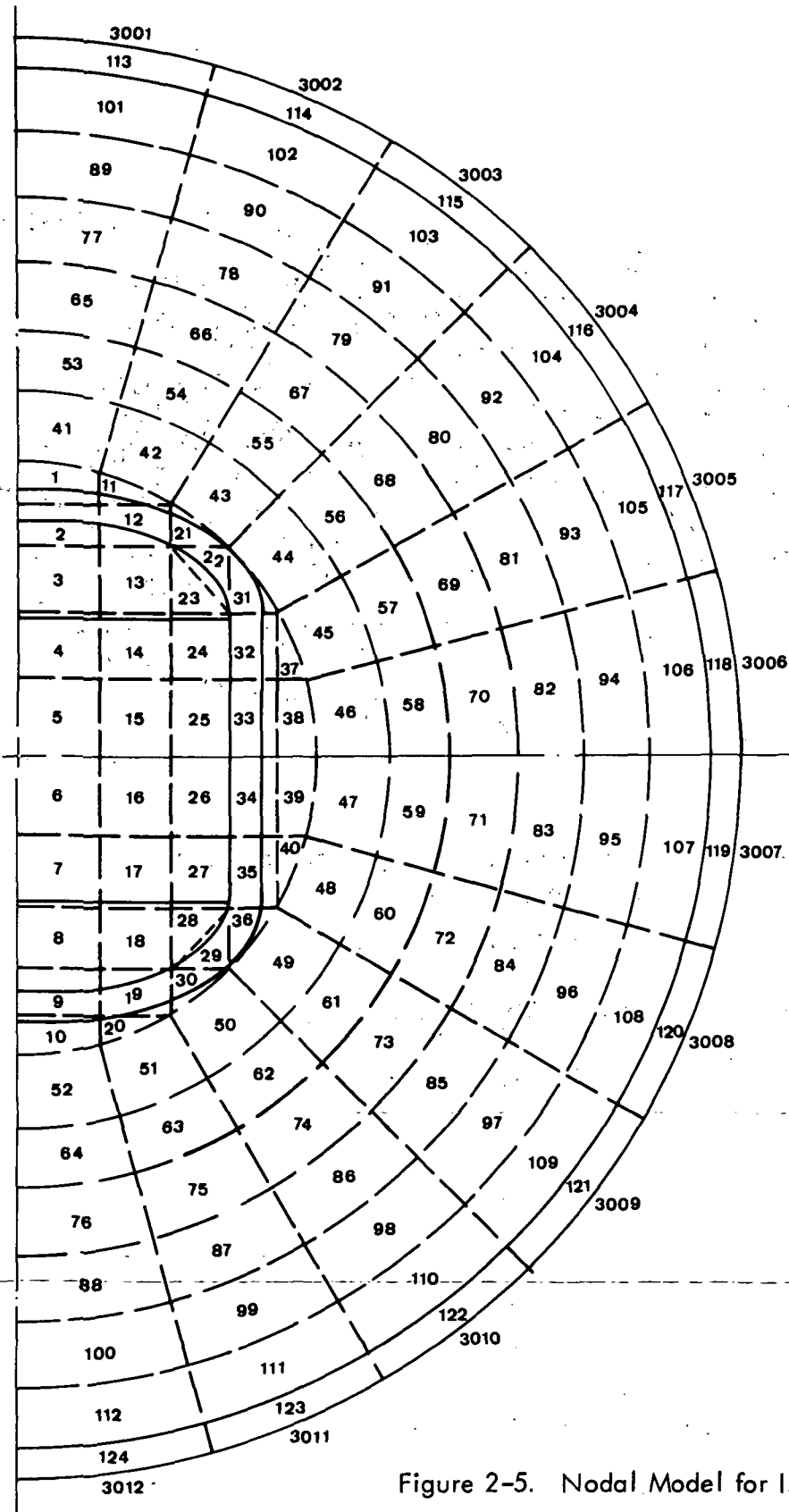
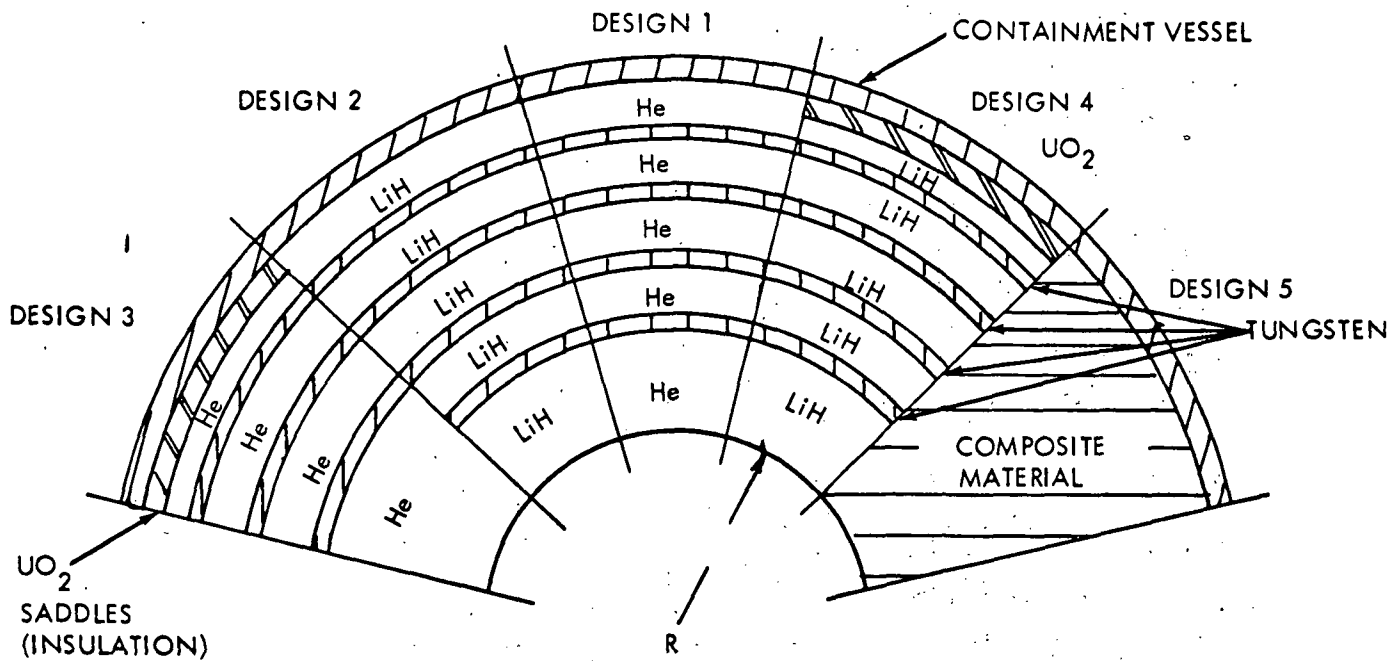


Figure 2-5. Nodal Model for In-Pile Test Model



- DESIGN 1 - HEAVY METAL WATER SHIELD WITHOUT WATER
- DESIGN 2 - LITHIUM HYDRIDE SHIELD
- DESIGN 3 - HEAVY METAL SHIELD WITH HEAVY INSULATION
- DESIGN 4 - LITHIUM HYDRIDE SHIELD WITH HEAVY INSULATION
- DESIGN 5 - COMPOSITE MATERIAL SHIELD

Figure 2-6. Reactor Shield Designs

shield layers. Nodes that were radiation gaps in Design 1 are LiH nodes in Design 2. Design 3 consists of 3 heavy metal shield layers separated by helium gaps with a layer of UO_2 insulation adjacent to the containment vessel. Nodes 63-74, 87-98, and 111-122 in Figure 2-3 would represent the 3 shield layers. Nodes 135-146 represent the UO_2 . Design 4 is identical to Design 2 except that the layer of UO_2 insulation adjacent to the containment vessel is included. Design 5 consists of a composite shield with all the space between the core and the containment vessel containing UO_2 spheres filled with LiH.

4. Geometries - See Section 2.1.3.
5. Sodium heat pipes adjacent to containment vessel wall-full operation and 50 percent operation can be considered. Also, configurations can be analyzed that do not contain heat pipes.
6. Containment vessel-single wall containment.
7. Ground burial due to impact - zero, partial, and full burial is provided for undeformed configuration. Partial and full burial is provided for the deformed configuration. Soil property data representative of results from Sandia test programs are included.
8. Fission products for the reactor plants are represented by four groups. The groups escape the core at rates that are functions of time and core temperature. Deposition of the fission products occur on the four W shield layers and the containment vessel. Deposition can be followed by vaporization dependent on local temperatures. The products move radially outward (layer by layer) following deposition and subsequent reevaporation. For the undeformed model, 4π redistribution is considered while for the deformed model, redistribution can only occur in the undeformed region. Uncondensed fission products contribute to pressure buildup. The heat of vaporization of fission products is neglected.

9. Heat generation rates for the in-pile test model are assumed to be in the core until the UO_2 reaches its melting point; the energy is then released to the shield layers and "walked out" radially based on the local temperature. The fuel deposited on the shield layers is worth more due to the increased attenuation of the neutron flux.
10. Metal-water reactions are considered in the core for the moderator and reflector water reacting with the stainless steel and molybdenum structure. Energy released or absorbed by the reaction is considered a heat generation in the core. Hydrogen released by the reaction contributes to the pressure buildup.
11. The core melts (Moly, UO_2 and AM-355 heats of fusion are modeled) and displaces as a unit as opposed to allowing portions of the core to displace while others remain stationary.
12. LiH melting and displacement is considered and the heat of fusion is modeled. However, with any of the shield options provided, elimination of voids - formation of a solid mass - after melting is not considered. Likewise, displacement of the LiH does not result in mass conservation.
13. Tungsten melting and displacement is considered and the heat of fusion modeled.
14. Pressure buildup due to uncondensed fission products, hydrogen released from metal-water reactions, and trapped helium gas is treated.
15. Hoop stress and creep rupture failure analysis of the containment vessel is treated.
16. The time increment is expanded by a factor of 2 each time the number of iterations required for convergence at a previous time is less than 20.

17. Normal TAP-A input is available for geometry changes, material changes, and temperature changes. Limited nodal structure changes can be made with caution to prevent invalidating parts of the analysis such as component displacement and fission product redistribution.

2.1.5 Input and Output Options

The quantity of input data required for the operation of any computer program becomes particularly important whenever the program is to be employed for analysis of many different configurations. For this reason, the input data requirements of ESATA were minimized. The general types of input data that are required are as follows: (Section 4.0 of Reference 1 defines specific input data requirements.)

- One card to identify the amount of computer space required by the problem to be analyzed.
- Title cards.
- Initial and final time for the calculation and the starting time interval.
- Convergence criteria for the calculation.
- Set of numbers (triggers) which will identify the reactor concept to be analyzed, the physical configuration of the power plant, etc.
- Gross dimensions of the core, shield, and containment vessel.
- Initial temperatures of the core, shield, containment vessel, soil, and ambient environment.
- Weights of core components; i.e., fuel, clad, structure, and coolant.
- Normal reactor operating power level.
- Initial internal pressure.
- The times during the transient period when output data is desired.

The following general types of data will be included in the output from the ESATA code package: Section 5.0 of reference presents a detailed description of the output data.

- Time point in the afterheat decay transient.
- Temperatures and temperature distributions for all system components.
- Location of all heat sources in the system: including the general location of the four fission product groups.
- Percentage of the core that has melted.
- An identification of all system materials on a nodal basis that have initiated melting and the corresponding percentage that is molten.
- Internal pressure, containment vessel stress level, and the percent of containment vessel (creep-rupture) life used.

2.2 SUBROUTINE DESCRIPTION

A general description of each subroutine is given in this section. Appendices A to E contain equations and experimental data for those subroutines that were added to the basic TAP-A program to form the ESATA program.

2.2.1 Program Control and Call Subroutines

ESATA Main Program

This is the main program for the ESATA computer code. It contains the operational logic by which all primary subroutines of the program are called in the process of analyzing the temperature response of the reactor plant models. The order in which the operational subroutines are called is presented in Figure 2-2 and described in Section 2.1.1. In addition, since ESATA is a variable dimensional program, the sizes for most matrices used

in the calculations are computed based on the input data in this portion of the program. The titles and main program control trigger for specifying the analysis option are also read in the main program.

Subroutine SCALL

This is an intermediate subroutine used in conjunction with the main program to call other subroutines in the program. Since ESATA is a variable dimensioned program, all subroutines contain large argument lists in the calling statements. Several subroutines are called more than once from the same subroutine. To provide for efficient use of computer space, an intermediate subroutine, SCALL containing one argument is used to call the appropriate subroutines at the desired point in the computations.

2.2.2 TAP-A Functional Subroutines

The following subroutines were developed originally for TAP-A program usage and extended where necessary for usage compatible with the afterheat temperature analysis option of the ESATA program. Reference 1 contains additional information relative to the subroutines described below.

Subroutine INPUTT and INPUTA

These subroutines read input for performing the calculations. They consist of ESATA input data required for the heat transfer models (HTM) contained in the program for performing the afterheat analysis and the standard TAP-A data input routine. For analyses where changes to the heat transfer models are desired, certain changes can be accommodated using the standard TAP-A input.

Subroutine OUTPUT

It prints the following data at predefined time intervals during the decay transient:

- Time point in the afterheat decay transient
- Internal, surface, and boundary temperatures
- Location of all heat sources in the system
- An identification of all system materials on a nodal basis that have initiated melting and the corresponding percentage that is molten
- Location of core relative to the shield and containment vessel
- General location of the four fission product groups
- Total system pressure
- Containment vessel stress level and percent of creep-rupture life used.

Subroutine POWER

This subroutine calculates internal heat generation and material capacitances. Heat generated at different nodes in the model are determined in subroutines FISSON and REACT for fission product heating and metal-water reactions respectively. These individual heating rates are summed in this subroutine on a per node basis. Heat capacitances for each node in the model are also computed. If a standard TAP-A run is made, this subroutine selects from the input data the heat generation rate for each node.

Subroutine STCALC

This subroutine calculates surface heat transfer coefficients and containment vessel surface temperatures.

Subroutine INOUT

This subroutine prints the input data, initial conditions, geometry data generated by HTMGGEN or read in, and heat generation rates generated by FISSON and REACT.

Subroutine PUNCEM

This subroutine punches on cards the temperatures for each node at the final time step.

Subroutine XLTN

This subroutine does a linear interpolation of independent and dependent variables.

Subroutine CONDO

This subroutine calculates steady-state and transient temperatures for each node in the model through solution of the finite difference equations. In addition, a procedure for varying the time increment during the afterheat decay transient is included. The procedure consists of monitoring the number of iterations required for solution convergence and doubling the time increment for the next calculational step whenever the number of iterations is less than 20.

2.2.3 HTM Generation Subroutines

The subroutine HTMGGEN (including HTMGGN1, HTMGGN2, HTMGGN3, HTMGGN4, HTMGGN5) and associated subroutines VCAL1, VCAL2, VCAL3, VCAL5, and FIXPAM set up the appropriate nodal geometry from the three nodal models described in Section 2.1.3 based on the input data option.

A detailed description of these subroutines including representative equations is presented in Appendix A.

2.2.4 Heat Generation Subroutines

For the general heat transfer calculation option, heat generation rates are supplied to the program via input data for each node. For the afterheat temperature analysis option, heat generation rates for each node are calculated internally. There are two sources for heat generation in ESATA. One source is the fission product decay energy which is calculated in FISSON based on the normal reactor operating power level which is an input variable. The other source is the heat released or absorbed during the water to metal reactions in the core which is calculated in the subroutine REACT. A general description of the subroutines is presented below. Detailed descriptions including supporting equations, curves, and data are presented in Appendix B. Energy absorption associated with phase changes are simulated in the capacitance calculation by effective specific heats. However, the heat of vaporization of fission products is neglected.

Subroutine FISSON

This subroutine calculates heat generation rates based on fission product decay, release from the core, and deposition followed by reevaporation from specific shield layers on the containment vessel. This subroutine classifies fission products in four groups according to their volatility (Table 2-1). These groupings are allowed to exist (depending on temperature) in the core, on four heavy metal (W) shield layers (for example, nodes 39 to 50 in Figure 3-1), the containment vessel, and in the vapor state. Heat generation rates are assigned to those nodes in the heat transfer models where groupings of fission products are located. Part, all, or none of the nodes in each of the shield layers or containment vessel may receive fission products.

For each fission product group, a time dependent energy decay rate is defined, shown in Figure 2-7. The fission products are allowed to escape gradually from the core. The percent of fission product escape is defined for each grouping on a time and temperature basis. A

TABLE 2-1
YIELDS AND CHARACTERISTICS OF
IMPORTANT FISSION PRODUCT ELEMENTS

	Isotope	Normal Boiling,		Weight Percent of	
		(°R)	(°K)	Yield After 1 Year of	Irradiation*
A. High Volatility	Kr	216	120	1.4	17.5
	Xe	297	165	15.3	
	Br	598	332	0.1	
	I	821	456	0.7	
B. Intermediate Volatility	Cs	1724	958	10.2	29.5
	Te	2268	1260	1.6	
	Ru	8105	4503	5.5	
	Tc	8771	4873	2.8	
	Mo	9131	5073	9.4	
C. Low Volatility	Sr	2950	1639	4.0	8.0
	Ba	3434	1908	4.0	
	Sb	3443	1913	-	
D. Refractory	Sm	3375	1875	1.5	45.0
	Pr	5927	3293	3.4	
	Y	5501	3056	1.9	
	Nd	6053	3363	11.8	
	La	6557	3643	3.6	
	Ce	6737	3743	9.8	
	Zr	8276	4598	12.7	
	Nb	9365	5203	0.3	

* Assumed thermal neutron flux, 5×10^{12} neutrons/cm² sec

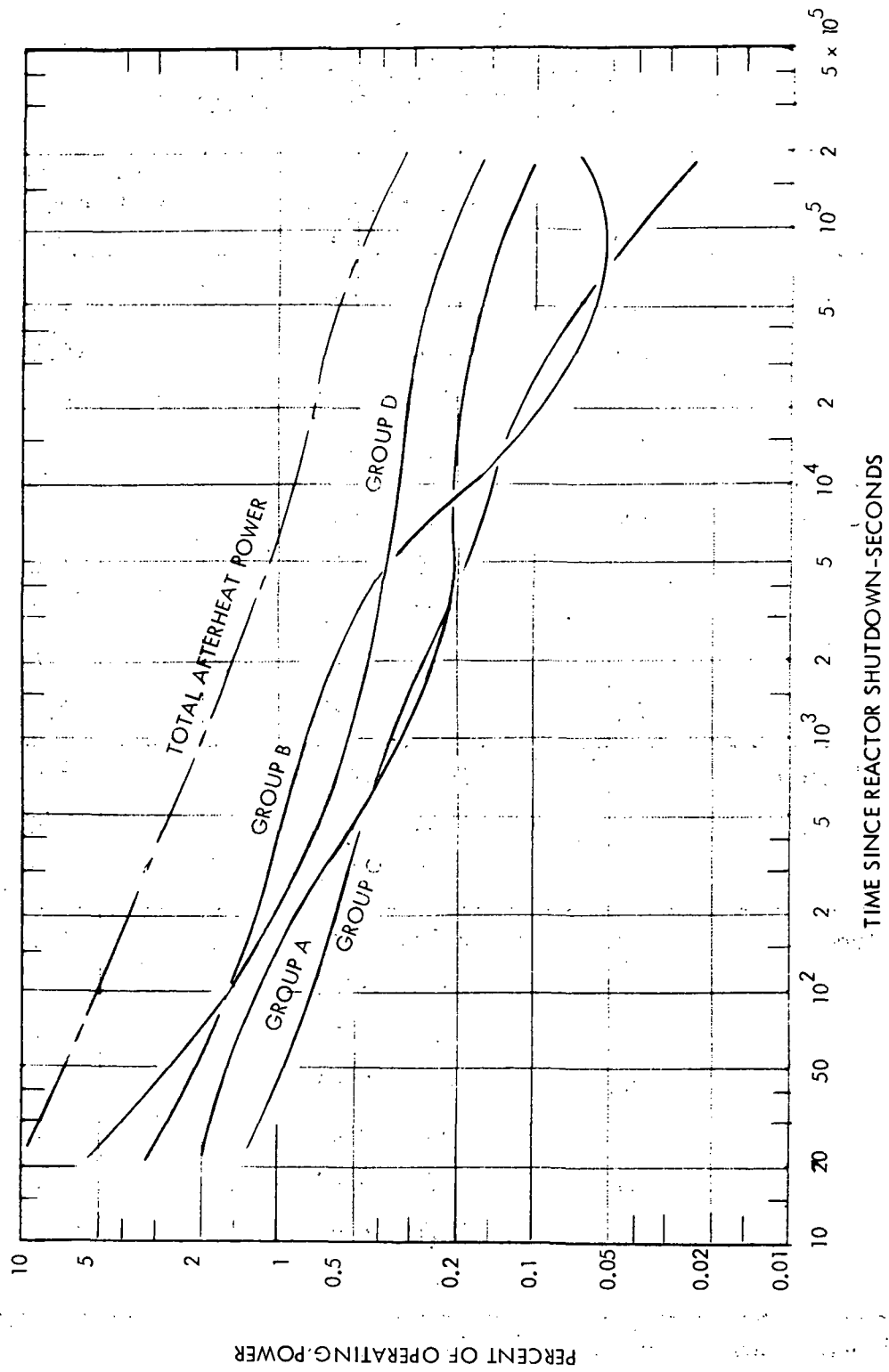


Figure 2-7. Fission Product Decay Curves

condensation temperature is defined for each grouping. A typical fission product deposition pattern reported by Castleman and Tang⁽¹²⁾ was used as a basis for selection of condensation temperatures, see Table 2-2. (It should be noted, that this subroutine was programmed such that the data used to define each of the four groups and the condensation temperature for each group can be easily modified when or if better experimental data becomes available.) If any node or nodes in the shield layer are below that temperature, then the fission products in that grouping are condensed on that layer. If the temperature is greater than the deposition temperature, the fission products are transported to the next layer. The decay energy associated with the condensed products is applied to the node as a heat generation term. Heats of condensation or vaporization are not considered. If a node in any layer has fission products and rises in temperature above the condensation (deposition) temperature, then the fission products are removed from that node and assigned to the next layer.

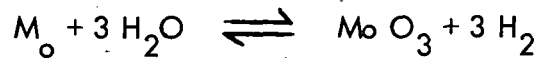
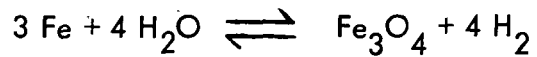
When fission products reach the containment vessel and are subsequently driven off, they are then considered as in the vapor state. The mass of fission products in the vapor state is considered in the pressure buildup.

TABLE 2-2
DEPOSITION PATTERNS IN THERMAL GRADIENT TUBE

Temperature Range	470 to 870°K	870 to 1070°K	1070 to 1670°K
Deposition Fission Product Group	A	B	C, D

Subroutine REACT

This subroutine calculates the heat generation or heat removal in the core due to metal-water reactions. The reactions considered for the water remaining in the gas core are:



The stainless steel-water reaction is considered prior to pressure tube melting (1770°K), and the molybdenum-water reaction is considered after the pressure tubes melt. The reaction rates are defined by the following equations as a function of core temperature and reaction areas (areas are a part of input).

$$R_{\text{SS-H}_2\text{O}} = \begin{matrix} (.1092) (A_{\text{PT}}) e^{(-19080/T)} & \frac{\text{lbm water}}{\text{sec}} & T \sim ^\circ\text{R} \\ (.00767) (A_{\text{PT}}) e^{(-10600/T)} & \frac{\text{kgm water}}{\text{sec}} & T \sim ^\circ\text{K} \end{matrix}$$

$$R_{\text{SS-Mo}} = \begin{matrix} (10.38) (A_{\text{Mo}}) e^{-(48646/T)} & \frac{\text{lbm water}}{\text{sec}} & T \sim ^\circ\text{R} \\ (.731) (A_{\text{Mo}}) e^{-(27026/T)} & \frac{\text{kgm water}}{\text{sec}} & T \sim ^\circ\text{K} \end{matrix}$$

Where A_{PT} is the pressure tube surface area, A_{Mo} is the clad surface area and T is the temperature representative of those surfaces.

The mass of water that is reacted is summed and compared to the initial mass of water in the system which is an input value. The heats of reaction for both reactions are stored versus temperature. The total heat release or absorbed in the core is calculated for each time step based on the reaction rate and the corresponding heat of reaction. This total heat is distributed among the core nodes by a volume weighted basis.

2.2.5 Property Data Subroutines

Several subroutines and functions are used to store property data and calculate effective property data to simulate internal interface conditions. Appendix Contains a detailed description of these subroutines. All data used in these subroutines are presented in tabular form there. A general description follows:

Subroutine VARK

This subroutine defines the thermal conductivity for each node and calculates the thermal conductance between each node in the model. It calls the SHELDK and PROTK functions described below. VARK contains logic to calculate an effective conductivity for simulation of sodium heat pipe operation. Curves have been defined for a maximum heat flux versus temperatures representative of 100 percent sodium heat pipe operation. Based on a predefined ΔT of 20°F (11°K) between adjacent heat pipe nodes, thermal conductivities are calculated from the heat flux at the calculated heat pipe node temperature. If adjacent heat pipe nodes exceed a temperature drop of 20°F (11°K), then the thermal conductivity is adjusted to prevent the heat flux from exceeding its maximum value. For 50 percent operation the heat flux and thus thermal conductivity are divided by two. VARK also contains the logic to calculate effective conductivities for the soil to containment vessel contact coefficient, vessel to air interface of radiation and natural convection, and air to air nodes.

Function SHELDK

This function calculates the effective thermal conductivity to simulate radiation from core to shield and between shield layers. It assigns high or low conductivities for one dimensional heat transfer paths through materials or across interfaces. It also assigns a large thermal conductivity for the homogenized core representation.

Function PROTK

This subroutine stores thermal conductivity data versus temperature for 10 materials used in the gas-cooled thermal reactor concept. It does a linear interpolation of this data to define a thermal conductivity for a prescribed material and temperature.

Block DATA

This subroutine stores density, melting point temperature, and the effective specific heat to simulate the heat of fusion for ten basic materials. The effective specific heat is defined for a temperature differential of 50°F (27.8°K) by the equation

$$C_p' = \frac{H_{fg}}{\delta T}$$

Where $\delta T = 50^\circ R (27.8^\circ K)$ (prescribed arbitrarily).

Function PROCP

This subroutine stores specific heat data versus temperature for ten materials used in the gas cooled reactor concept. It does a linear interpolation of this data to define a specific heat for a prescribed material and temperature.

Subroutine CPCAL

Defines effective specific heat and density for all materials (components) not defined by basic material properties; for example, defines effective properties for the homogenized gas-cooled thermal reactor core.

2.2.6 Core-Shield Melt and Displace Subroutine

Two subroutines are used to simulate the melting and displacement of the core and shield. A general description of these subroutines follows with a detailed description in Appendix D.

Subroutine TMPCAL

This subroutine corrects temperatures in the core and shield to account for the heat of fusion during phase changes of various materials. In the subroutine PROCP and the DATA block are defined effective specific heats simulating the heat of fusion spread over a prescribed ΔT of 50°R (27.8°K). Namely,

$$C_p' = \frac{H_{fg}}{\delta T} \quad \text{where } \delta T = 50^\circ R (27.8^\circ K)$$

These data are defined for six materials used in the core and shield—molybdenum, UO_2 , tungsten, AM-355, lithium hydride and a composite of UO_2 and LiH. TMPCAL simulates phase changes for these six materials as separate components and also simulates the effect of phase changes of the three materials representing the homogenized gas core; namely, molybdenum, UO_2 and AM-355.

After a temperature convergence is obtained in CONDO for a particular time step, the temperatures of all nodes assigned one of the above materials are compared to their melting point temperature plus the band of 50°R (27.8°K) above the melting used to simulate the phase change. Dependent upon the percent of melting, the previous calculated temperature and the present temperature for a node relative to the 50°R (27.8°K) melting band the temperature is corrected by a set of equations defined in Appendix D. The fraction of melting is

$$X_{\text{mel}} = \frac{(T - T_{\text{mp}})}{\delta T}$$

where T is the corrected temperatures

T_{mp} is the melting point temperature.

X_{mel} - fraction of melting

When this function is one melting is completed. Equations are defined to simulate the correct value of H_{fg} irrespective of the number of time steps to go through the melting and irrespective of the magnitude of the old and new node temperature relative to the melting band.

Subroutine CSMELT

This subroutine reassigns material properties for various nodes to simulate the movement of the core and shield as a result of melting. It is oriented specifically to the deformed and undeformed models and is restricted to the five shield options and prescribed shield materials for those options. Replacement of materials would invalidate this model.

In the undeformed model with void spaces between the core and shield, the entire core will "drop" to the first tungsten shield layer (nodes 39 to 50 in Figure 2-3) when the core structure is completely molten. It will then collapse and fill up layers and nodes inside the first shield layer from the bottom until the volume of nodes assigned core properties equals the volume of solid core material. The core will rest on the first layer until the first layer melts. When the first shield layer melts, the shield and core will come in contact with the next shield layer. Similarly when the second, third, and fourth layers melt they will become in contact with the adjacent layers. "Walkout" to the containment vessel is thus simulated.

With the shield filled with LiH, the core will not drop immediately on the first heavy metal shield layer. The core will first displace through the LiH inside the first shield layer. The displacement will be on a row-by-row basis. When a row of LiH nodes are entirely molten, the entire core will displace 1 row. When the core has dropped onto the first heavy metal shield layer, then it will collapse into a volume representative of the volume of solid core materials. As above, the core will rest on the heavy metal shield layer until the layer melts. When the shield layer melts, the shield layer and core will drop onto the next shield layer if the LiH separating the two layers is molten.

If the shield contains UO_2 insulation of the inner surface of the containment vessel, the UO_2 will not be displaced by the core. Also, when the composite shield material is used, core displacement is not treated. This option was "set up" for UO_2 spheres filled with LiH and the UO_2 will not be displaced since the specific gravities of the core/ UO_2 are similar. With any of these shield options slumping of the shield material to a solid mass - elimination of voids - after melting is not considered.

In the deformed model, the structural support of the core and shield layers are assumed to be destroyed. With the shield configurations containing voids, all shield layers are in

contact with each other, the core, and the containment vessel. When the core structure melts it will collapse and fill the base of the first heavy-metal shield layer. Further displacement will not occur since the specific gravity of the assumed tungsten is greater than that of the core. With the LiH filled configuration, the shield layers, core, and containment vessel are separated by LiH. Core and shield displacement will occur only when an entire row of LiH becomes molten. If UO_2 is between the outer shield layer and the containment vessel, it will not be displaced. If the composite shield option is used, no displacement occurs.

In all of the above described displacements, the core mass is maintained constant to provide for proper simulation of the core capacitance. Displacement of the LiH layers does not result in mass conservation, however.

2.2.7 Pressure and Stress Subroutine

Subroutine PRESUR

This subroutine calculates the pressure buildup inside the containment vessel, the maximum hoop stress level of the containment vessel, and the percent life used on a creep rupture basis.

Three components are considered in the pressure buildup; namely, the helium cover gas, hydrogen released from the metal-water reaction, and non-condensed fission products. This subroutine takes the vapor masses calculated in other subroutines and calculates the partial pressures of each component based on the perfect gas law. The total pressure is calculated and used to calculate a hoop stress based on the radius and thickness of the containment vessel. The Larsen Miller parameter is calculated based on SS-316 creep rupture data and the maximum containment vessel temperature using the following:

$$(60 - LM)^{0.496} - (\log_{10} \sigma)^{1.2} = 1.2 = 0$$

where LM = Larsen-Miller parameter

σ = stress level

The time to failure is computed from the standard Larsen-Miller equation

$$LM = (T + 460) (a + \log_{10} \tau) 10^{-3}$$

where T = temperature of the vessel in °F

a = experimental constant having a value of 20 for the 316 stainless steel material

τ = time to failure at the applied stress (σ) level

The percent of life used in each time step is calculated based on the time increment divided by the time to failure (τ). The percent of life used is summed to determine the total used up for fraction of life. When this fraction equals 1 rupture is assumed to occur.

3.0 TASK II HEAT TRANSFER CALCULATIONS

Eight HTM's were defined for performing heat transfer calculations and analysis using the ESATA program described in Section 2.0. Six of these HTM's represent design variations of a helium cooled thermal reactor power plant shown in Figure 2-1. These HTM's considered both deformed, and underformed power plant models, various shield configurations, percent of ground burial, and various heat pipe performance. The calculations were run for sufficient times to characterize the temperature transient of each HTM and to determine the integrity of the containment vessel. Section 3.1 briefly describes the helium cooled thermal reactor power plant. Sections 3.2 and 3.3 describe the HTM's analyzed and the results obtained. The comparison and discussion of the HTM's were the requirements of Task III and are presented in Section IV.

3.1 HELIUM GAS COOLED THERMAL REACTOR POWER PLANT

A schematic of the power plant and containment system is shown in Figure 2-1. A reactor core is contained in a pressure vessel which is surrounded by gamma and neutron shielding. The shielded reactor is surrounded by a containment vessel for protection in the event of an impact.

The core fuel pins are cooled by high pressure helium which is contained by pressure tubes. Water is provided as the moderator. The water moderator is isolated from the pressure tubes by a layer of high temperature thermal insulation. A typical unit designed to provide 300 thermal megawatts to helium at 1730°F can be enclosed inside a spherical reactor containment vessel of less than 20 feet outside diameter. Pertinent reactor characteristics are shown in Table 3-1. Principal materials of construction are shown in Table 3-2.

3.2 HTM DESCRIPTION

The 8 HTM's that were analyzed are tabulated in Table 3-3. They represent design variations of a helium cooled thermal reactor powerplant with the water moderator removed. The first HTM was a checkout problem to demonstrate an optional shield configuration

TABLE 3-1
REACTOR CHARACTERISTICS

Power to coolant (helium), MW	300
Total reactor power, MW	326
Reactor inlet pressure, psi	1500 (1034 N/cm ²)
Reactor inlet temperature, °F	1000 (811°K)
Operating lifetime, hours	1000
Active reactor core, diam., in.	66 (167.6 cm)
Active reactor core, length, in.	42 (106.7 cm)
Core pressure drop, P/P	<.03

TABLE 3-2
MATERIALS OF CONSTRUCTION

Fuel element clad	Molybdenum alloy TZM
Fuel element supports	Hastelloy X
Pressure tube layers	Hastelloy X, M in K 2000 and Austenitic steel (AM-355)
Reactivity control plate	Stainless steel - cadmium "sandwich"
Pressure vessel	Austenitic steel (AM-355)
Heavy material layers in shield	Tungsten

TABLE 3-3
 HEAT TRANSFER MODELS

<u>HTM Number</u>	<u>Description</u>
1	UO ₂ /LiH Shield checkout problem
2	Undeformed model Tungsten (W) shield-water removed, UO ₂ adjacent to CV 0 heat pipes 33 percent burial
3	Undeformed model W shield, LiH filled, UO ₂ adjacent to CV 0 heat pipes 33 percent burial
4	Deformed model W shield, LiH filled, UO ₂ adjacent to CV 0 heat pipes 33 percent burial
5	Undeformed model W shield, LiH filled, UO ₂ adjacent to CV 0 heat pipes 50 percent burial
6	Inpile test model Flux distribution No. 1
7	Undeformed model W shield, LiH filled, UO ₂ adjacent to CV 100 percent heat-pipes 50 percent burial
8	Deformed model Composite shield of LiH filled UO ₂ spheres 0 percent heat pipes 33 percent burial

consisting of the LiH filled heavy metal shield with a layer of UO_2 adjacent to the containment vessel. The shield option features a detachment of the UO_2 in the upper portion of the model when the LiH adjacent to it melted. HTM 2, 3, 5 and 7 were cases to analyze the undeformed model with alternate shield options, percent burials, and heat pipe options. HTM 4 and 8 were to analyze the deformed model with alternate shield options. HTM 6 was the in-pile test model with an initial heat flux distribution. Table 3-4 summarizes the initial temperature and pressure conditions for the six reactor plant cases. Table 3-5 summarizes the core mass and fuel pin surface areas used for these six cases. The radii and shield layer thicknesses are presented in Table 3-6. The after-heat power decay profile is described in Appendix B. The normal operating level for these cases was 300 M watts. The in-pile test model was run based on a 4K watt power level with $610^{\circ}R$ ambient temperature.

3.3 HTM RESULTS

3.3.1 HTM-1, LiH/ UO_2 Shield Option Checkout Problem

A unique design feature was incorporated into the W/LiH/ UO_2 shield configuration. This feature consisted of supporting the UO_2 with a low melting point material such as aluminum. During the transient heating period, this material would melt before the containment vessel reached an excessive temperature level in the top portion of the vessel. With the support structure molten the dense UO_2 would fall away from the top of the vessel and displace through the LiH. LiH with a larger thermal conductivity would then provide some "thermal shorting" to the top of the vessel.

This effect was simulated in the ESATA program for both the undeformed and deformed models. In the undeformed model the temperature of LiH adjacent to the UO_2 in the upper portion of the model (nodes 123-130 in Figure 3-1) was compared to the melting point for LiH_2 . When any one of these nodes exceeded its melting point, all the UO_2 in nodes 135 to 142 were replaced by a high conductivity material (material number 25) to simulate the displacement of UO_2 through molten LiH. In the deformed model LiH in nodes 100-109 are checked for melting, and the UO_2 in nodes 110 to 119 are displaced when applicable.

TABLE 3-4
INITIAL TEMPERATURES AND PRESSURES

	<u>Temperature</u> °R	<u>°K</u>
Clad	3310	(1839)
Structure	1660	(922)
Water	672	(373)
Shield	960	(533)
Containment Vessel	560	(311)
Ambient	560	(311)
Internal pressure	350 psi (241 N/cm ²)	

TABLE 3-5
CORE MASS AND AREA

	<u>Mass - Lbs.</u>	<u>(Kgm)</u>
Molybdenum in core	10,260	(4658)
UO ₂ in core	1,914	(869)
Pressure vessel and support structure	17,939	(8144)
Water left in core (5% of original)	163	(74)
	<u>Area ~ in²</u>	<u>(Cm²)</u>
Pressure tube surface area	133,490	(861,010)
Clad Area	2,721	(17,500)

TABLE 3-6
KEY RADII AND THICKNESSES

Overall core radius	37 inches (94 cm)	
Overall core height	76 inches (193 cm)	
Shield layers		
	<u>Inner Radius (in.)</u>	<u>Thickness (in.)</u>
First layer	54 (137 cm)	3.95 (10 cm)
Second layer	61 (155 cm)	0.91 (2.3 cm)
Third layer	66 (167.6 cm)	1.18 (3 cm)
Fourth layer	71 (180 cm)	0.61 (1.55 cm)
UO ₂ insulation thickness	1.5 inches (3.8 cm)	
Containment vessel inner radius	118 inches (300 cm)	
Containment vessel thickness	2 inches (5.08 cm)	

TABLE 3-7
TABULATION OF HTM-1 UO₂ DETACHMENT

<u>Time (Sec)</u>	<u>LiH Temperature - °R</u> (Nodes 123-131)	<u>UO₂ Temperature - °R</u> (Nodes 135-143)	<u>Material</u> (In Nodes 135-143)
0	5000 (2778 °K)	5000 (2778 °K)	UO ₂
60	4152 (2307 °K)	5000 (2778 °K)	UO ₂
120	4152 (2307 °K)	4994 (2774 °K)	LiH
180	4152 (2307 °K)	4993 (2773 °K)	LiH

This feature was checked with the use of the ESATA program. The undeformed model was defined with the W/LiH/ UO_2 shield. Temperatures in the shield and containment vessel were initialized above the melting point of LiH, and the program was executed for three time steps.

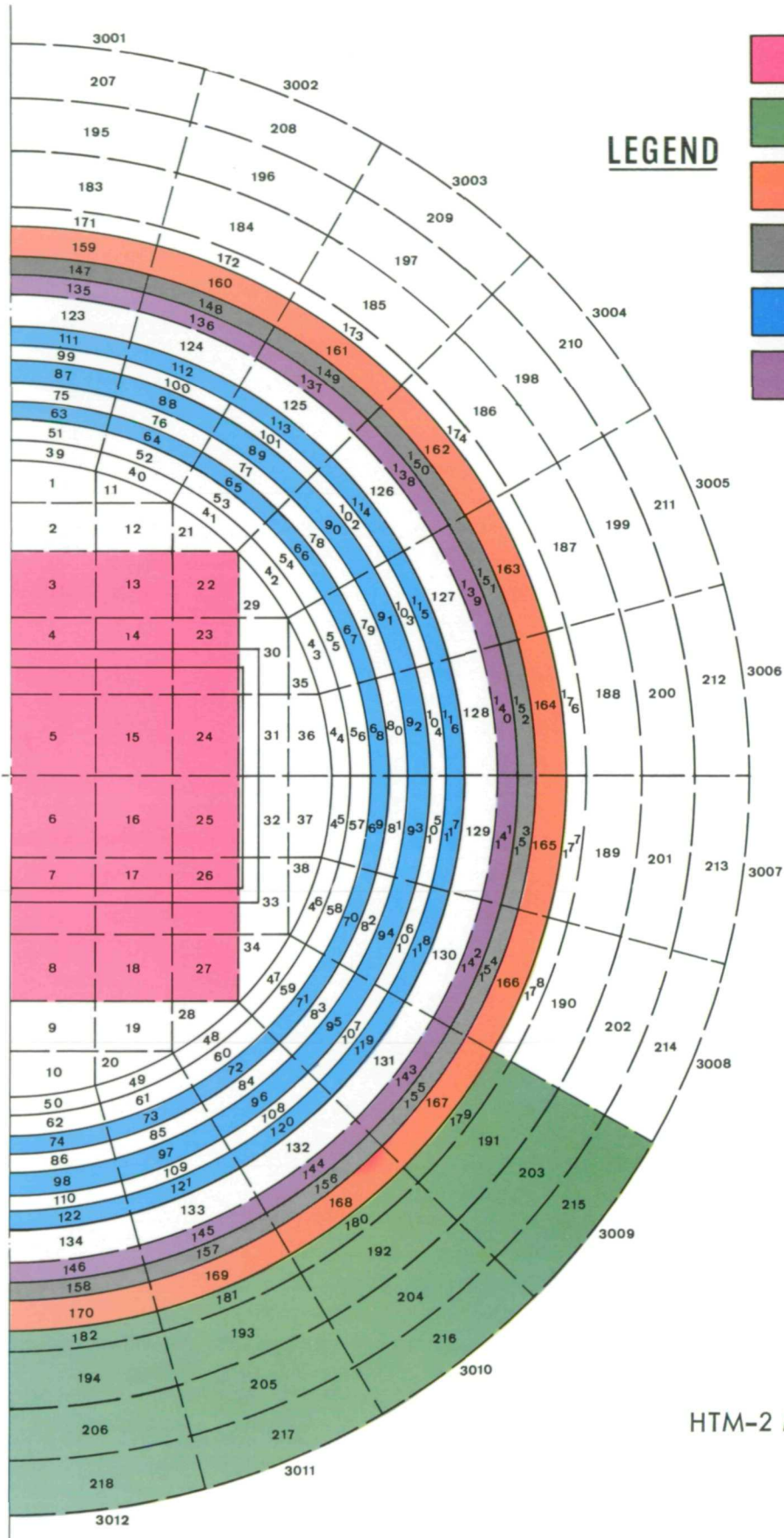
Table 3-7 summarizes pertinent results from this transient. Temperatures were initialized in the LiH (nodes 123-131) and UO_2 (nodes 135-143) at 5000°R (2778°K). The first time step was executed, and the temperatures in the LiH were corrected down to 4150°R (2306°K). The TPCAL subroutine was defined to correct temperatures (for heat of fusion) of materials above their melting at any time step if the fraction of melting has not been calculated to completion ($X_{\text{mel}}=1.0$). Since the fraction of melting is initialized at 0.0 for all components, this subroutine would correct the temperatures during the first time step for those nodes having temperatures over their melting point as if they had gone through their melting point.

For the next time step (from 60 to 120 seconds) the material in nodes 135 to 143 was changed from UO_2 to the high thermal conductivity material resulting in negligible temperature changes. The switching of materials was verified. This concluded the analysis of this problem since HTM-1 was designated as a checkout problem for verification of the simulation techniques.

3.3.2 HTM-2 Results

HTM-2 consisted of analyzing the undeformed model with the heavy metal-water shield with UO_2 wrapped inside the containment vessel. This case considered 33 percent burial without any heat pipes operating. The HTM-2 model was run for 20,000 seconds of operation under the influence of the afterheat power decay profile. Figure 3-2 shows the location of the core, shield layers, and soil in the nodal model for HTM-2.

Figure 3-3 is an axial profile of temperatures in the core, shield, and containment vessel. At about 300 seconds the core temperature response was flattened due to the melting of the 18,000 lbs (8172 Kgms) of core structure. Approximately 300 seconds were required



LEGEND

- CORE
- EARTH
- CONTAINMENT VESSEL
- HEAT PIPE
- TUNGSTEN
- UO₂

Figure 3-2.

HTM-2 Model Description

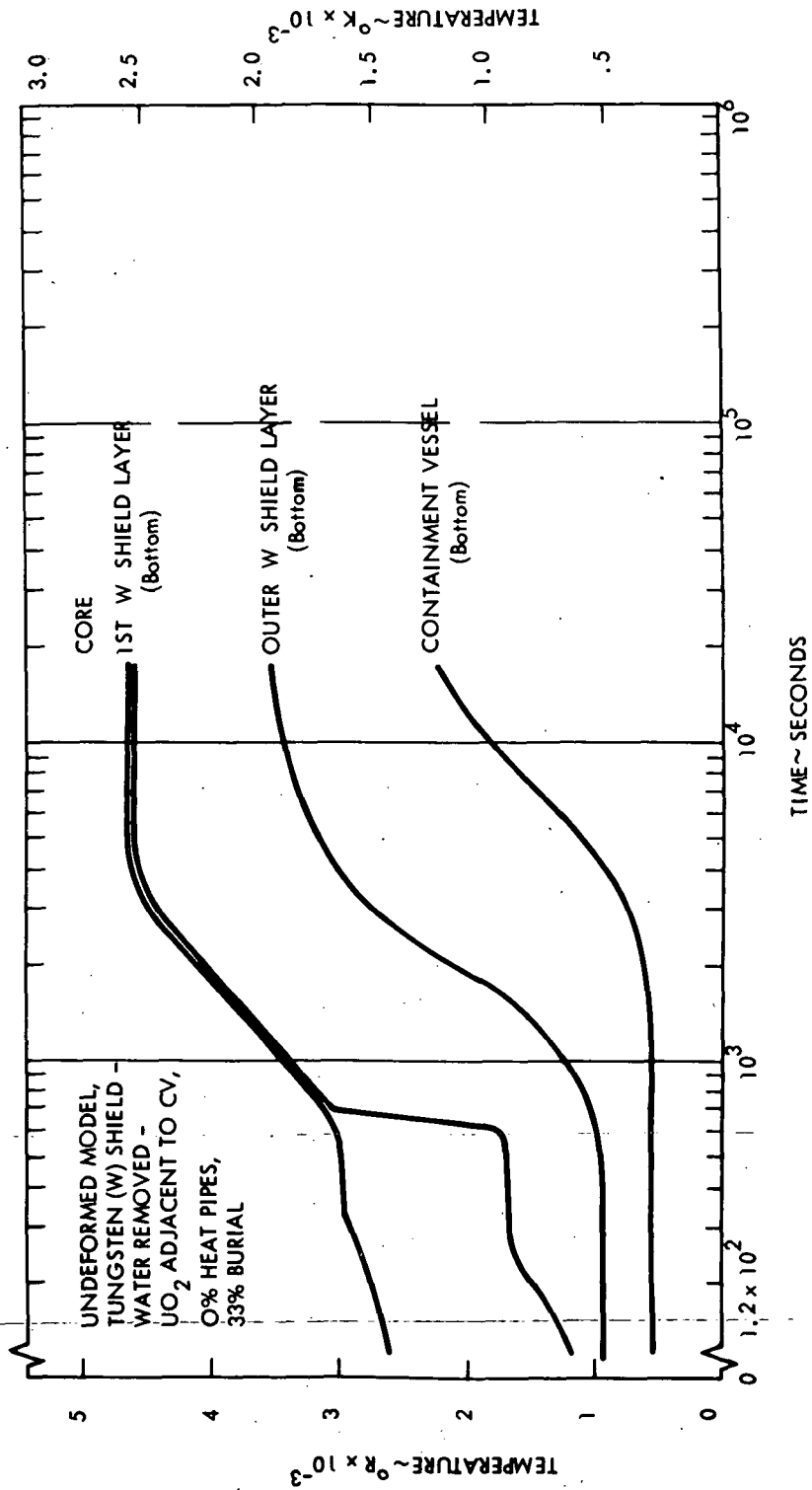


Figure 3-3. Temperature History for HTM-2

for the core structure to completely melt. This time period was checked by hand calculations based on an average core heat generation rate of 8 megawatts corresponding to this time period. The core capacitance was represented by the heat of fusion of the core structure smeared over a 50°F (27.8°K) interval plus contributions due to the capacitances of molybdenum and UO₂.

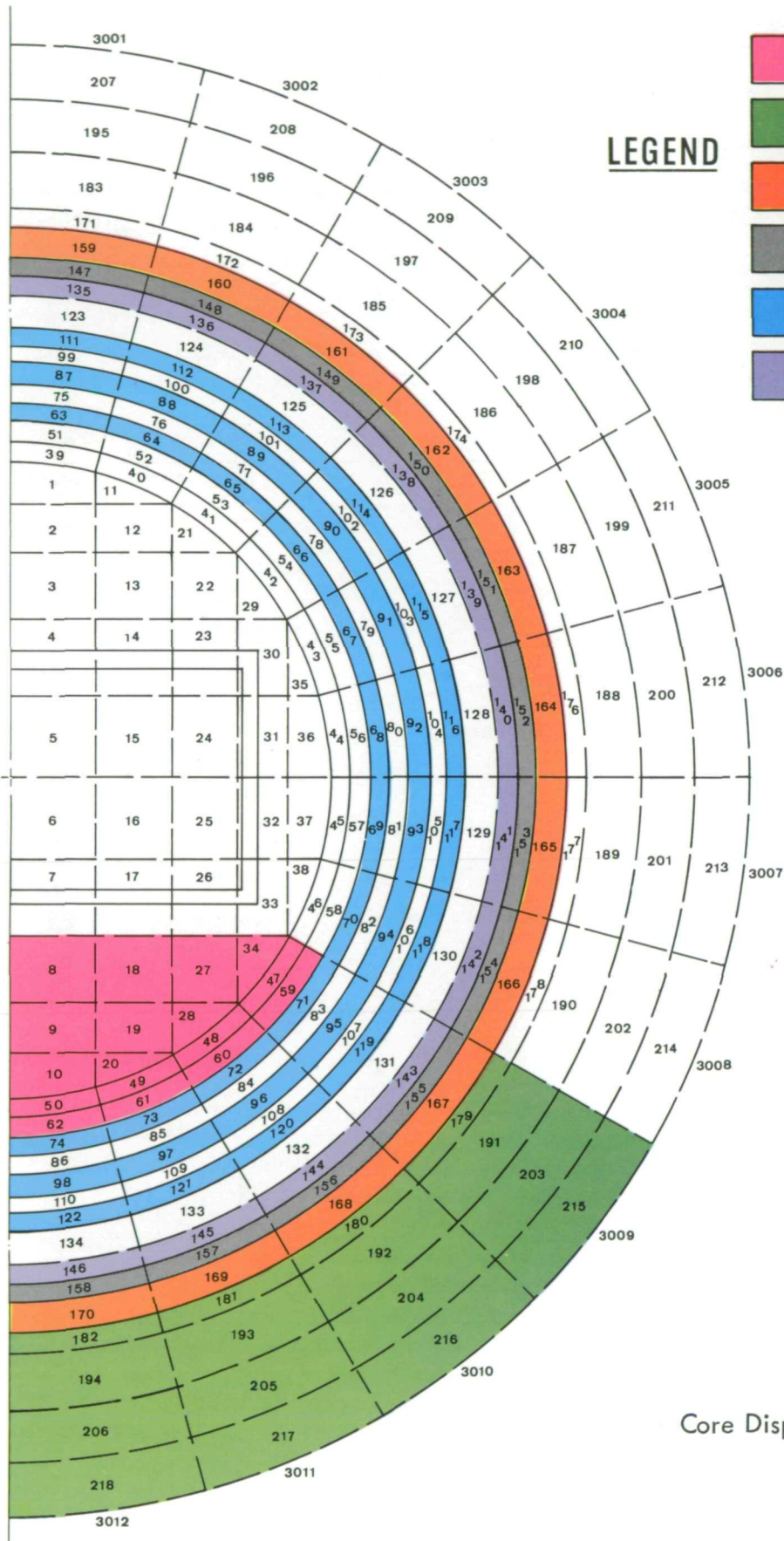
After completion of melting of the structure, the core dropped onto the first shield layer which for this shield configuration was nodes 63 to 74. Nodes 8-10, 18-20, 27, 28, 28-50, and 60-62 were representative of the core, as shown in Figure 3-4. The slope of the core temperature response before and subsequent to the structure melting was compared to hand calculated values using the expression:

$$\frac{dT}{d\tau} = \frac{Q_{\text{gen}}}{C_p V}$$

where Q_{gen} is the heat generation rate, C_p is the specific heat, V is the core volume, T is temperature and τ is time. This equation assumes negligible heat transfer from the core. Good agreement was obtained up to approximately 1400 seconds. Beyond this time heat transfer from the core is significant.

The first shield layer below the core represented by node 74, rapidly responded to contact with the core and subsequent to the time of contact followed the core response. The core and first shield layer reached a peak of 4600°R (2556°K), at about 5000 seconds and remained flat during the remainder of the transient. The third shield layer represented by node 122 responded more slowly due to the radiation gaps separating the shield nodes and due to the capacitance of the first shield layer. This layer was still increasing in temperature at 18,000 seconds and had achieved a temperature of 3500°R (1944°K).

The bottom of the containment vessel represented by node 170 did not receive any appreciable amount of heat until about 2500 seconds after which it started to heat



LEGEND




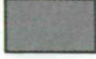


-  CORE
-  EARTH
-  CONTAINMENT VESSEL
-  HEAT PIPE
-  TUNGSTEN
-  UO₂

Figure 3-4.

Core Displacement for HTM-2

significantly. After 18,000 seconds it had reached 2200°R (1222°K) and was still rising significantly. At 18,000 seconds the top of the containment vessel had reached 1300°R (722°K). At 18,000 seconds the internal pressure had increased from 350 psi (241 N/cm^2) to 1200 psi (827 N/cm^2) and the stress level was 35,000 psi ($24,100\text{ N/cm}^2$). The rupture point of the containment vessel was calculated to be 12,000 seconds. At this point the pressure was 1150 psi (793 N/cm^2) and the peak containment vessel temperature was 1950°R (1083°K).

Figure 3-5 shows the temperature profile circumferentially around the containment vessel at different periods during the transient. The temperature profile along the vessel is flat but at two levels with essentially a step change between the two levels. The smaller temperature level corresponds to the section of the containment vessel that is adjacent to air and the greater temperature level corresponds to the vessel section adjacent to the soil indicative of the greater thermal impedance of the soil. The steep temperature drop circumferentially in the vessel at the soil to air interface is indicative that the vessel thermal resistance circumferential is sufficiently large such that very little heat is redistributed circumferentially in the vessel particularly during the response period when most of the heat is being absorbed by the vessel. For example at 13,700 seconds, node 167 (Figure 3-4) a containment vessel node adjacent to the soil just below the soil-to-air interface is receiving 46 Btu/sec (49 kwatts) from fission product generation plus 35 Btu/sec (37 kwatts) by conduction radially from the insulation. Of this total, 7 Btu/sec (7 kwatts) are conducted radially to the soil, 75 Btu/sec (79 kwatts) are absorbed, and 4 Btu/sec are conducted circumferentially to node 166 which is adjacent to air.

Figure 3-6 shows the location of the four groups of fission products during the transient without regard to the percent on each layer. For example at 500 seconds, Group A is deposited in the core and on the second W shield layer. Groups B, C and D are deposited in the core and on the first shield layer. The Group A fission products were completely escaped from the core after 2500 seconds and had walked through the shield layers to be completely

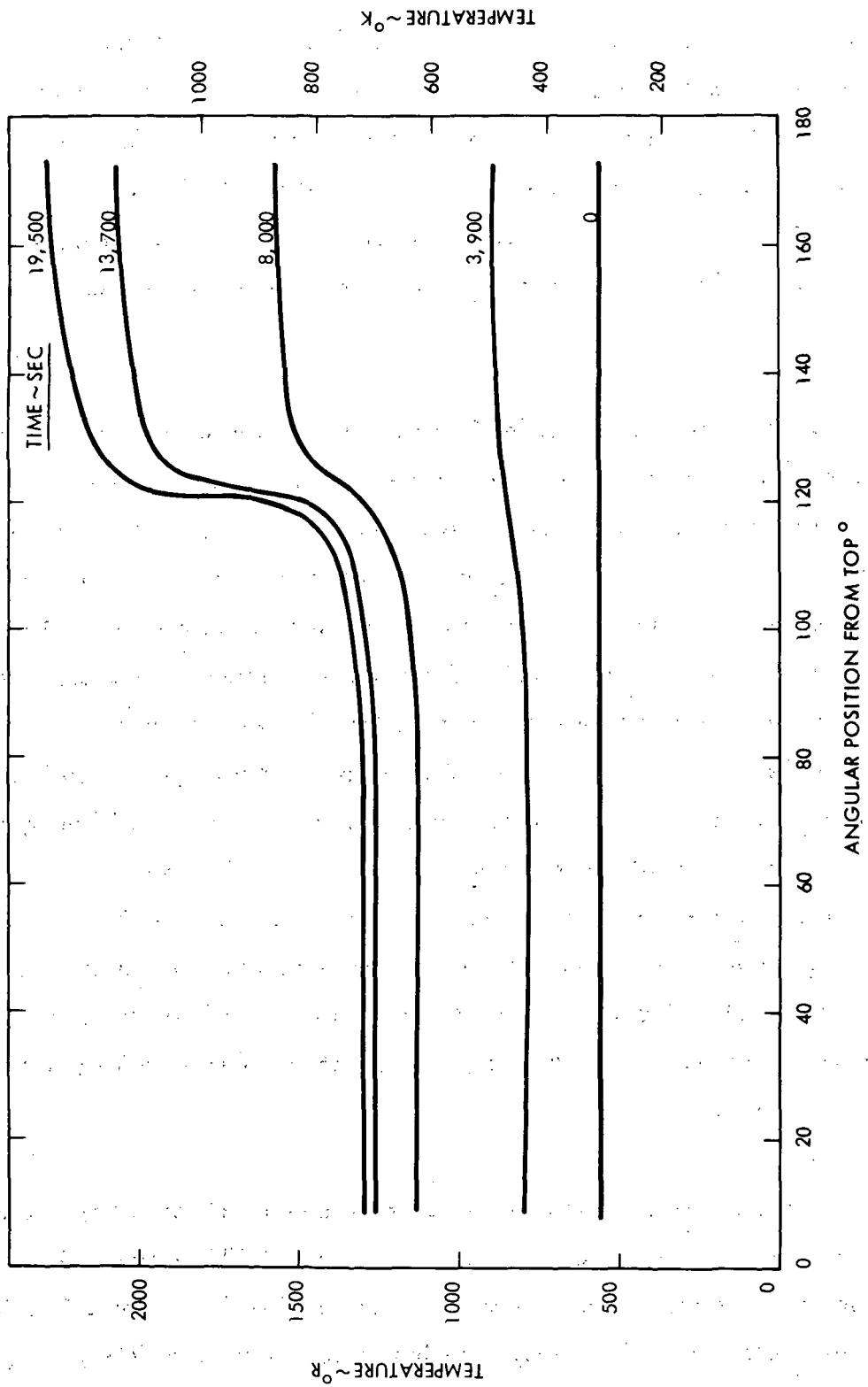
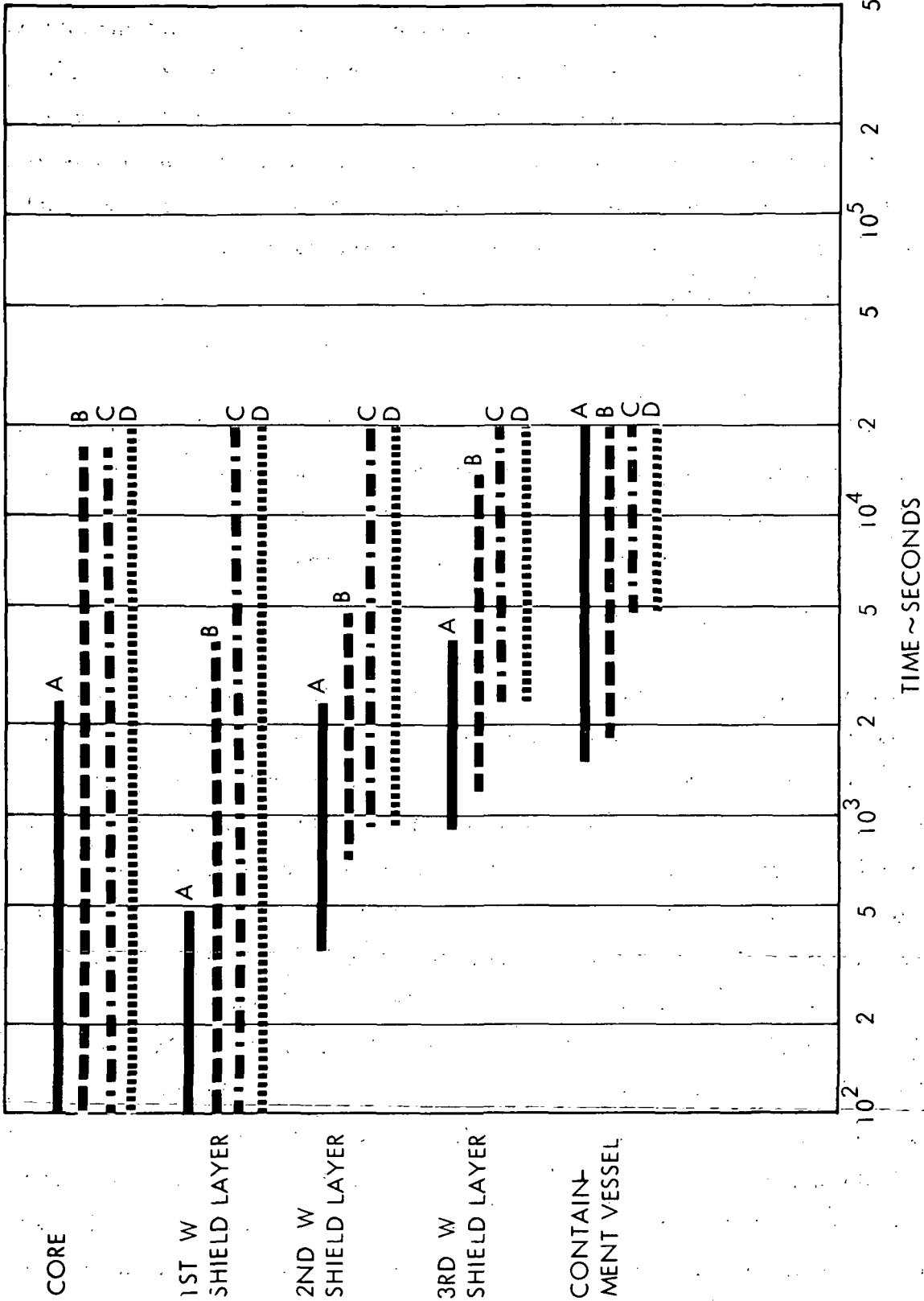


Figure 3-5. Containment Vessel Circumferential Temperature Profile for HTM-2



613623-188

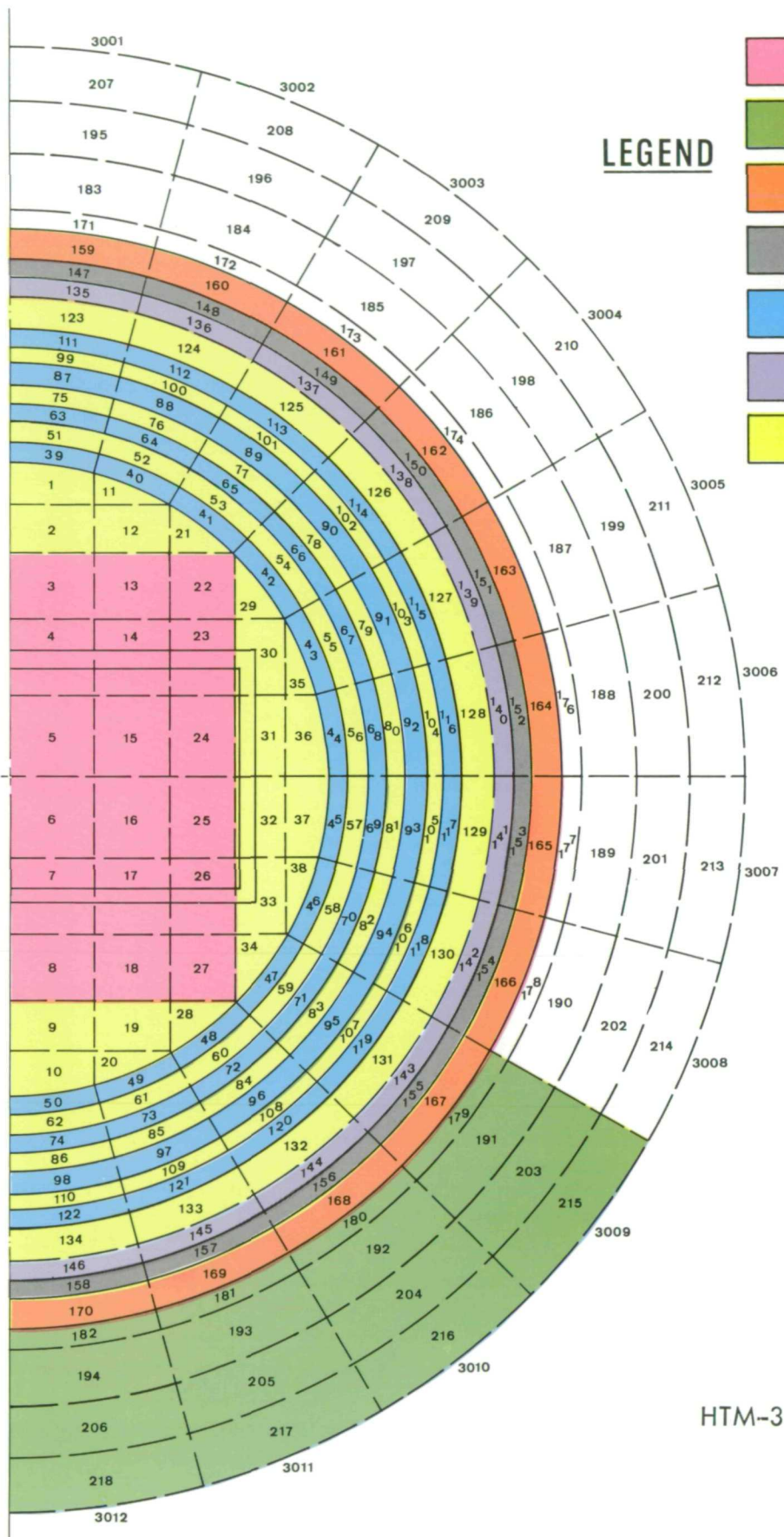
Figure 3-6. Fission Product Redistribution for HTM-2

deposited on the containment vessel after 4000 seconds. Groups B and C were not completely driven from the core until after 18,000 seconds. Group B first reached the containment vessel at about 2000 sec and was being entirely deposited on the containment vessel after 14000 seconds, however. Group C and D were deposited on portions of all the shield layers and the containment vessel. At the end of the 20,000 seconds, all of Groups A and B were deposited on the containment vessel. Ninety-two percent of Group C was on the first layer with only a trace reaching the containment vessel. Seventy-five percent of Group D had left the core of which 70 percent was deposited on the first shield layer.

3.3.3 HTM-3 Results

The HTM-3 model consisted of the undeformed model with the W/Li/ UO_2 shielding combination. This case was run without heat pipes and with 33 percent soil burial. Figure 3-7 illustrates the nodal material representation. HTM-3 was run for 110,000 seconds of operation under the influence of the afterheat power decay profile. The time increment varied from 60 seconds initially to 7680 seconds at the end of the transient.

Figure 3-8 is an axial profile of temperatures in the core, shield, and containment vessel. The initial response of the core for this model is very similar to that of the HTM-2 model. The time to reach and melt the core structure was essentially the same which indicated that (excluding fission product escape) very little heat is transported to the LiH shield during the initial time period. During the subsequent time period, the core peaked at 4800°R (2667°K) at approximately 5000 seconds which was 300°R (167°K) higher than HTM-2. In the 5000 to 20,000 second time period the core cooled down to 3800°R (2111°K) as its heat was absorbed by the relatively cold LiH adjacent to it. During this period the core started to displace LiH. At 14,000 sec a layer of LiH nodes was displaced by the core in the model as shown in Figure 3-9. At 24,000 seconds the core dropped onto the first W shield layer and displaced all the LiH as shown in Figure 3-10. This resulted in the steep temperature response of the first shield layer as shown in Figure 3-8. Subsequent to this the core and first shield layer rose to 4200°R (2333°K) and was flat for the remainder of the transient. The increase in core temperature during this period was a result of a reduction in core surface area when it is on the shield surface; also, the LiH adjacent to the core has become molten and is rising in temperature.



LEGEND


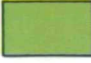





-  CORE
-  EARTH
-  CONTAINMENT VESSEL
-  HEAT PIPE
-  TUNGSTEN
-  UO₂
-  LIH

Figure 3-7.

HTM-3 Model Description

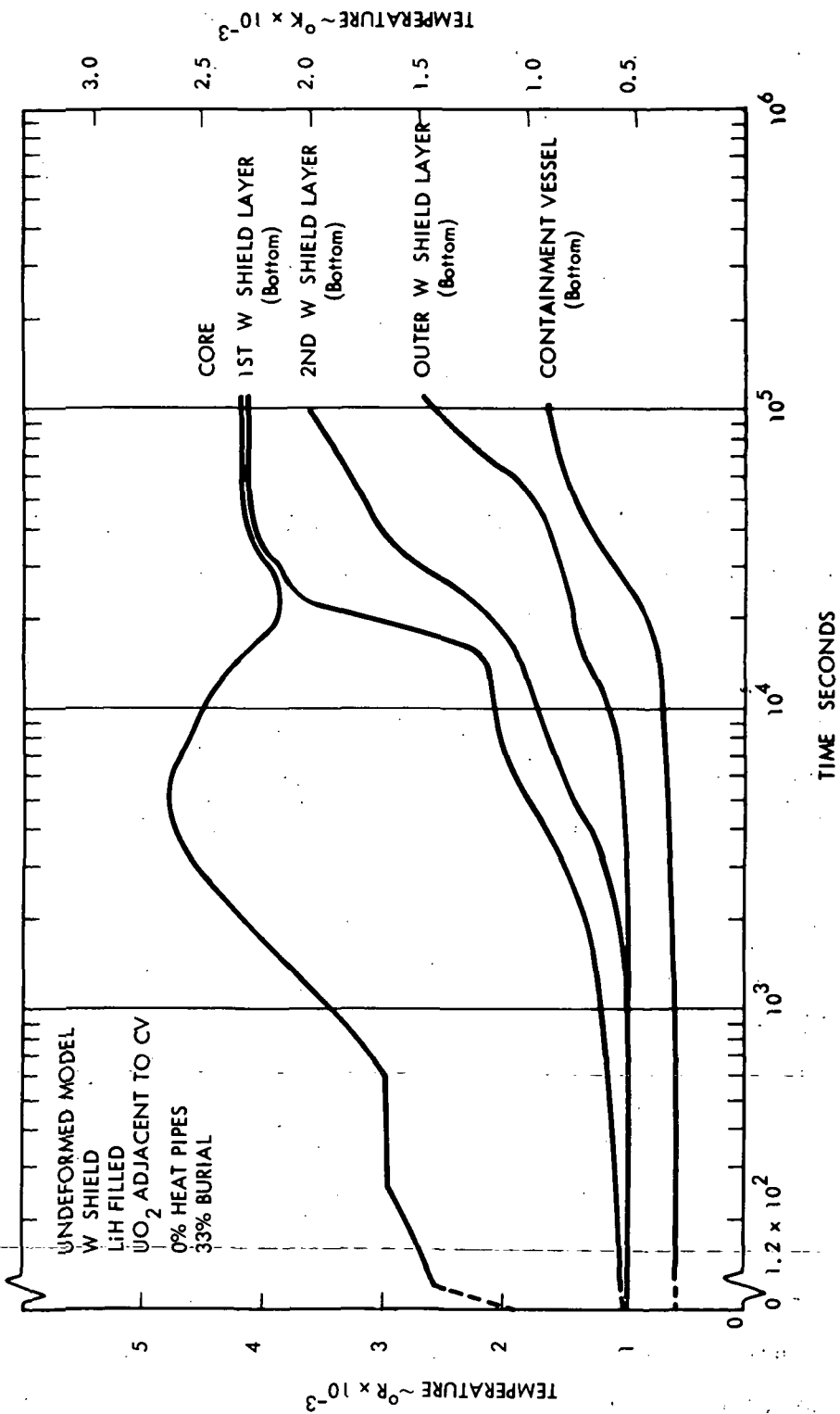


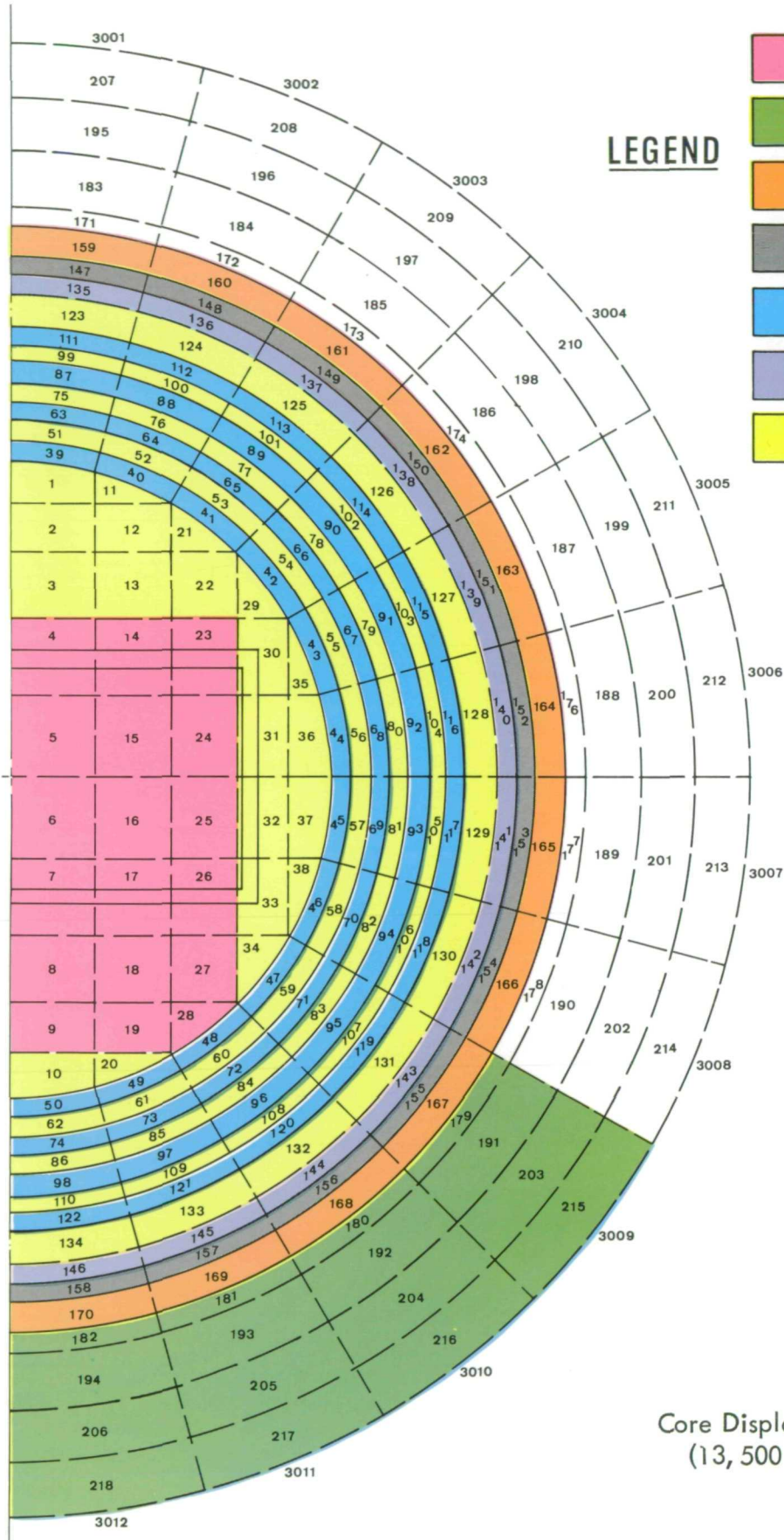
Figure 3-8. Temperature History for HTM-3

in temperature. The response of the second and outer W shield layers are also shown in Figure 3-8. The response of the shield layers are marked by several changes in slope. The initial rise in the shield layers in the 2000-15,000 second range is caused by fission product deposition as indicated in Figure 3-11, which shows the walk out of fission products versus time. In the vicinity of 1700 °R (944 °K) the upward response of the shield layers are slowed due to the melting of LiH adjacent to them. After LiH adjacent to the shield layers is molten, the shield layers responded to the drop of the core onto the first shield layers plus the continued deposition of fission products on these layers. During this period, LiH between the first and second layers increase in temperature to levels beyond its dissociation temperature. Dissociation of LiH was not considered.

The bottom of the containment vessel does not begin to rise significantly until the 20,000 second period when the Group A fission products reach the containment vessel. At 100,000 seconds the containment vessel reached 1600°R (889°K) and was still rising.

As shown in Figure 3-11, only Groups A and B reached the containment vessel in 100,000 seconds for HTM-3. Groups C and D had just started to condense on the fourth shield layer at about 100,000 seconds. This slower walk out of fission products in HTM-3 is directly attributed to the presence of LiH delaying the response of the shield layers and containment vessel. After 110,000 seconds all of Group A and 84 percent of Group B were deposited on the containment vessel. The remainder of Group B had not left the core. Group C was deposited on all four shield layers with a percent breakdown from the 1st to 4th layers of 7 percent, 27 percent, 40 percent and 12 percent respectively. The remaining 14 percent had not left the core. The breakdown for Group D was 5 percent, 19 percent, 27 percent, and 8 percent for the four layers with 41 percent of Group D still in the core region.

Figure 3-12 shows the circumferential temperature profile of the containment vessel at various points in time. Similar to HTM 2, a step change in the circumferential temperature profile of the containment vessel occurs at the soil/air interface. The presence of LiH adjacent to the containment vessel did not significantly alter the temperature profile.



LEGEND



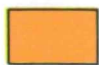




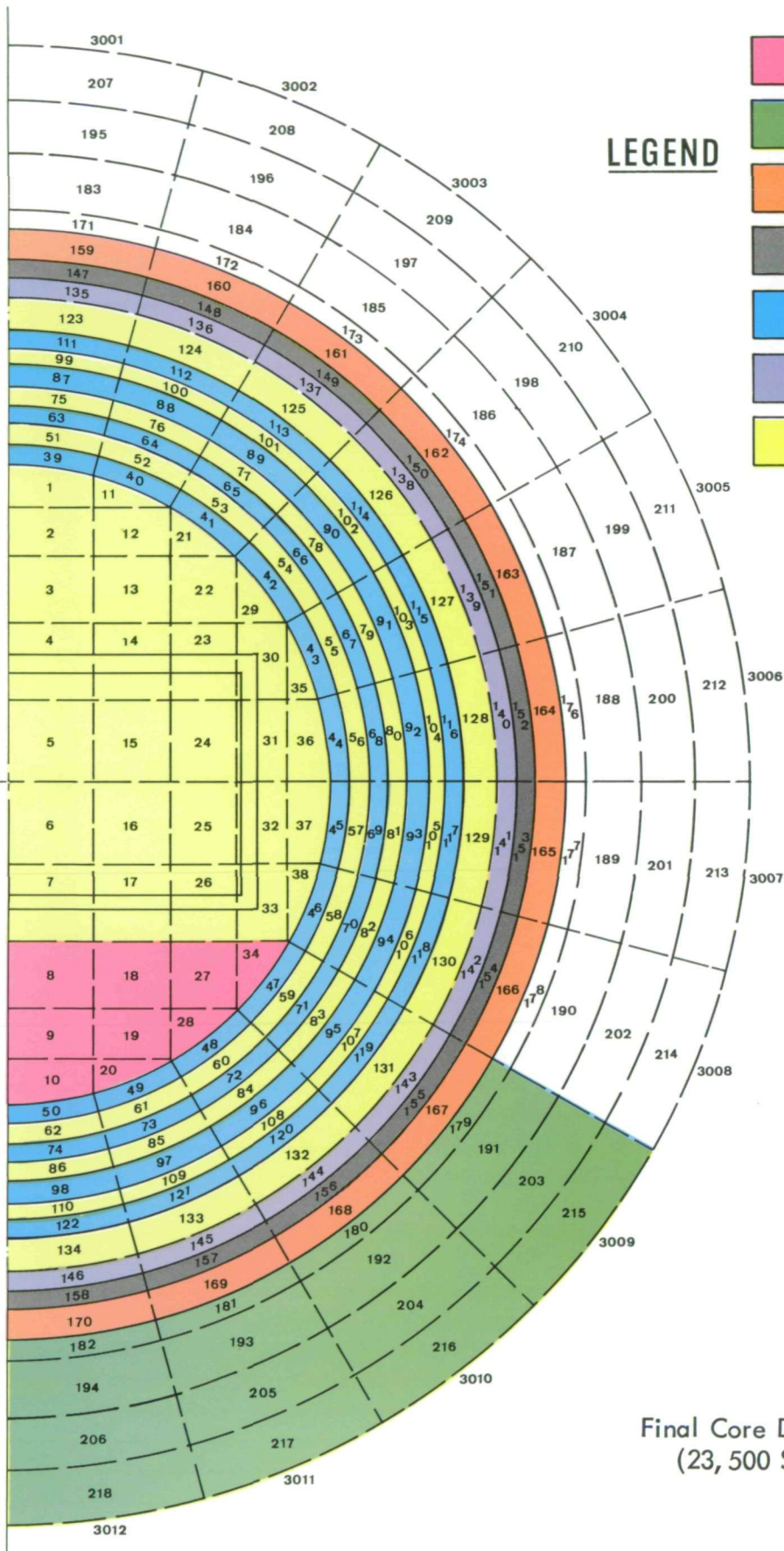
-  CORE
-  EARTH
-  CONTAINMENT VESSEL
-  HEAT PIPE
-  TUNGSTEN
-  UO₂
-  LiH

Figure 3-9.

Core Displacement for HTM-3
(13,500 Sec - 23,500 Sec)



LEGEND






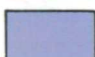
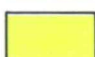
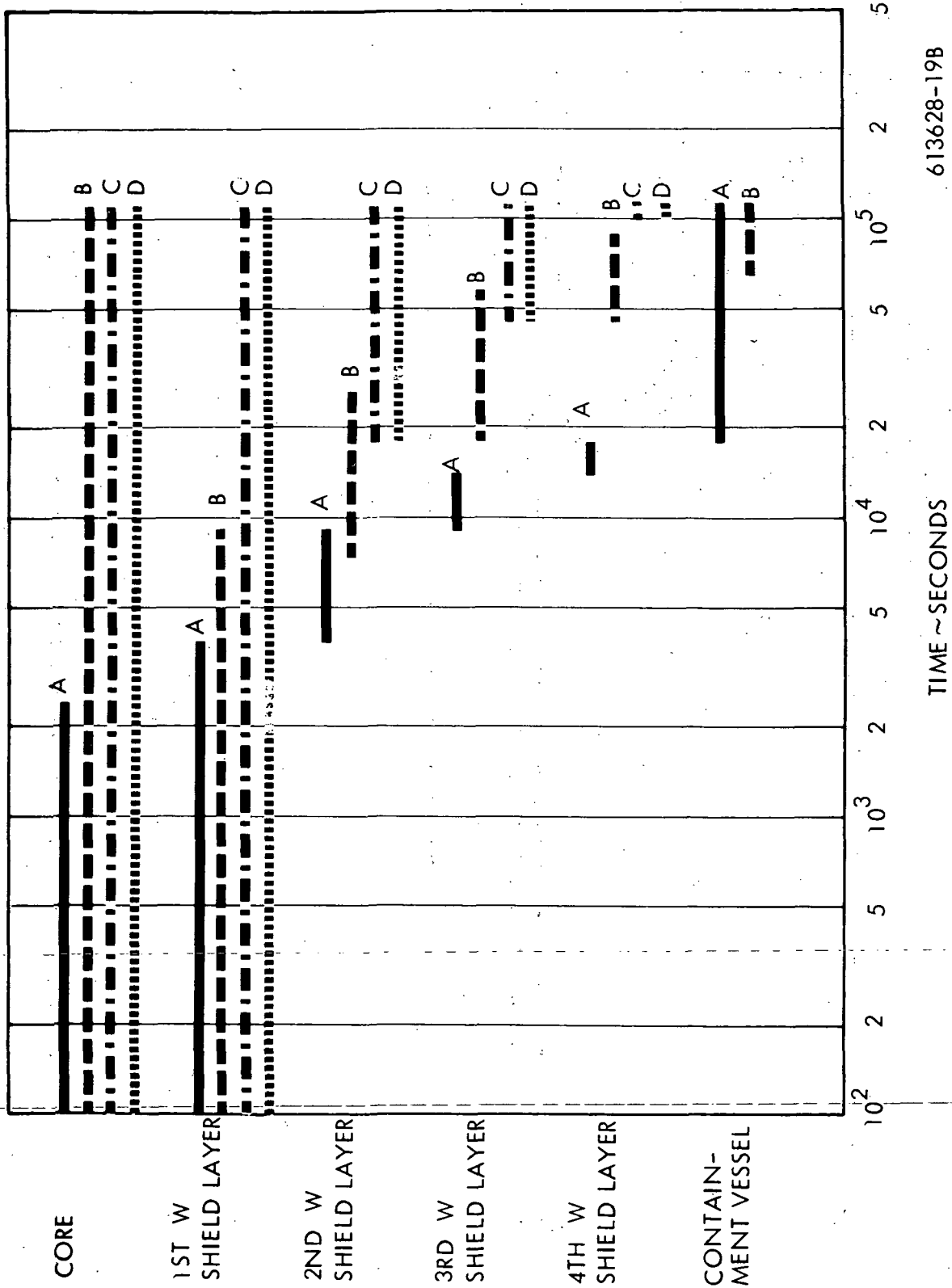
-  CORE
-  EARTH
-  CONTAINMENT VESSEL
-  HEAT PIPE
-  TUNGSTEN
-  UO₂
-  LiH

Figure 3-10.

Final Core Displacement for HTM-3
(23, 500 Sec - 110, 000 Sec)



613628-19B

Figure 3-11. Fission Product Redistribution for HTM-3

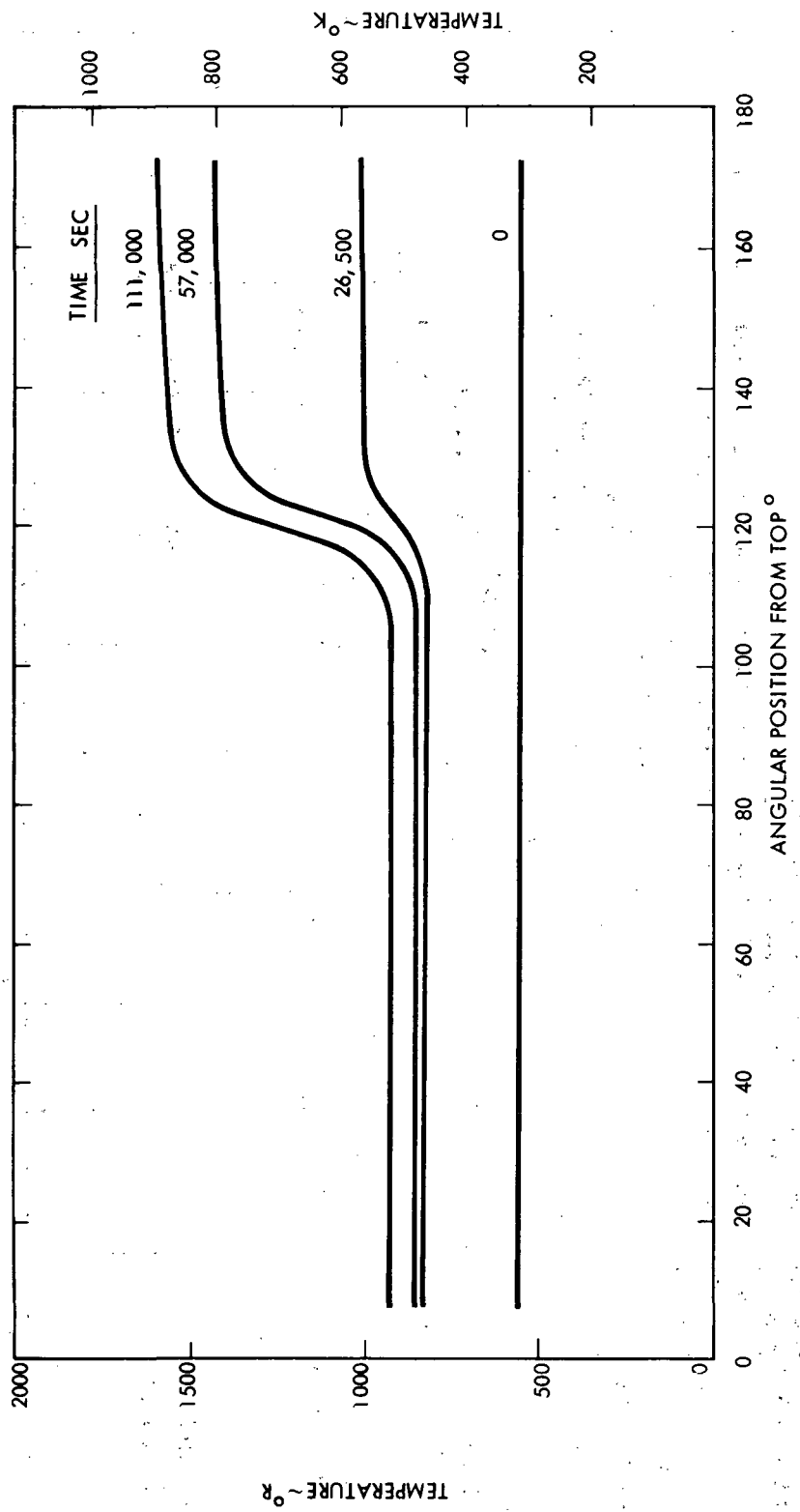


Figure 3-12. Containment Circumferential Vessel Temperature Profile for HTM-3

For HTM-3 the internal pressure level was 1880 psi (1296 N/cm^2) at 110,000 seconds with a stress level of 51,400 psi ($35,440 \text{ N/cm}^2$). Rupture for the containment vessel occurred at 95,000 seconds. The pressure and stress levels was 1420 psi (979 N/cm^2) and 42,000 psi ($28,960 \text{ N/cm}^2$), respectively. The maximum containment vessel temperature was 1650°R (917°K) at this point.

3.3.4 HTM-4 Results

The HTM-4 model consisted of the deformed model with a LiH/ UO_2 /W shield configuration. This case was run without heat pipes and with 33 percent soil burial. Figure 3-13 is a sketch of this model showing the material representation for this HTM. This model was run for 115,000 seconds of operation under the influence of the afterheat power decay profile.

Figure 3-14 is an axial profile of temperatures in the core, shield, and containment vessel for HTM-4. The core structure started to melt at 350 seconds and required approximately 600 seconds to completely melt which was considerably slower than the HTM-2 and HTM-3 cases. This is attributed to thermal shunting of an appreciable amount of heat through the LiH to the shield layers in the deformed base. The core, in fact, displaced molten LiH below it and dropped onto the first shield layer before the core structure was entirely molten as indicated in Figure 3-14 by the rapid increase of the 1st W shield layer temperature. In the period subsequent to the core structure melting, the core and the portion of the first layer just below the core rose gradually and leveled off at 4200°R (2333°K). The core and first layer displaced the LiH between the first and second layers at about 3000 seconds resulting in the second shield layer rising to the temperature level of the core and 1st layer. After 14,000 seconds the LiH between the shield layers at the bottom had been displaced and all the shield temperatures had risen to the core temperature. After 24,000 seconds the final layer of LiH between the outer shield layer and the containment vessel had been displaced.

Figure 3-15 shows the location of the core and shield at this point. The containment vessel in the base started to heat significantly at about 5000 seconds and rose to 4000°R (2222°K) after all the LiH had been displaced. The driving force for the rise of the layers and vessel

in the base was the inability of the soil below the vessel to dissipate the heat that could be conducted from the core through the shield to the soil. Figure 3-16 shows the temperature profile around the containment vessel starting from the top (Node 130 in Figure 3-13). As indicated by this figure the containment vessel around the top and side did not rise in temperature nearly as significantly as the well insulated base.

Figure 3-17 shows the redistribution of the fission products for HTM-4. Group A had completely left the core after 8000 seconds and was completely deposited on the containment vessel after 30,000 seconds. Group B fission products that were released from the core were being deposited only on the containment vessel after 80,000 seconds. After 105,000 seconds all of Groups C and D that had left the core were deposited on the containment vessel. At 115,000 seconds 90 percent of Group B, 89 percent of Group C, and 63 percent of Group D were on the containment vessel.

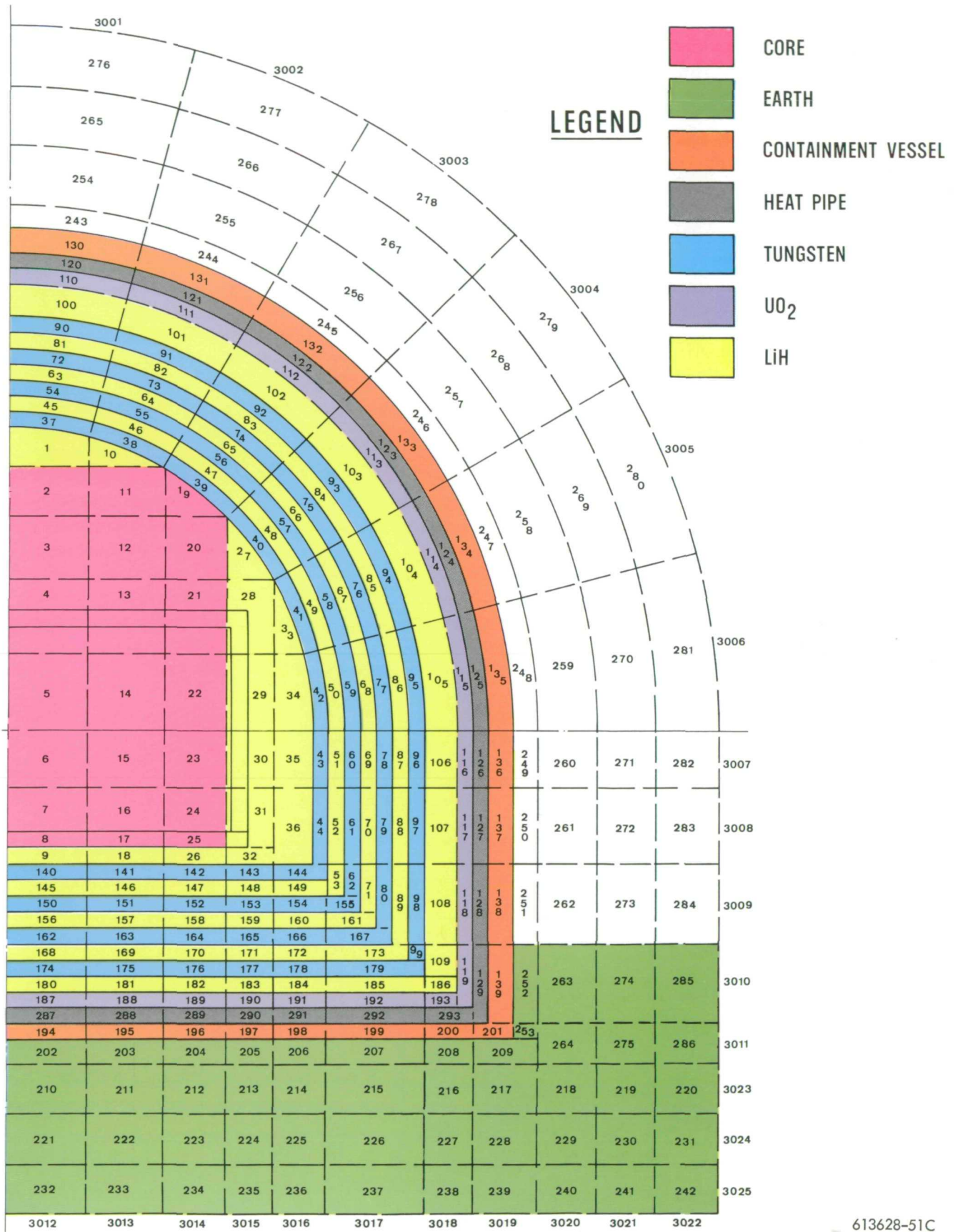
At the end of the 115,000 seconds, the internal pressure was 1810 psi (1275 N/cm^2) and the stress level was 53,500 psi ($36,888 \text{ N/cm}^2$). Containment vessel rupture occurred at 10,700 seconds. At this point the internal pressure was 1290 psi (889 N/cm^2) and the maximum containment vessel temperature was 1850°R (1028°K).

3.3.5 HTM-5 Results

The HTM-5 model consisted of the undeformed model with a W/ UO_2 /LiH shield configuration. This case was run without heat pipes and with 50 percent soil burial. Figure 3-18 is a sketch of this model showing the material representation for this HTM. This case differed from HTM-3 only in the percent burial. HTM-5 was run for 120,000 seconds of operation under the influence of the afterheat power decay profile.

Figure 3-19 is an axial profile of the temperature in the core, shield, and containment vessel for HTM-5. The characteristics of this transient were the same as those observed for HTM-3 without any noticeable difference in the peak containment vessel temperature even at the end of the transient period analyzed. The fission product redistribution shown in Figure 3-20 also differed only slightly with that obtained from the HTM-3 case. The containment vessel circumferential temperature profile presented in Figure 3-21 did reflect the difference in

Figure 3-13. HTM-4 Model Description



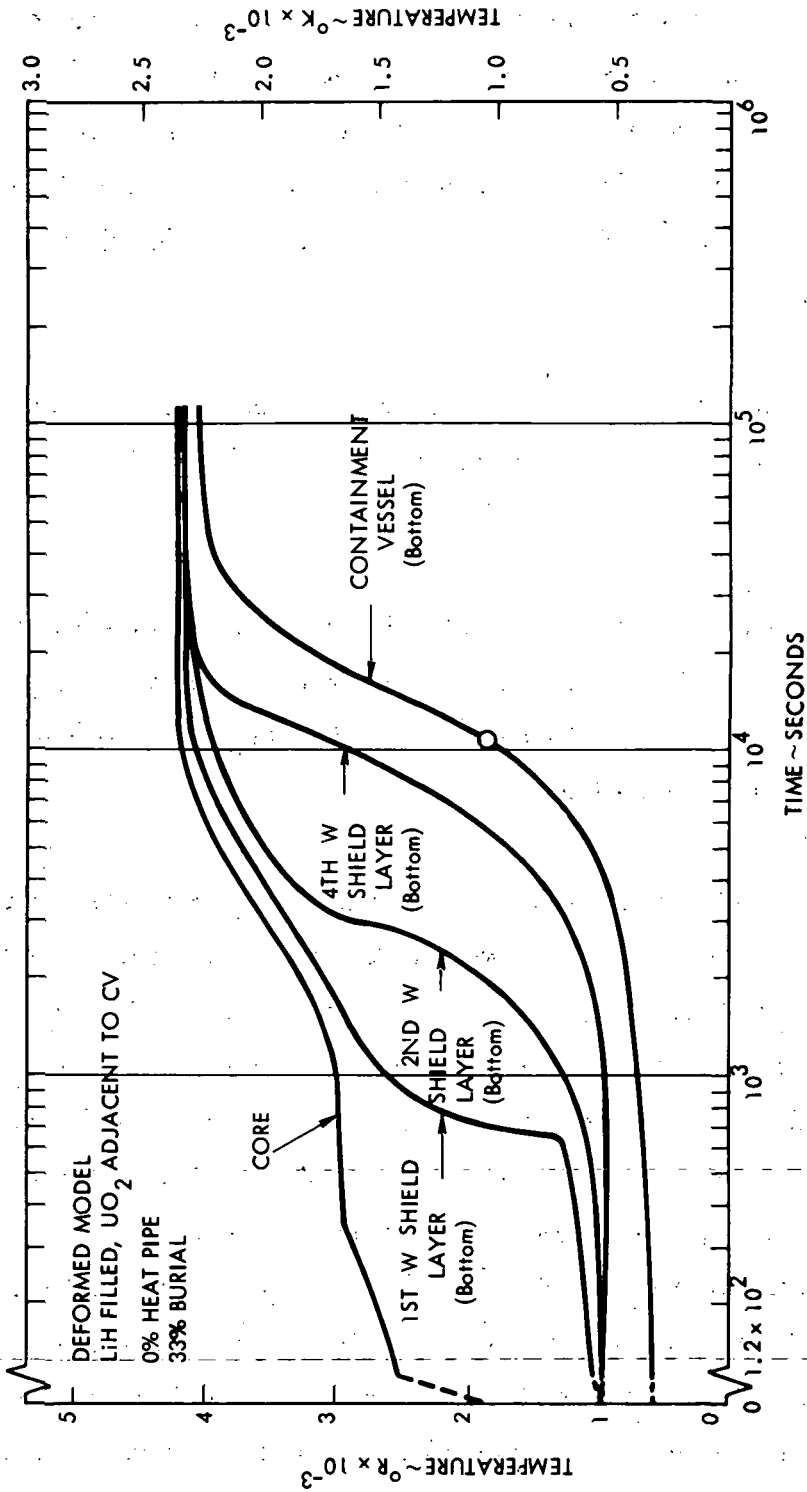


Figure 3-14. Temperature History for HTM-4

burial depth in terms of the transition point from the high temperature level adjacent to the soil to the lower temperature level for that part of the vessel exposed to the air. Because a smaller fraction of the vessel was exposed, the vessel temperature level in the exposed region was 1000°R (555°K) at 120,000 seconds for HTM-5 as compared to a 930°R (517°K) temperature level at 111,000 seconds for HTM-3 as shown in Figure 3-12. The peak temperature was 1650°R (917°K) for HTM-5 versus 1630°R (905°K) for HTM-3, only a minor difference.

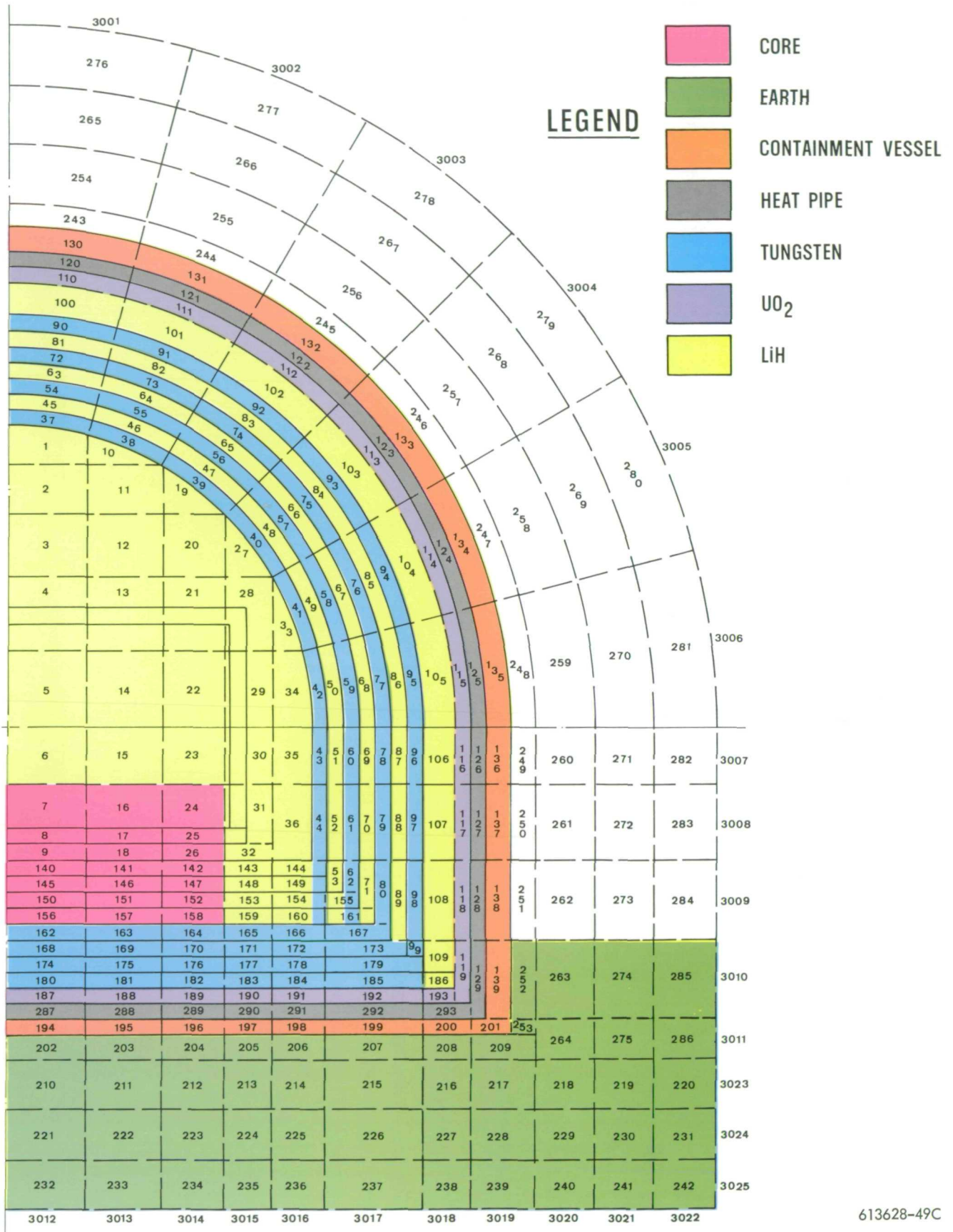
The rupture point for HTM-5 was 89,000 seconds. The pressure level was 1420 psi (979 N/cm^2) and the maximum containment vessel temperature was 1650°R (917°K).

3.3.6 HTM-6 Results

The HTM-6 model was the in-pile test model (Figure 2-5). This test model consists of enriched UO_2 fuel pins clad in molybdenum surrounded by depleted UO_2 contained in a 5-inch diameter Inconel sphere. It will be tested in the Plum Brook Reactor Facility to simulate a reactor core melt-down condition.

A case was run with initially a 4 K watt power prior to the release of enriched HO_2 into the depleted UO_2 shield zones. The 4 K watts represent the mean power level with all heat sources located in the core. As the fuel melts, redistribution is initiated. The method of heat source redistribution consists of energy leaving the core as the enriched UO_2 melts (5500°R (3056°K)) and is deposited on colder UO_2 zones in the shield (less than 4500°R (2500°K)). In the model, the heat sources are deposited on the intermost layers below 4500°R (2500°K). As node temperatures in a layer increase and exceed 4500°R (2500°K), the heat sources are transported to the next layer. In this manner heat sources move radially outward layer by layer. The heat generation for a heat source is increased radially outward due to the reduced shielding of the UO_2 as the distance to the surface becomes smaller. An escape temperature, condensation temperature, and a radial power factor array are defined in FISSION to characterize this heat source distribution.

Figure 3-15. Core and Shield Displacement for HTM-4
(23,700 Sec - 115,000 Sec)



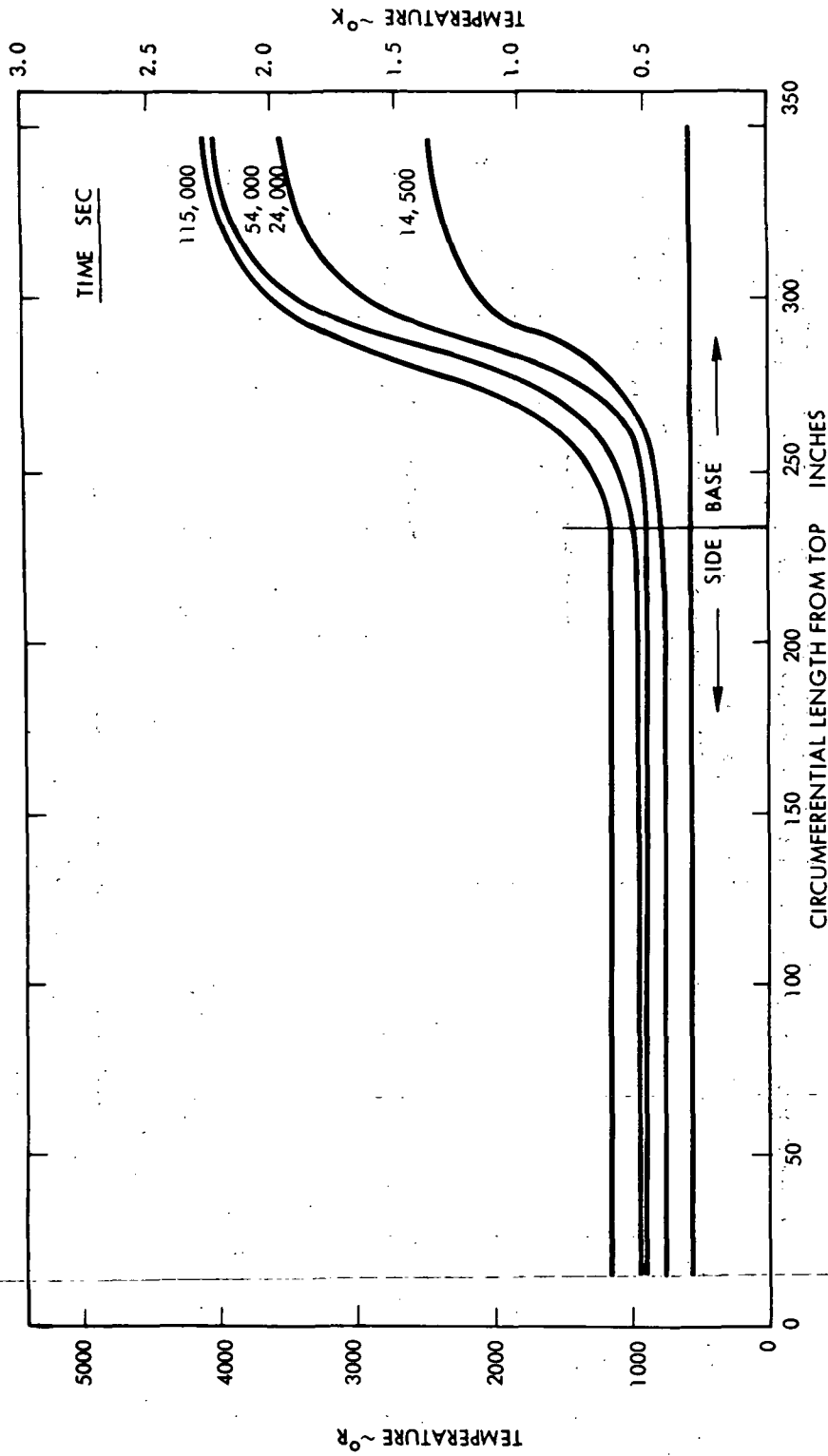


Figure 3-16. Containment Vessel Circumferential Temperature Profile for HTM-4

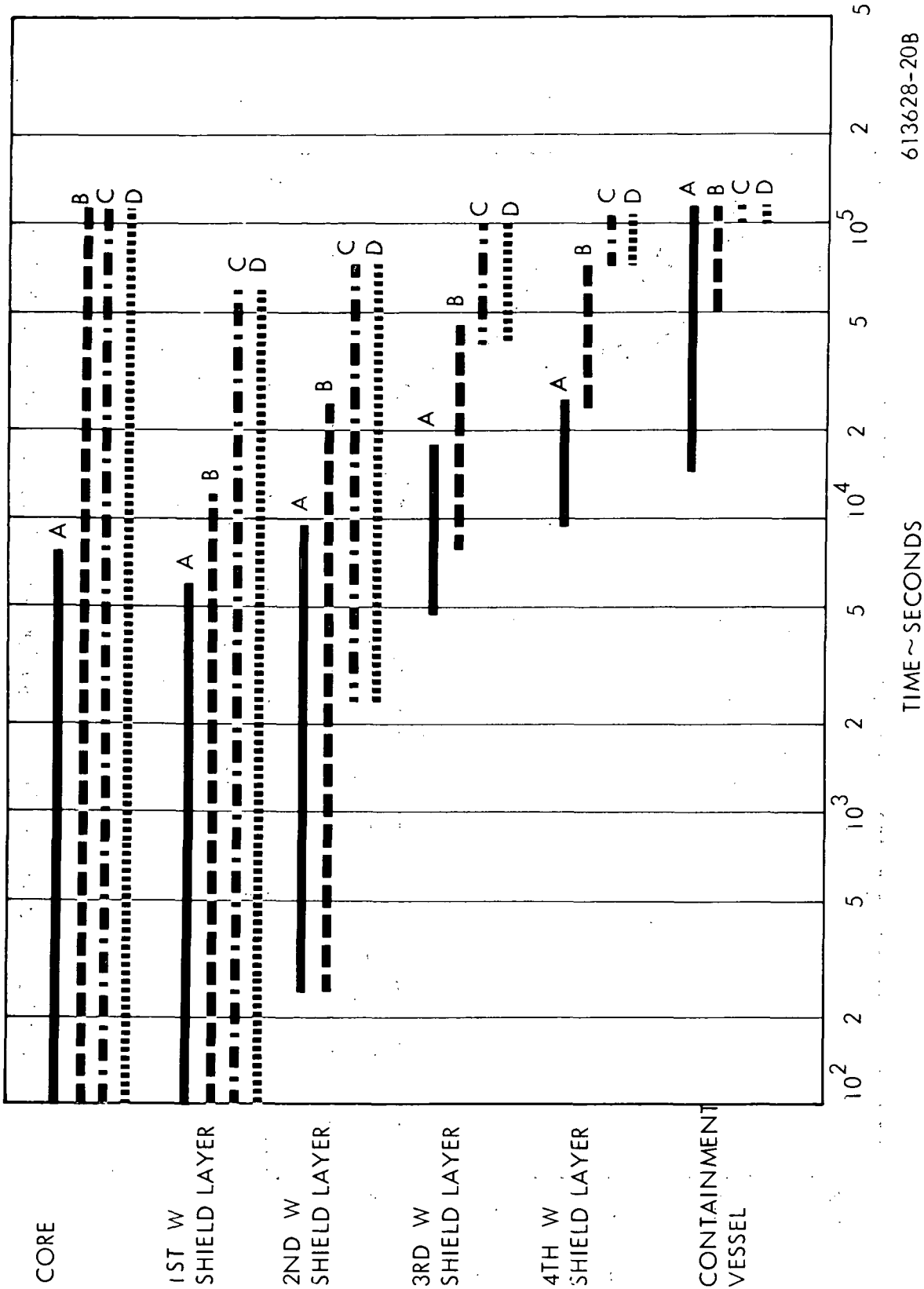
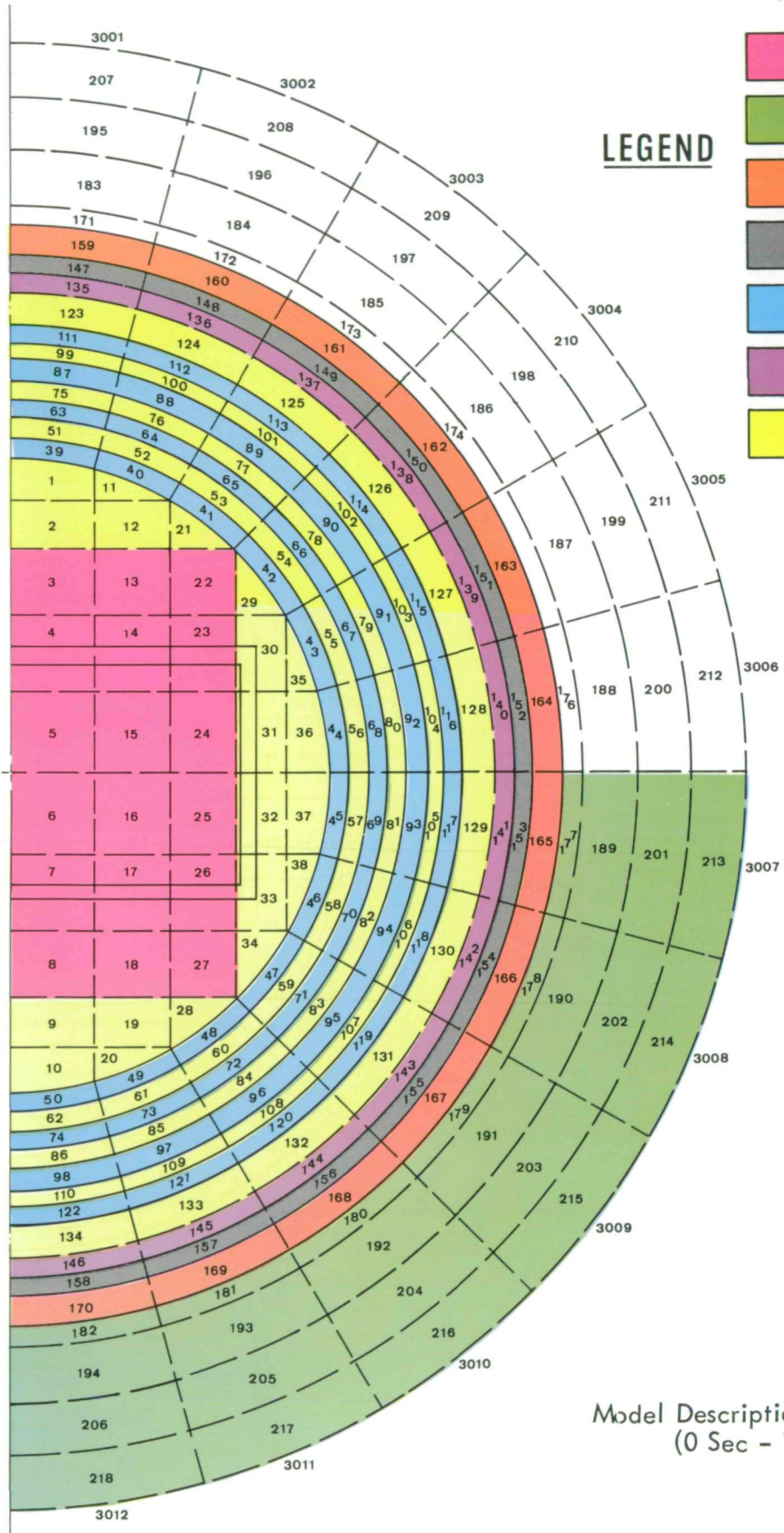


Figure 3-17. Fission Product Redistribution for HTM-4

613628-20B

TIME ~ SECONDS



LEGEND

- CORE
- EARTH
- CONTAINMENT VESSEL
- HEAT PIPE
- TUNGSTEN
- UO₂
- LIH

Figure 3-18.

Model Description for HTM-5 and HTM-7
(0 Sec - 13,500 Sec)

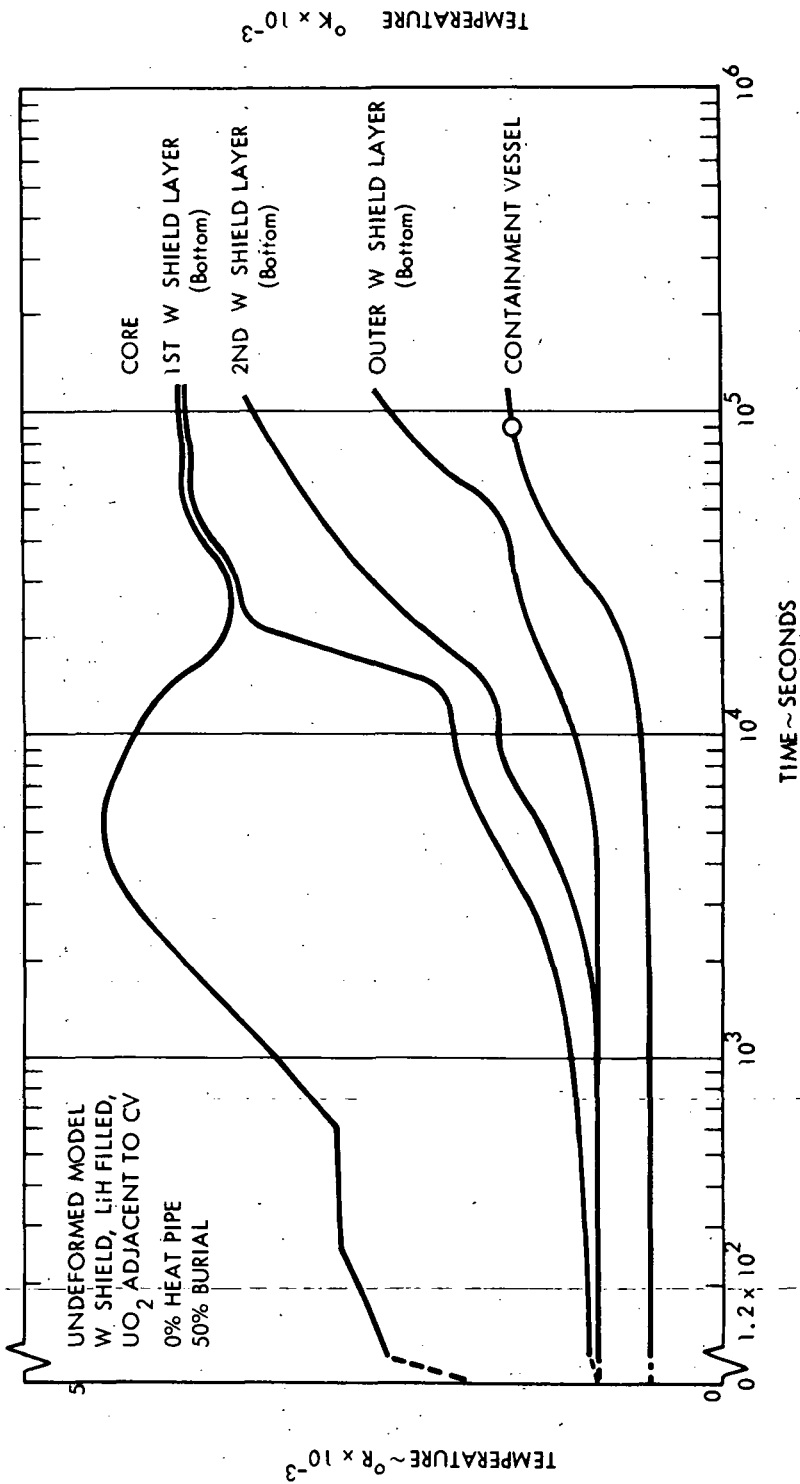


Figure 3-19. Temperature History for HTM-5

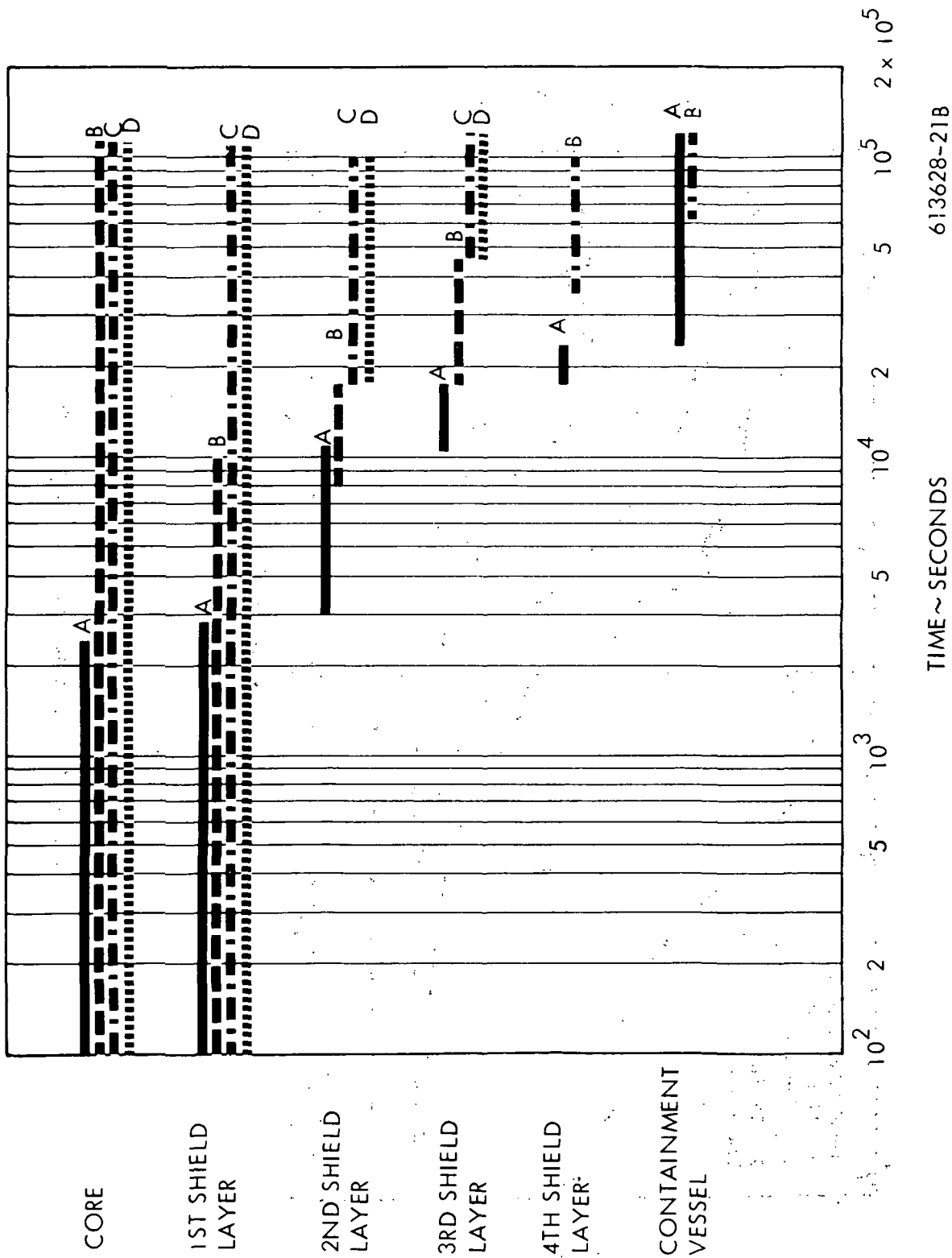


Figure 3-20. Fission Product Redistribution for HTM-5

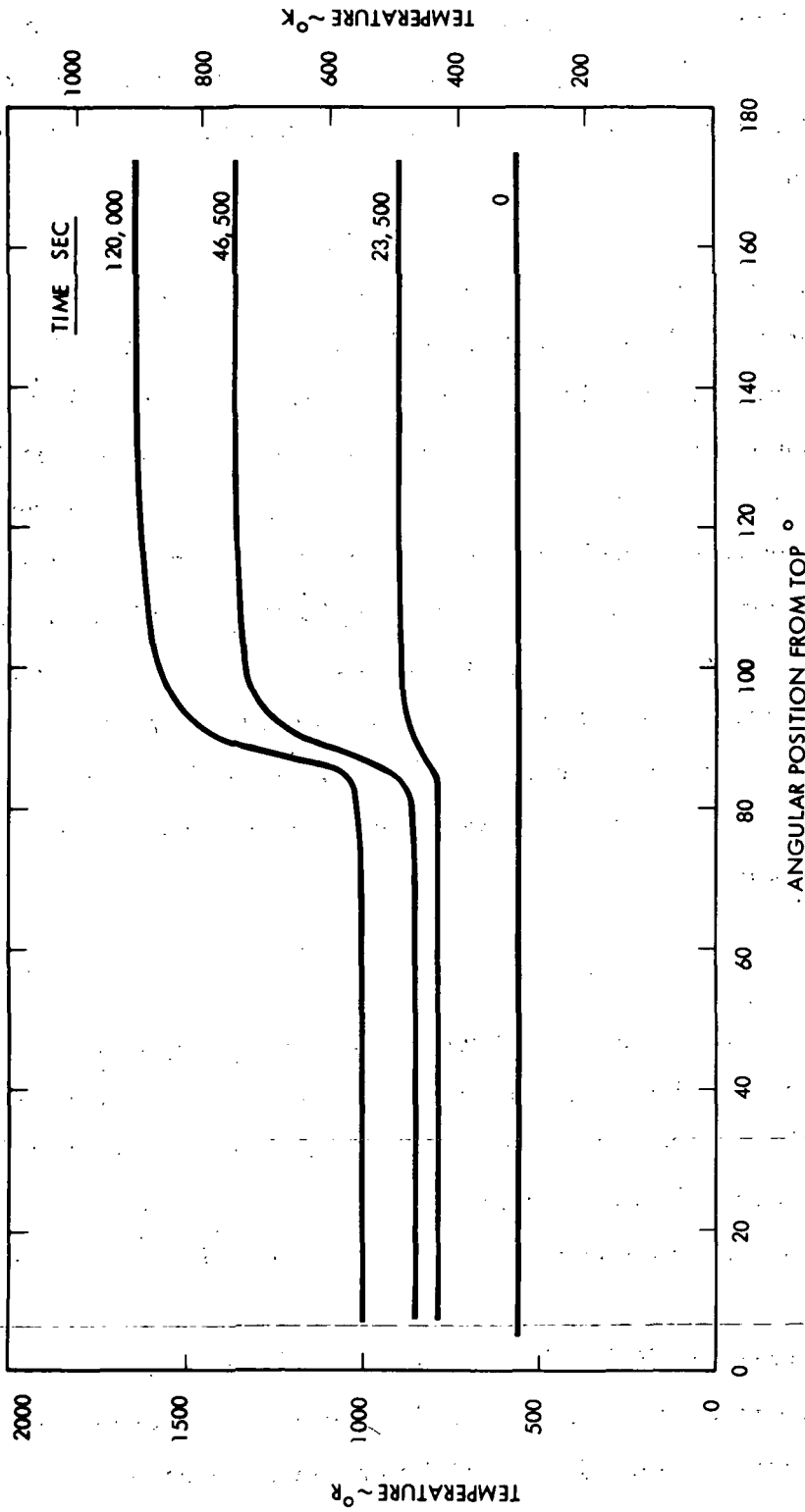


Figure 3-21. Containment Vessel Circumferential Temperature Profile for HTM-5

The 4 K watt case was run for 6000 seconds. The time step was maintained of 30 seconds throughout the transient with a 2 percent convergence criteria on the heat flow. This was required as a result of the steep gradients imposed by the relative large amount of energy generation versus the system capacitance. Larger time steps induced considerable instability in the temperature profiles.

Figure 3-22 shows the temperature profile axially from the center of the core to the bottom of the containment vessel. As indicated in Figure 3-22 the center of the UO_2 core melted within 300 seconds. At this point the heat source left and was deposited out on the depleted UO_2 in the shielding area. The core center eventually stabilized at about 4500°R (2500°K), the temperature level at which condensation occurs. The heat sources were driven entirely from the core after 1200 seconds and eventually walked out layer by layer to the fourth and fifth shield layer after 2100 seconds. Because of the reduced shielding capability radially outwards, the power generation level had risen from 4 K watts to 10 K watts. Thermal equilibrium of the system was reached with the heat sources located in the third and fourth layers. The shield temperatures stabilized at about 4300°R (2389°K) in the fourth layer and the core center-line stabilized at 4600°R (2555°K). The shield surface temperature was stabilized at 2550°R (1417°K) at this point.

3.3.7 HTM-7 Results

The HTM-7 model consisted of the undeformed model with a $\text{W}/\text{UO}_2/\text{LiH}$ shield configuration. This core was run with 50 percent soil burial and with 100 percent heat pipe operation. The representation of this model is the same as for HTM-5 which is shown in Figure 3-18. This case differed from Case 5 only in the condition of heat pipe operation. HTM-7 was run for 200,000 seconds of operation under the influence of the afterheat power decay profile.

Figure 3-23 is an axial profile of the temperatures in the core, shield, and containment vessel for HTM-5. The characteristics of this transient were the same as those observed from HTM-3 and HTM-5 with the exception of the containment vessel temperature response from about 50,000 seconds on out to 200,000. During this period the sodium heat pipes are in an operating mode as a result of reaching their operating range about 1390°R (772°K). As a result the

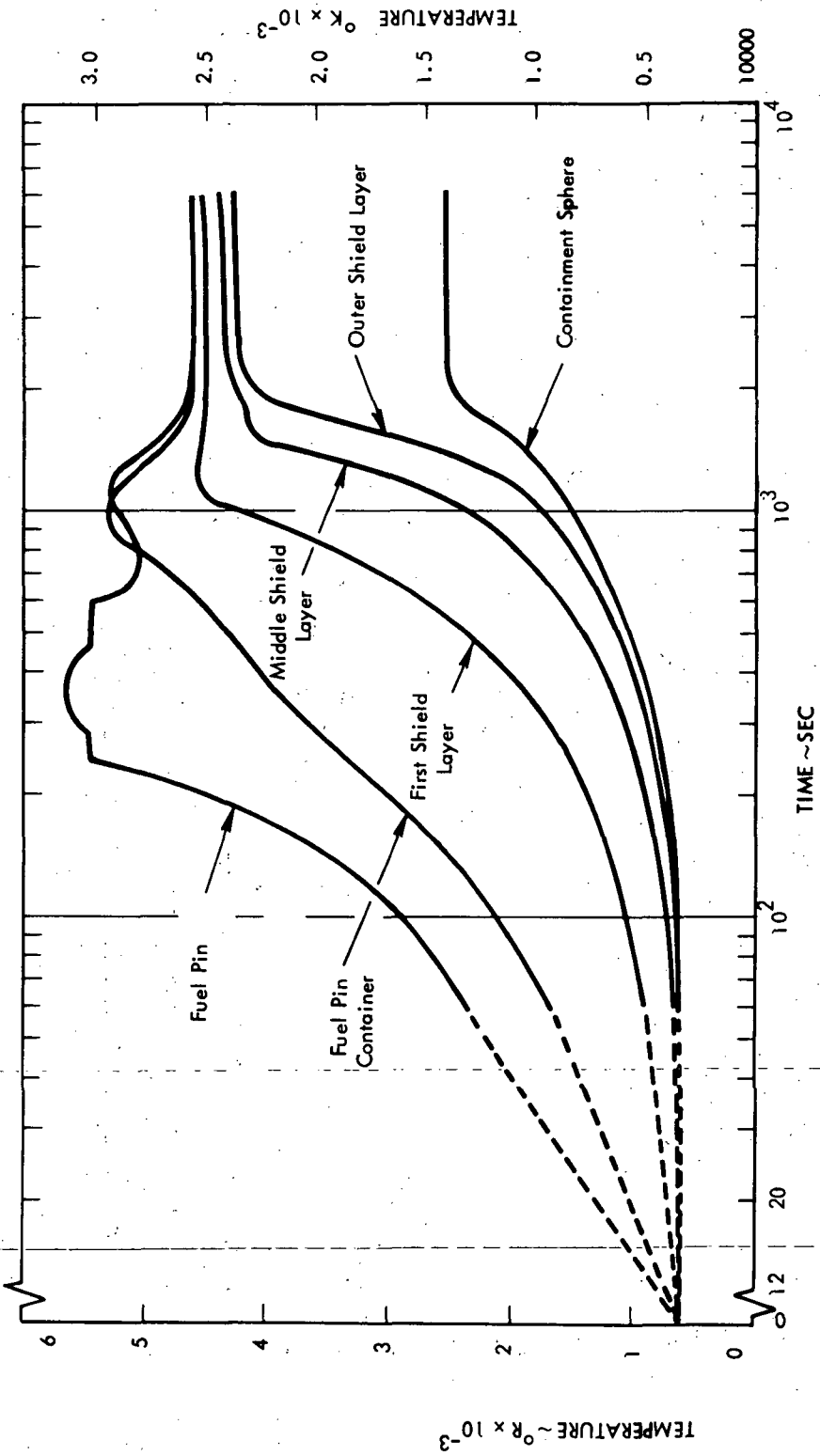


Figure 3-22. Temperature History for HTM-6 (In-Pile Test Model) Axial Profile

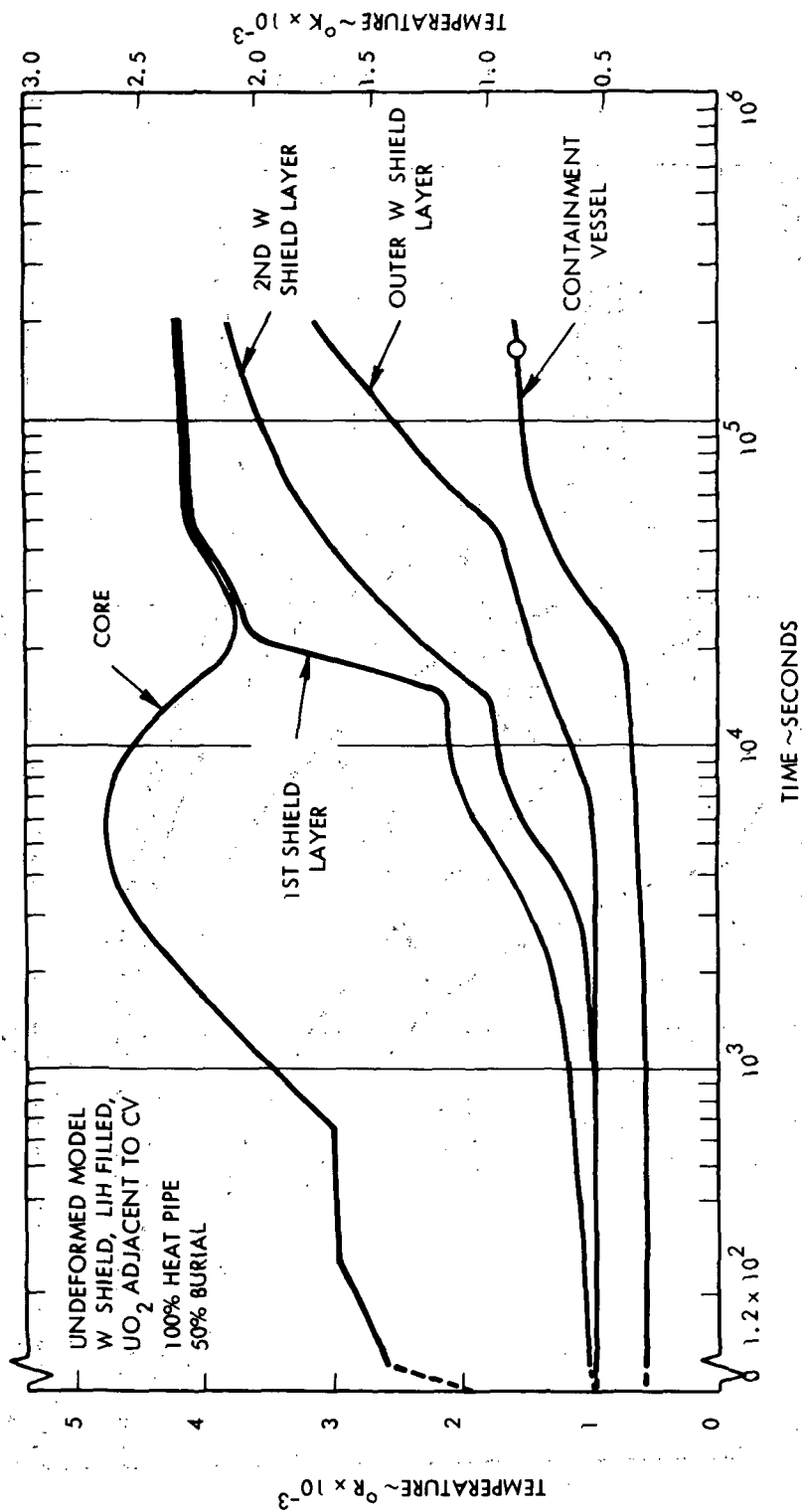


Figure 3-23. Temperature History for HTM-7

peak containment vessel temperature was approximately 150°R (83°K) lower for HTM-7 than for HTM-3 or HTM-5 at 110,000 seconds into the transient. The temperature profile circumferentially around the containment vessel is shown in Figure 3-24 for various times. After 50,000 seconds when the heat pipes are operating, the slope across the region adjacent to the soil to air interface was more gradual than that shown just prior to the heat pipe operating region. Comparison of Figure 3-21 for HTM-5 and Figure 3-24 at 120,000 sec also illustrate a more gradual slope indicative of the additional heat transport capability of the heat pipes. An isothermal containment vessel was not obtained, however. The peak containment vessel after 200,000 seconds was 1600°R (889°K).

Figure 3-25 shows the fission product redistribution for this case which was very similar to Figure 3-20 for HTM-5. After 200,000 seconds Groups C and D had started to reach the containment vessel. At this point 100 percent of Group A and 86 percent of Group B was on the containment vessel. The remaining 14 percent of Group B was in the core. The breakdown for Group C fission product deposition was 4 percent, 1 percent, 22 percent, 54 percent and 7 percent for the 1st through 4th shield layer and the containment vessel respectively. Twelve percent of the Group C fission products had not escaped the core. For Group D the breakdown was 4 percent, 1 percent, 15 percent, 37 percent, and 5 percent respectively with 38 percent of Group D remaining in the core.

For this case the containment vessel did not rupture until after 170,000 seconds. At this point the internal pressure was 1610 psi (1110 N/cm^2) and the maximum containment vessel temperature was 1560°R (867°K).

3.3.8 HTM-8 Results

The HTM-8 model consisted of the deformed model with a composite shield simulating LiH filled UO_2 spheres. This case was run without heat pipes and with 25 percent soil burial. A preliminary set of thermal properties were used to represent the composite shield. The thermal capacitance of LiH with its heat of fusion at 1700°R (944°K) was modeled. The thermal conductivity was representative of UO_2 . The density of LiH was used for capacitance

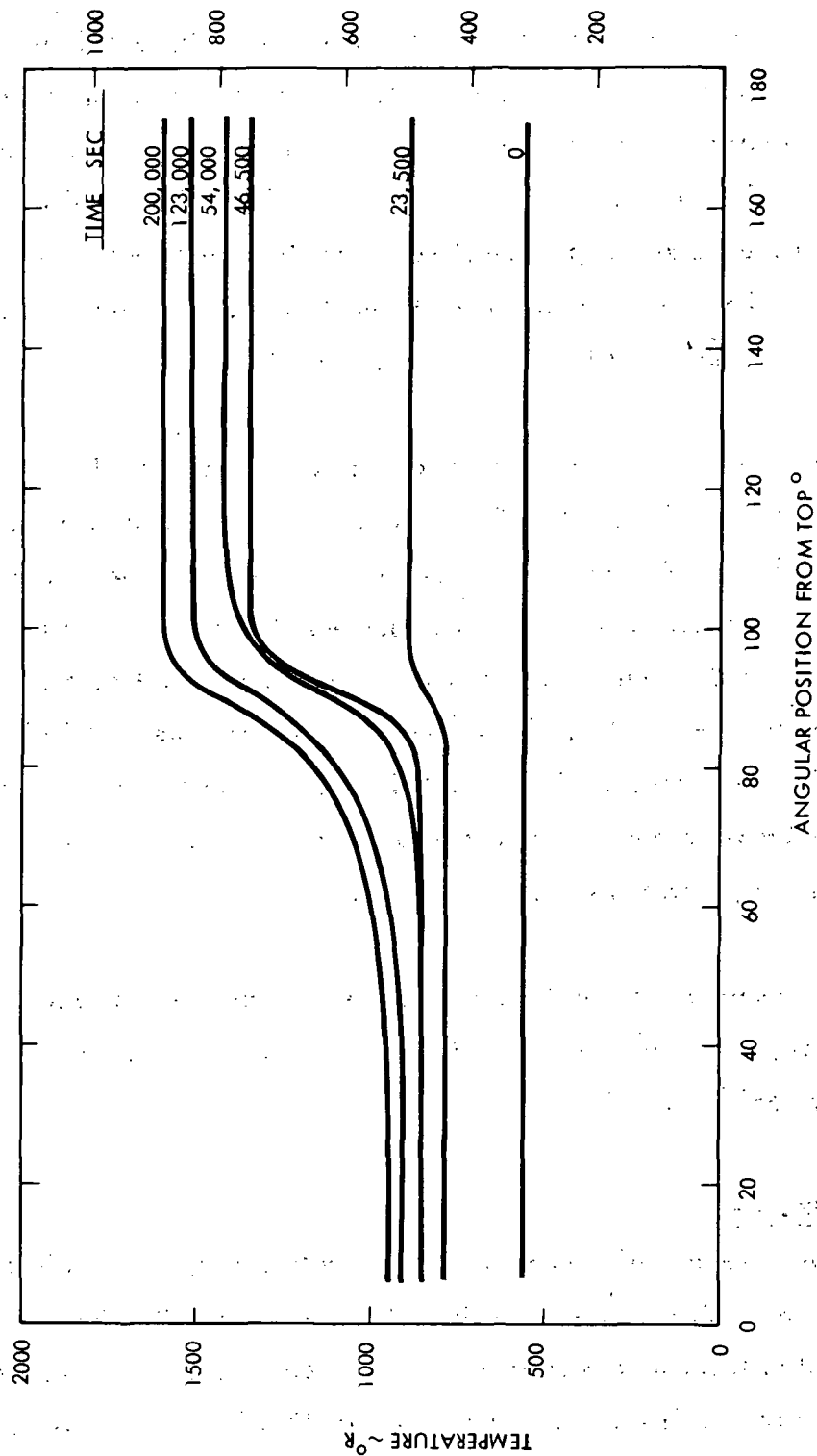
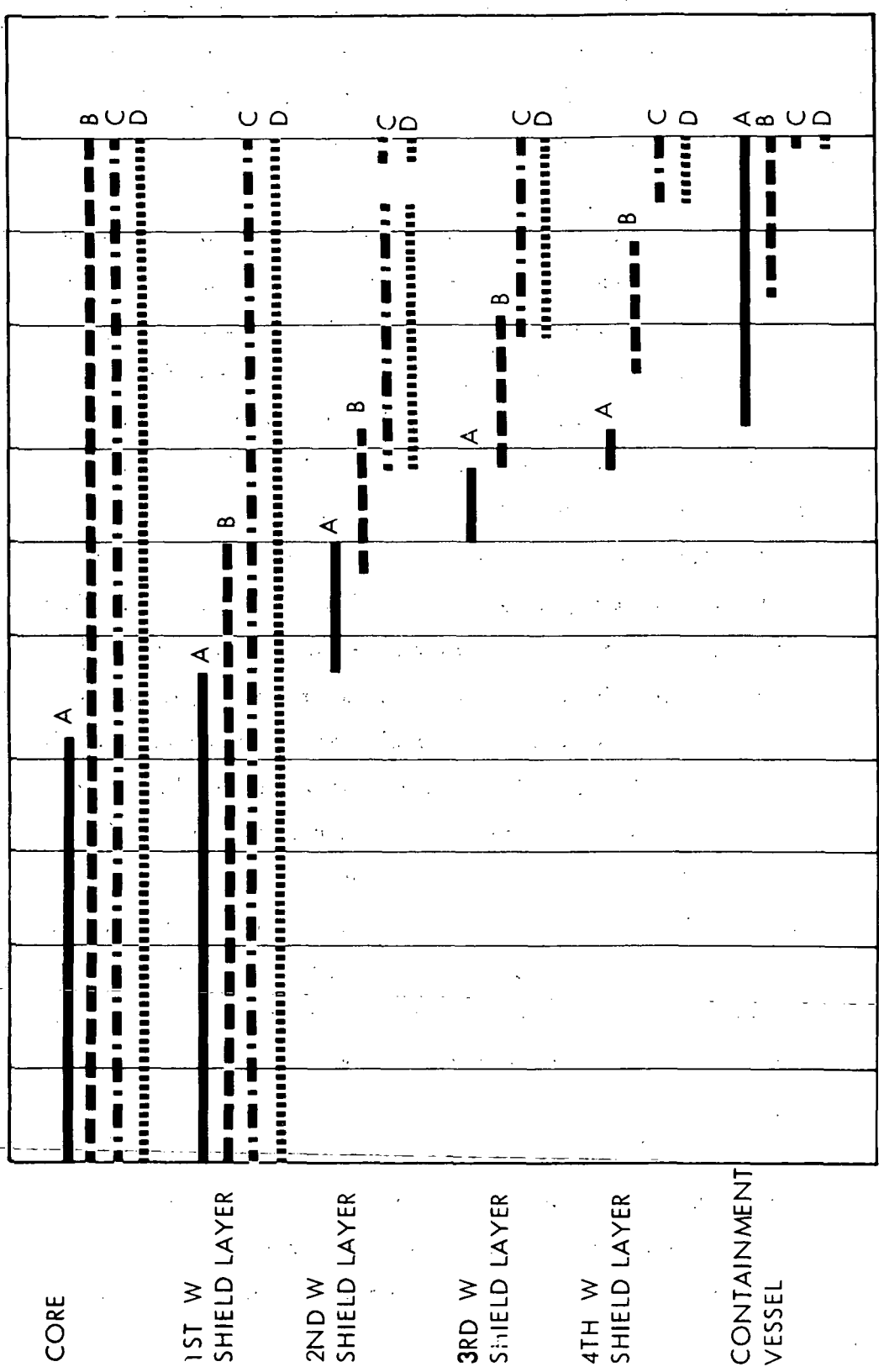


Figure 3-24. Containment Vessel Circumferential Temperature Profile for HTM-7



10² 2 5 10³ 2 5 10⁴ 2 5 10⁵ 2 5
 TIME ~ SECONDS

613628-22B

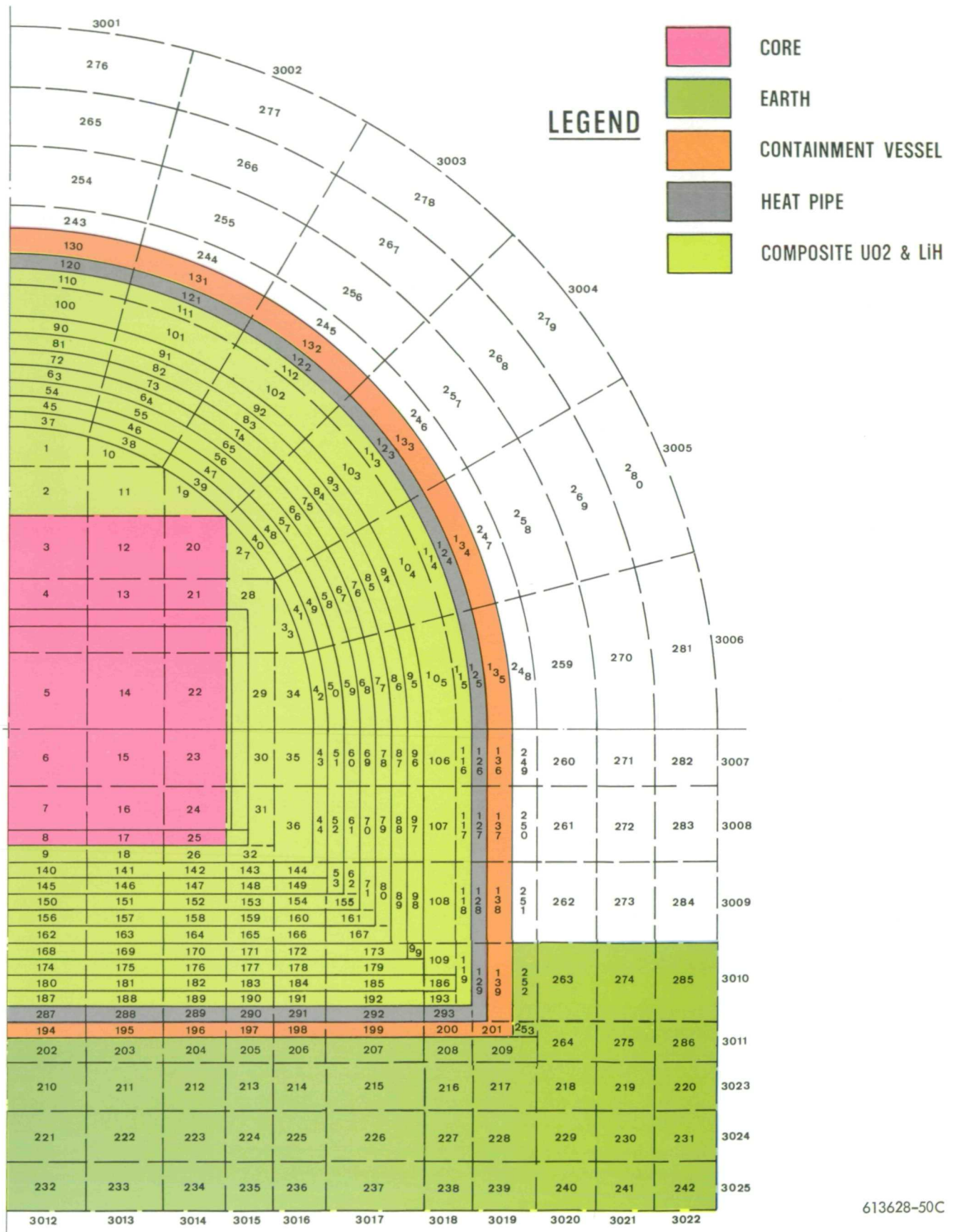
Figure 3-25. Fission Product Redistribution for HTM-7

purposes; however, UO_2 density and melting point were considered in the sense that the core was not allowed to displace the composite shield. Figure 3-26 is a sketch of this model showing the material representation for this HTM. This model was run for 112,000 seconds of operation under the influence of the afterheat power decay profile.

Figure 3-27 is an axial profile of temperatures in the core, shield, and containment vessel for HTM-8. The core structure started to melt at 350 seconds and required approximately 350 seconds to melt which was similar to results of the undeformed models and much quicker than HTM-8. This indicated that much less heat was getting out of the core and shorting to the bottom with the W shield layers replaced by the low conductivity, high capacitance material. Without any displacement occurring the core was thermally shielded and therefore rose to a temperature level of approximately 5200°R (2889°K) before it peaked. The peaking and subsequent decay was attributed to the continued decay and escape of fission products from the core. The shield layers significantly lagged the core due to their low conductivity, high capacitance, no displacement characteristics. Furthermore the containment vessel at the bottom did not start to rise significantly until 20,000 seconds into the transient. After 110,000 seconds it had reached 1700°R (944°K). Figure 3-28 shows the temperature profile of the containment vessel starting from the top. The top and side of the containment vessel remained uniform in temperature. At the corner of the containment vessel between the side and bottom, the vessel runs cooler late in the transient. The bottom of the vessel, thermally insulated by the soil, runs progressively hotter radially towards the center. Although it is reasonable to expect a corner farthest removed from the heat source to run cooler than the rest of the system, this case is amplified by the fact that the bottom is thermally insulated and the side portion of the vessel down to node 138 is receiving fission products whereas the corner is not receiving fission products.

Figure 3-29 shows the redistribution of fission products for HTM-8. Because the core peaked at slightly above 5000°R (2778°K), Groups A, B, and C were completely deposited on the containment vessel, 88 percent of Group D left the core of which 75 percent were deposited on the containment vessel.

Figure 3-26. HTM-8 Model Description



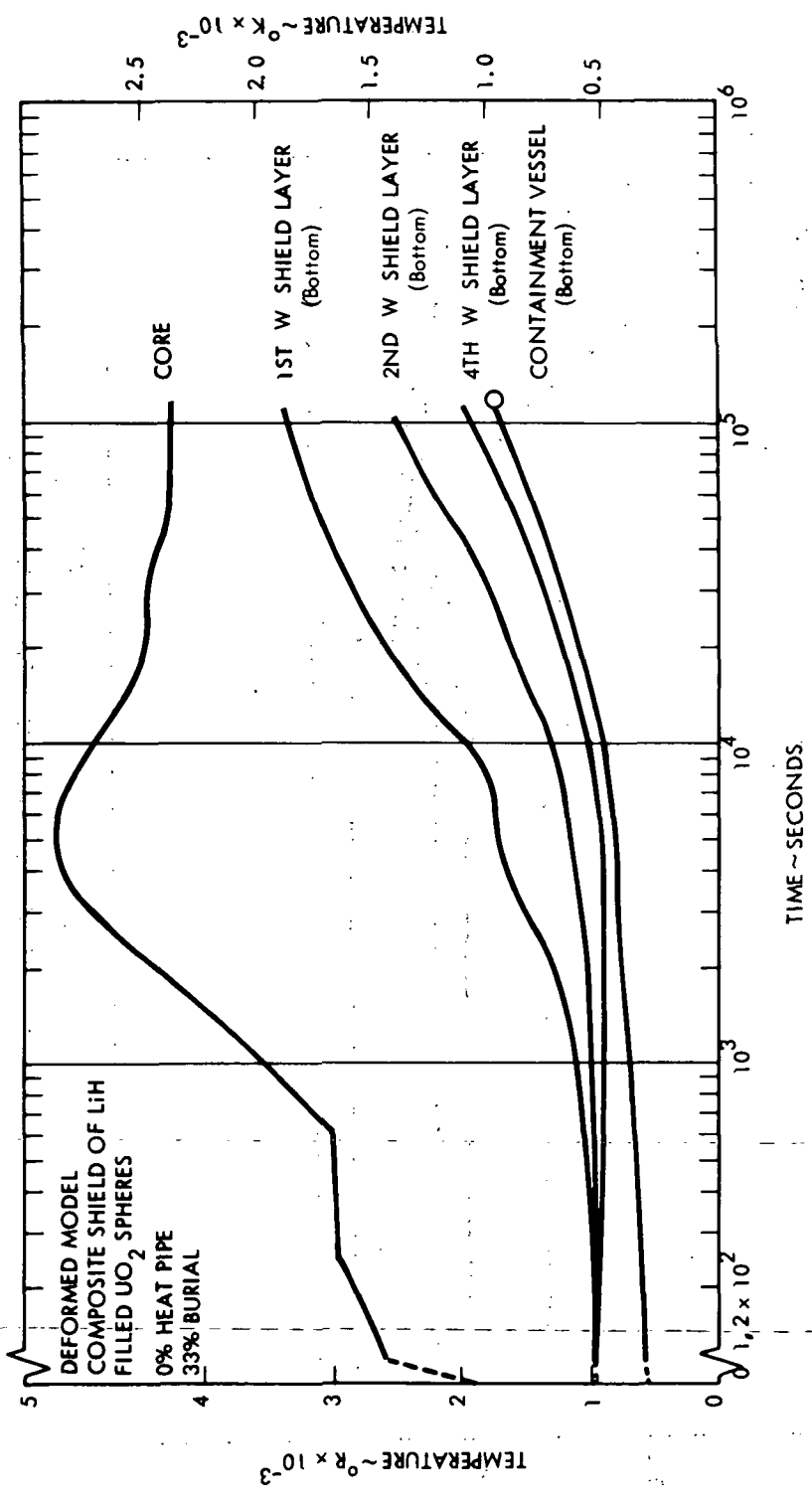


Figure 3-27. Temperature History for HTM-8

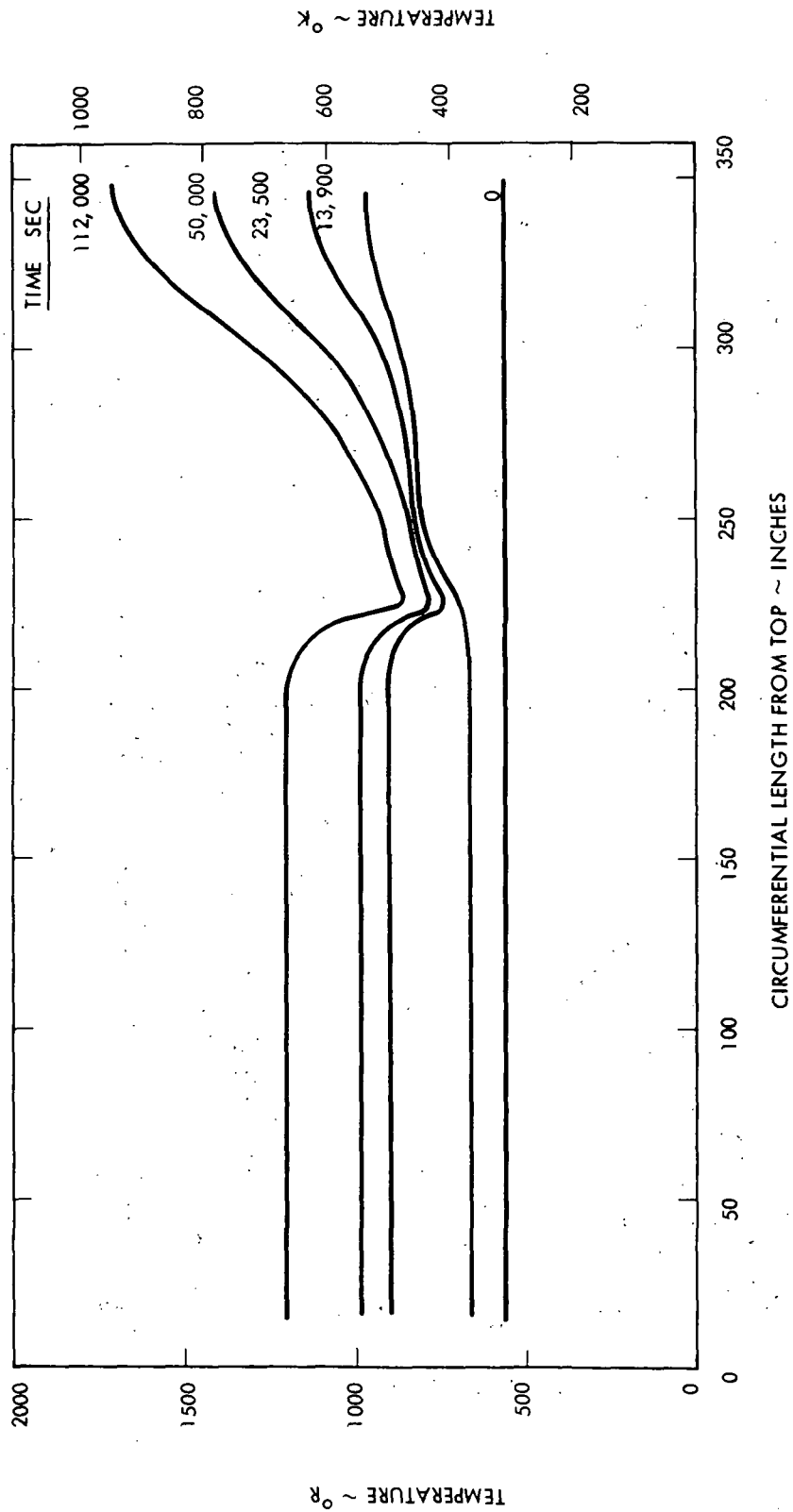
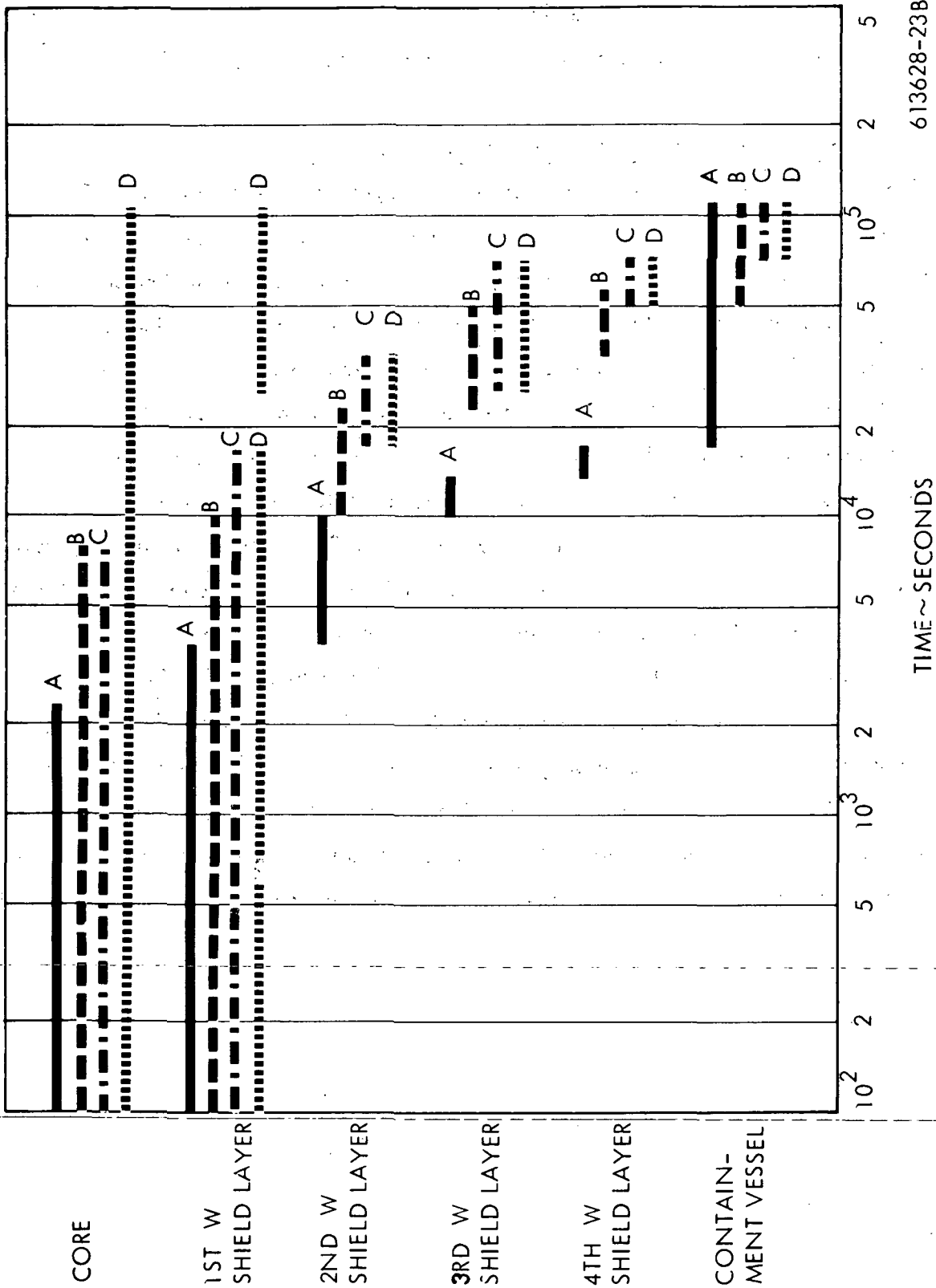


Figure 3-28. Containment Vessel Circumferential Temperature Profile for HTM-8



613628-23B

TIME ~ SECONDS

Figure 3-29. Fission Product Redistribution for HTM-8

The containment vessel rupture occurred at 112,000 seconds. At this point the pressure was 1050 psi (724 N/cm^2) and the maximum containment vessel temperature was 1710°R (950°K).

3.3.9 Comparison of Containment Vessel Temperatures and Pressures

Figure 3-30 compares the maximum containment vessel temperatures determined for HTM's 2, 3, 4, 5, 7 and 8 versus time. Figure 3-31 compares the internal pressure for these cases. HTM-2, the undeformed model with radiation gaps, and HTM-4, the deformed model with a W/LiH/ UO_2 shield experienced the earliest and steepest temperature responses on the containment vessel. The pressure buildup consequently for these two cases was more rapid than for the other cases. Rupture failure for these cases occurred around 10,000 seconds. The three undeformed models with W/LiH/ UO_2 (HTM-3, 5, 7) indicated much slower temperature and resultant pressure responses with only minor differences between them. Rupture occurred for two of these three cases, at about 100,000 seconds. Heat pipe operation, HTM-7, extended the rupture life to 170,000 seconds. HTM-8 the deformed model with the composite shield was initially similar in temperature response to HTM-4. Because the core was not displaced in HTM-8, the HTM-8 response remained gradual unlike HTM-4. Eventually it was similar in temperature level to the HTM-3, 5, and 7 cases. The void space for this composite shield was assumed to be greater than in the LiH filled shields. As a result the pressure level lower than for the other cases. The rate that it built up was also slower; however, this was a result of the transfer of fission products to the containment vessel resulting in lower shield temperatures on the side and top. Rupture for this case was around 100,000 seconds.

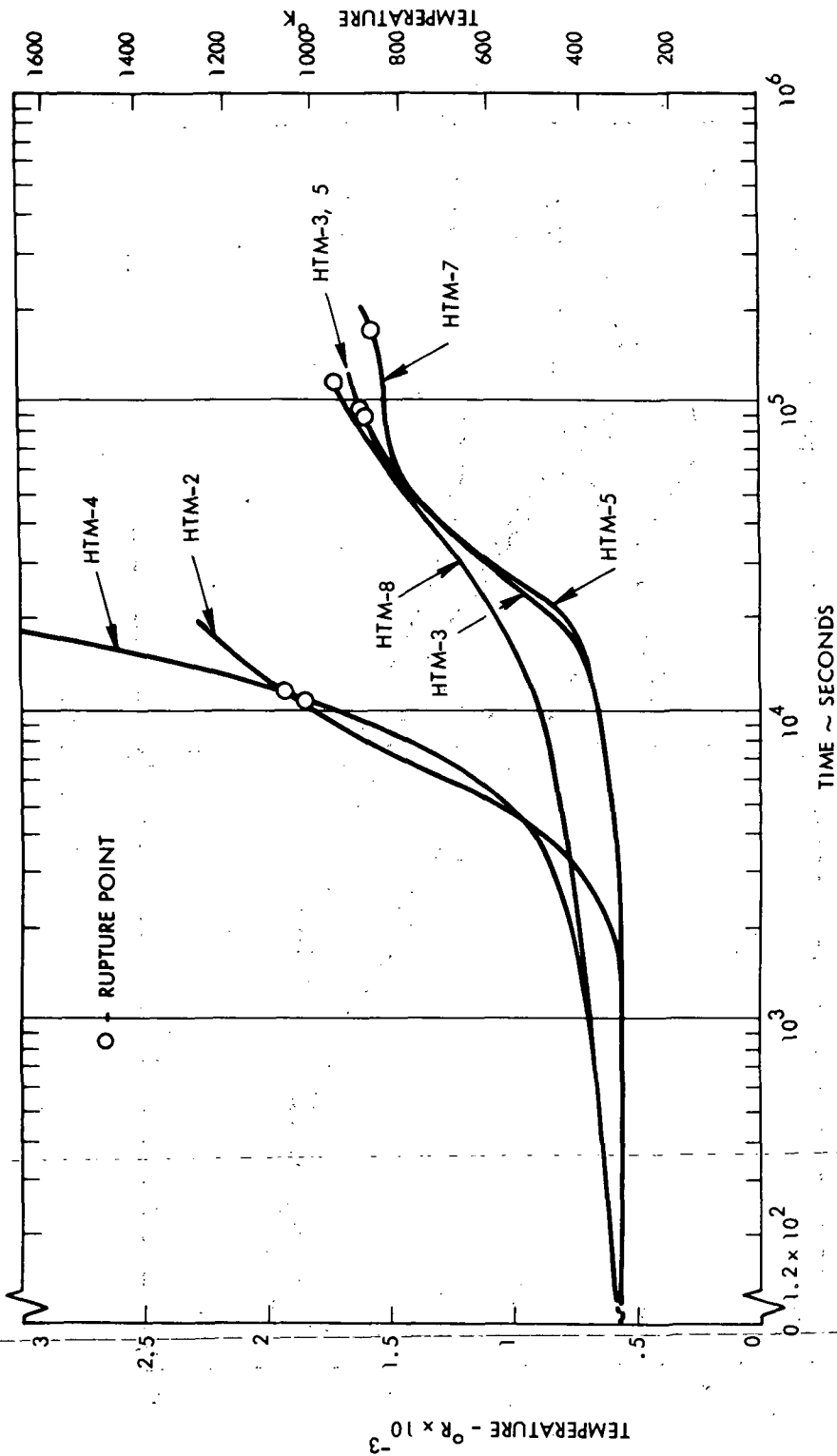


Figure 3-30. Comparison of Peak Containment Vessel Temperature

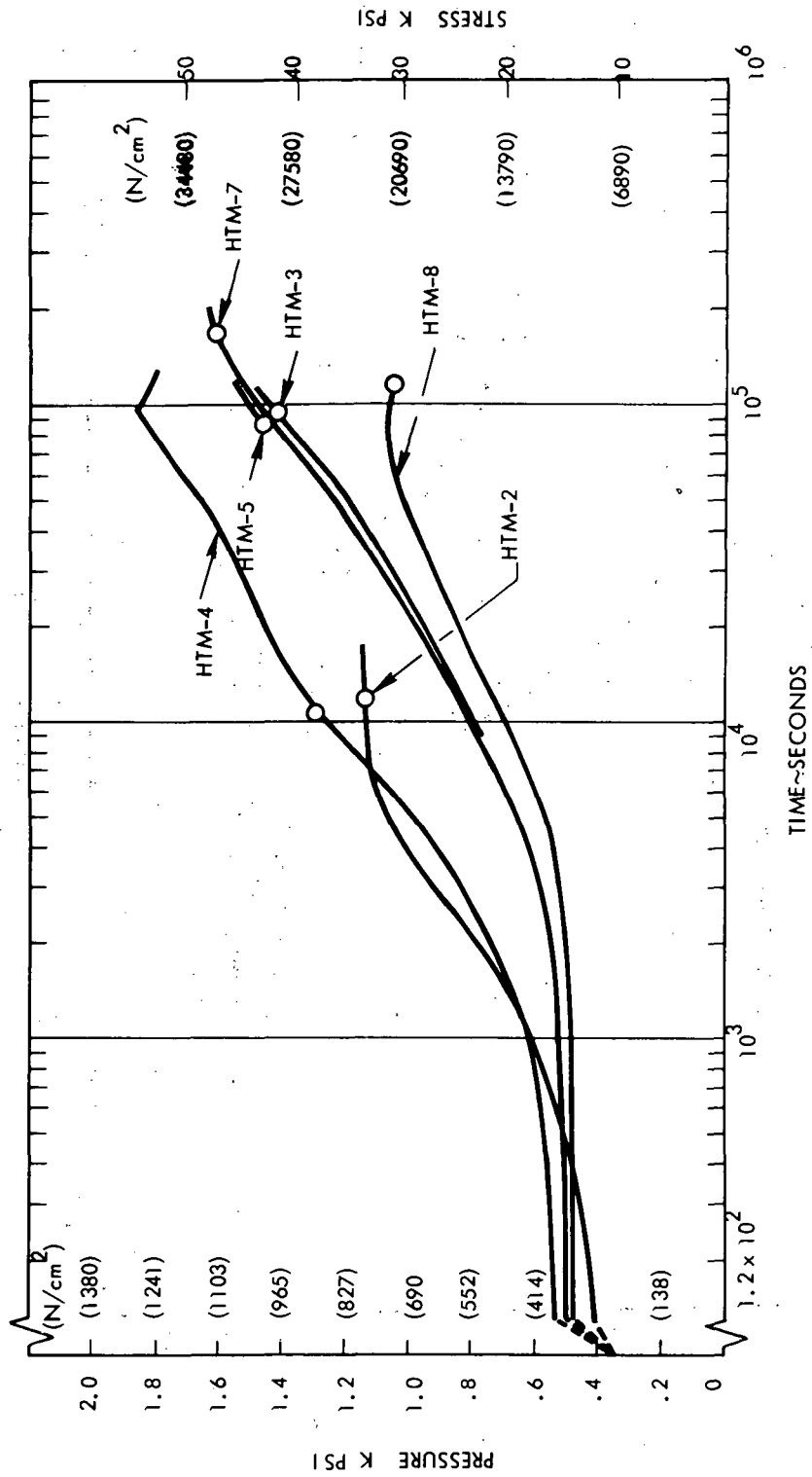


Figure 3-31. Comparison of Internal Pressure and Containment Vessel Stresses

4.0 TASK III DISCUSSION OF RESULTS

In the contract nine questions were identified for response as part of the requirements of Task III. Results obtained in the course of the study suggest that additional analyses would be required to provide quantitative answers for some of the nine questions. Also several interesting points, not covered by the nine questions, have been identified. This section has, therefore, been divided into a subsection for answering the nine contractual questions and a subsection for other points of discussion.

4.1 CONTRACTUAL QUESTIONS AND DISCUSSIONS

4.1.1 Question: What pressure could the containment vessel contain without rupture?

What are the uncertainties of the answer?

Answer: Containment vessel rupture occurred with internal pressures ranging from 1000 psi to 1600 psi as shown in Figure 3-31. Preliminary calculations performed to date are considered inadequate to define percent accuracy.

Discussion: The mechanism causing containment vessel structural failure for these HTM's is creep rupture. The rupture point is a function of the internal pressure and temperature time history of the containment vessel. A specific pressure, therefore, cannot be defined. For the four undeformed models and two deformed models analyzed the pressure level varied from 1000 psi to 1600 psi at the time rupture occurred as shown in Figure 3-31, Section 3.3.9 (based on an initial pressure of 350 psi). HTM-8 the deformed model with a composite shield, failed at the lowest pressure level of 1030 psi.

The initial helium gas internal pressure inside the containment vessel and the amount of moderator and reflector water remaining in the core following impact strongly influence the "time to failure" of the containment vessel. For example, if the initial pressure of the helium gas were reduced, the resultant pressure level for a given temperature level in the shield would correspondingly be reduced. The pressure history would therefore be less severe, and the time to failure of the containment vessel for a given temperature response would be extended.

4.1.2 Question: Does heavy insulation help lower the containment vessel temperature?

Answer: A comparison of shields with and without insulation was not available. Of the six HTM's identified and analyzed which pertain to the reactor power plant, five of the shield configurations include the heavy insulation and the sixth consists of the composite shield.

4.1.3 Question: Does the effect of lithium hydride as a heat sink lower system temperature throughout the post impact period?

Answer: LiH significantly delays the system temperature response as indicated by the comparison of HTM-2 and HTM-3 in Figure 3-30.

Discussion: HTM-2 and HTM-3 provide a direct comparison of designs with and without LiH shields. Both are undeformed models with W shield layers and UO_2 adjacent to the containment vessel. Both consider 33 percent burial without any heat pipe operation. Figure 3-30 in Section 3.3.9 compares the containment vessel temperature for both cases. The containment vessel for HTM-2 which had void spaces between the W layers started to heat significantly at 2000 seconds, indicating a delaying effect by the LiH.

4.1.4 Question: How far can the containment vessel penetrate the soil before its surface temperature becomes excessive?

Answer: Burial depths of 33 percent for the undeformed and for the deformed models resulted in containment vessel failure. Burial depths less than these amounts were not considered.

4.1.5 Question: Does the soil melt? What effect does this have on the containment vessel surface temperature?

Answer: In HTM-4 the peak containment vessel temperature reached 4000°R (2222°K) within 100,000 seconds. The average temperature of the soil depth of 30 inches was 350°R . This is well below the soil fusion temperature of 2300°R (1280°K).

Because of the high containment vessel surface temperature, local soil melting will occur and will delay somewhat the containment vessel temperature response. The model was not defined

in sufficient detail to illustrate this effect. The number of soil nodes in the model could be increased by using the standard TAP-A input data option

4.1.6 Question? Is the containment vessel surface temperature affected by the surface deformation?

Answer: Deformation can significantly decrease the time to failure as indicated by the comparison of HTM-3 and HTM-4 in Figure 3-30.

Discussion: HTM-3 and 4 provide a comparison of designs containing W/LiH/UO₂ shields with no heat pipes in an undeformed and deformed configuration. This comparison shown in Figure 3-30 indicates that the containment vessel temperature rise for the deformed model is significantly greater than for the undeformed model. In the case of the composite shield configuration, differences between the deformed and undeformed models were not as significant since displacement of the core relative to the containment vessel does not occur. It should also be noted that in the deformed model with a LiH/W shields the thickness of LiH between W layers in the base was assumed to 1 inch with a diametrical reduction of the containment vessel to be 30 percent.

The degree of deformation was based on experimental data from rocket sled tests of two foot diameter spheres (30). The thickness of LiH was estimated without experimental verification. The time to melt and displace the core through the LiH layer is directly related to the thickness of the LiH layers. The containment vessel temperature response is therefore, strongly dependent on the assumed thickness of LiH.

4.1.7 Question: Identify those parameters which affect the containment vessel surface temperature that cannot be controlled by design. Determine the magnitude of their effect.

Answer: Afterheat decay profile, amount of trapped helium gas, and containment vessel material are three parameters that cannot be controlled without significant design modifications.

Two alternatives exist in changing the afterheat decay profile which are changing the fuel form and changing the mission time. Changing the fuel form would require a redesign of the system and negate much of the present development work. Changing the mission time is not a desirable change since it would impair the applicability and usefulness of the system.

Another parameter that may be difficult to modify is the amount of helium trapped in the system. This parameter affects the containment vessel temperature, but more significantly it is the primary source for excessive internal pressures resulting in creep rupture. A quick removal system for dumping all the helium coolant prior to an accident would be effective if it could be incorporated in the design. Another parameter that could be adjusted only through redesign of the shield and containment vessel is the choice of materials for the containment vessel. This design parameter, however, effects the impact requirements of the containment vessel.

4.1.8 Question: What effect does fission product redistribution have on the containment vessel temperature?

Answer: Deposition of the fission products on the containment vessel results in a significant temperature rise as indicated by Figures 3-3 and 3-8 for HTM-2 and 3.

Discussion: Comparison of the temperature response curves with the fission product redistribution graphs have indicated that the containment vessel temperature response has been influenced very significantly by the location of the fission products. In fact, deposition of fission products into the containment vessel is more predominate than conduction and radiation in the undeformed model in terms of increasing the vessel temperature. Only in the deformed model is the thermal conduction path to the bottom of the containment vessel more significant.

One feature that the codes do not contain is the deposition of the fission products on the insulation adjacent to the inside of the containment vessel. When the fission products transport outward they go from the W shield and LiH shield to the containment vessel.

Under actual conditions this would not happen since the fission products would deposit on the insulation.

4.1.9 Question: Can vessel temperature be kept below failure limits without heat pipes? If not, what percent of heat pipes must be operable to be effective in keeping containment vessel temperature from becoming excessive?

Answer: The results of the HTM's calculated indicate that the time to failure is significantly increased by the use of heat pipes as shown in Figure 3-30 by the comparison of HTM-5 and 7. Some consideration should be given to alternate heat pipes which operate at a lower temperature level in an attempt to keep the vessel in a temperature range where negligible creep occurs. The present analyses performed with the heat pipe calculation procedure still indicated a significant temperature gradient around the containment vessel as shown in Figure 3-24.

4.2 GENERAL DISCUSSION

This section will review the effects of the geometry options, heat generation sources, melting, and pressure buildup on the temperature/pressure response of the containment vessel.

4.2.1 Model Options

Results with the deformed and undeformed models were obtained for a W/LiH/ UO_2 shield without heat pipes (HTM-4 and HTM-3). The comparison of the two indicated more severe heating of the bottom in the deformed case than in the undeformed case caused by the dropping of the core through the LiH layers. The time required to rupture the containment vessel is a strong function of the time to melt LiH. In the deformed model the LiH thickness was fixed at 1 inch for each layer. Furthermore the degree of diametrical deformation of the containment vessel was 0.3. Because of the sensitivity to LiH melting, a quantitative comparison of the deformed and undeformed model is very dependent on how good of an estimate can be made for the thickness of the LiH separating the W layers in the deformed base. To date, impact testing suggests that voids or gaps between layers will be closed on impact but the test results do not provide a quantitative value of the LiH layer thickness.

The in-pile test model was analyzed (HTM-6) with initially a 4 kwatt power level prior to the release of enriched UO_2 into the depleted UO_2 shield zones. This model is a two-dimensional representation of a configuration that will have a three dimensional flux distribution. Figure 3-22 presented in Section 3.3.6 shows the temperature distribution for HTM-6. This temperature distribution reflects results based on a heat source relocation model of fuel leaving the core as the UO_2 melts and depositing on colder zones in the shield. For this model gravitational effects on the fuel relocation have been neglected. The temperature response of the system is strongly influenced by the escape temperature assumed from the core and the allowable temperature deposition and vaporization in the shield. These two parameters are defined in the code along with factors defining the increased heat generation radially outward for a given mass of enriched UO_2 vapor. These parameters can be readily varied with minor coding changes along with the input value of the initial power level to provide a capability for parametrically evaluating the in-pile test model and for matching test data. If, however, a centerline cannot be defined about which the heat fluxes are nearly symmetrical, then the two-dimensional model will be limited in its adequacy to match the test data and a more extensive three dimensional analysis may be indicated.

4.2.2 Shield Options

Of the five shield options, three were considered in the six applicable HTM's which include the W/water shield with water removed and with a UO_2 layer adjacent to the containment vessel, the W/LiH/ UO_2 shield and the composite shield. HTM-2 and HTM-3 provided a direct comparison of the design with and without a LiH shield. Figure 3-30 in Section 3.3.9 compares the containment vessel temperature for both cases. The containment vessel for HTM-2 which had void spaces between the W layers started to heat significantly at 2000 seconds into the transient. HTM-3 however, did not start to heat significantly until 20,000 seconds, indicating a delaying effect by the LiH. The presence of LiH extended the stress rupture lifetime from about 10,000 seconds for HTM-2 to 100,000 seconds for HTM-5. Over the 20,000 second period analyzed for HTM-2, the peak containment vessel temperature was significantly greater than that for HTM-3. Although HTM-2 has less capacitance than HTM-5 and would cool faster, the slopes of the curves shown in Figure 3-30 indicate that a cross over in vessel temperature during the cooldown cycle, if it were to occur at all, would not occur within

200,000 seconds. With an initial pressure of 350 psi (24 n/cm^2), the rupture point is well before 200,000 sec for both cases; therefore, a crossover is not important. If the helium in the system could be removed such that the pressure buildup is much slower, the stress rupture life would be extended further to the point that possibly the temperature response during periods beyond 200,000 sec would be important in determining the utility of LiH.

HTM-4 and HTM-8 are two deformed models that compare a LiH/W shield to a composite shield that prevented core displacement and provided significant capacitance. Figure 3-30 indicated that with considerable deformation, the response rate of the containment vessel in the deformed region is much greater. Providing a dense insulation that prevented the core displacement extended the rupture lifetime from 12,000 seconds to 120,000 seconds. This comparison indicates that although LiH significantly delays the vessel temperature response, a composite shield with sufficient capacitance can provide even better protection particularly with deformation occurring. The composite shield analyzed points out the advantage of preventing core displacement and driving the core to a temperature level such that fission products escape to the upper regions exposed to the ambient.

The five shield options provide flexibility in terms of comparison of each shield with the other. Additional shield configurations can be considered by replacement of material properties. For example, the composite material can be replaced by a material having any melting point, thermal conductivity and specific heat; however, it is limited to materials having a density greater than or equal to that of the core components. This is due to restricting the displacement of the core for this shield model. Similarly, the tungsten shield layers and the UO_2 insulation layer adjacent to the containment vessel can be replaced by components whose density is greater than the core components. LiH, however, can only be replaced by materials whose density is less than that of the core components.

4.2.3 Heat Pipe Operation

In the cases analyzed to date stress rupture failure has occurred with or without heat pipes. Lifetimes without heat pipes have been as long as 100,000 seconds. One hundred percent

heat pipe operation was considered in the undeformed model with a W/LiH/ UO_2 shield based on sodium heat pipe properties. In Figure 3-30 comparison of the containment vessel temperature profiles for HTM-5 and HTM-7 indicated that flattening of the peak containment vessel did occur. Creep stress rupture did occur in both cases; however, the lifetime was extended from 100,000 to 170,000 seconds. Sodium heat pipe operation becomes effective at temperatures above 1400°R which unfortunately is within 200°R of the level at which significant weakening of the vessel occurs. As a result an appreciable amount of creep rupture will occur in the operating regime for a sodium heat pipe. Some consideration should be given to alternate heat pipe fluids which operate at a lower temperature level in an attempt to keep the vessel in a temperature range where negligible creep occurs. The present analyses performed with the heat pipe calculation procedure still indicated a significant temperature gradient around the containment vessel as shown in Figure 3-24. Further effort could indicate whether this implies that heat pipes cannot provide a uniform temperature profile or if there is opportunity for improvement in the heat pipe modeling procedures. A possible quick check is to represent the heat pipes by a thermal conductivity much larger than that used to date as representative of heat pipe operation.

4.2.4 Soil Burial

The deformed model is limited to burial depths ranging from 33 percent to 100 percent surface contact in increments of 8.33 percent. A minimum burial of 33 percent was set for the undeformed model. If less than 33 percent burial is desired for the undeformed model, the HTMGEN subroutine can be revised with a few minor changes or the standard TAP-A could be used to change the material representation.

In the deformed model, 0 to 100 percent burial is treated. Increments of 8.33 percent are provided from 50 to 100 percent burial.

4.2.5 Fission Product Decay and Redistribution

The fission product escape and redistribution procedure was defined to provide the capability for considering four groupings independent of each other with separate decay, escape, and

deposition criteria. As described in Appendix B, the data search performed in this contract provided limited data to define accurately the time and temperature profiles for all four groupings. As a result some judgment was used in defining the curves contained in the program. As better data becomes available it can be easily inserted in the FISSON subroutine to provide a better simulation of fission products. The present decay rate in the code is for a 1000 hour mission based on NASA defined data.

The temperature response of the containment vessel to the deposition of fission products indicates a possibility for improvement of the fission product redistribution procedure. Fission product deposition is limited to the W shield layers and the containment vessel. Deposition on the LiH and UO_2 insulation is not considered. A significant amount of deposition followed by vaporization may occur on the LiH as opposed to vapor flow through the porous LiH. Likewise the fission products may deposit on the UO_2 insulation adjacent to the containment vessel. Based on the response of the containment vessel to fission product deposition, deposition of fission products on LiH and on the UO_2 insulation layer will delay the containment vessel temperature response and provide greater lifetimes.

4.2.6 Metal-Water Reaction

One mechanism not covered by the contractual questions was the consideration of metal-water reactions and their effect on containment vessel temperature and pressure response. In all the HTM's analyzed, the assumption was made that 95 percent of the moderator water in the core was removed. In addition, for HTM-2 which analyzed a W/water shield, all the water in the shield was removed. For all cases, therefore, the mass of water considered was 160 lbm (72.6 kgms). Typically the reaction of water with metal was completed within 180 seconds. The reaction that was analyzed was water reacting with the stainless steel pressure tubes. The mass of helium released was 18 lbm (8.2 kgms) and the pressure buildup due to this release varied from 51 psi (35 N/cm^2) in HTM-2 with voids between W shield layers to 186 psi (128 N/cm^2) in HTM-4; the deformed model filled with LiH. The heat released by this reaction was 9 percent of the total heat generated during this time period. The effect of the reaction on the temperature response was negligible. The contribution to the pressure buildup can be a

significant percentage; however, with 350 psi (241 N/cm^2) initial helium pressure the H_2 pressure was not dominant. It is obvious, however, that if a much larger percent of the moderator water is left in the core then the pressure buildup due to H_2 release can dominate. The effect on temperature response would be a steeper rate of increase in the core temperature initially; the effect on the overall temperature response would still be negligible. Control and removal of the moderator water is critical design parameter which can influence the survival of the containment vessel subsequent to impact.

4.2.7 Component Melting and Displacement

The ESATA program considers the heat of fusion for melting of molybdenum, UO_2 , AM-355, W, LiH, and the composite material. The lumped capacitance of the core includes the capacitance and when applicable the heat of fusion of molybdenum, UO_2 , and AM-355.

The core structure melting occurred in the 500 to 1000 second range for all the HTM's. The bulk core temperature did not reach the melting point for molybdenum or UO_2 in any of the transients.

For the undeformed model, a basic assumption was made that the core structure was intact and that the core could not drop until the structure was entirely molten. After structure melting was completed, the core would drop and fill the base of the first shield layer in HTM-2 which had voids between the core and shield layer. The dropping of the core significantly increased the first shield layer temperatures for HTM-2 as indicated in Figure 3-3 after 700 seconds. In the case with W/LiH/ UO_2 shields the core would drop a layer at a time through the LiH as the LiH melted. With a W/LiH/ UO_2 shield the core did not drop onto the first shield layer until approximately 15,000 seconds as shown in Figure 3-8 for HTM-3.

There are several simplifications in the modeling of the core displacement to the first shield layer which detract from the accuracy of the temperature time response. With a homogeneous core local melting of components in the core is not considered, and displacement is delayed until the entire mass of the core reaches the melting point of the structure.

The mass and the capacitance of the core is conserved during displacement. When the core displaces LiH, the mass of LiH is not conserved due to the different size of nodes above and below the core. The thermal resistance is adjusted however to account for a changing heat transfer path. LiH mass will be increased or decreased depending on the location of the core. Its effect is not expected to significantly alter the time to rupture of the containment vessel, because the percent change of total LiH mass (5-10 percent) is small and the change occurs well before rupture failure time (in HTM-3 the core drops to the first shield layer within 20,000 seconds while rupture of the containment vessel occurs at about 95,000 seconds.)

The UO_2 insulation layer adjacent to the containment vessel did not detach from the vessel wall for any of the HTM's analyzed with the exception of HTM-1. This was due to the low insulation temperatures that resulted for the cases analyzed. Additional design studies should be directed to provide for the detachment of the insulation layer in that portion of the containment vessel exposed to the air.

4.2.8 Pressure and Stress

Containment vessel stress analysis is based on a simplified creep-rupture model. The Larson-Miller parameter and the containment vessel percent life used is calculated for the maximum vessel temperature. The hoop stress in the containment vessel is calculated for both the undeformed and deformed model based on thin wall pressure vessel theory. Local stresses at the edge of the base in the deformed model are not considered in the analysis. The support provided by the compacted earth is also not considered for either model. The internal pressure buildup calculation is based on an average temperature of the heavy metal shield layers. In cases where voids exist between W layers this is a more representative temperature than with the voids filled with LiH. These considerations add uncertainty to the pressure buildup and stress rupture calculations. The containment vessel stress level and rupture time can therefore only be considered as representative values.

5.0 CONCLUSIONS AND DESIGN RECOMMENDATIONS

This program has resulted in the development of a computer program to analyze the afterheat distribution of a mobile nuclear power plant. The computer program analyzes an undeformed and deformed power plant. It considers a homogeneous core with five shield options. The code considers variable heat pipe operation and soil burial. It will also analyze an in-pile test model. Phenomena such as fission product redistribution, core/shield melt and displacement, and metal-water reactions are considered. The code also calculates transient temperature and pressure responses and performs a simplified creep rupture analysis of the containment vessel. Variable size, weight, and initial temperatures can be input to the code. The code was developed to minimize input data requirements. This program is operational on the NASA IBM-7094 II/7044 direct coupled system and the WANL CDC 6600 computer.

Eight HTM's were run and analyzed. These HTM's were primarily selected to verify the operability of the ESATA program options. However, the analysis of these HTM's has provided insight into some of the features that should be considered in future power plant designs. These features are:

- A composite shield material having the capacitance of LiH and a specific gravity equal to or in excess of UO_2 . Likewise, a LiH/W shield is preferable to a W/water shield with the water removed prior to impact.
- A heat pipe grid-work as an integral part of the containment vessel wall provided the heat pipes through design can withstand impact and remain operable.
- A layer of insulation adjacent to the containment vessel wall provided that fission product deposition through design occurs on the internal surface of the insulation and not on the containment vessel wall.

- A means for minimizing/eliminating the helium gas remaining in the containment vessel prior to impact.
- A means of minimizing/eliminating the moderator and reflector water remaining in the containment vessel prior to impact.

Specific conclusions pertaining to the HTM results and modeling procedures are described below:

1. Time before rupture ranged from 10,000 seconds for a deformed model to 170,000 seconds for an undeformed model with an initial internal pressure of 350 psi (241 n/cm^2). The internal pressure at rupture varied from 1000 psi (689 n/cm^2) to 1600 psi (1103 n/cm^2), and the peak containment vessel temperature varied from 1500°R (833°K) to 1900°R (1056°K) at rupture.
2. Time to rupture should be significantly increased by lowering the initial pressure through the addition of a means of removing helium prior to impact.
3. Without consideration of fission product deposition on the UO_2 insulation, the presence of the insulation adjacent to the containment vessel did not significantly affect the containment vessel temperature response when used in a LiH filled shield. Consideration of deposition of fission products on the UO_2 is expected to extend the life time of the vessel.
4. The use of LiH as a thermal capacitance material placed between heavy metal shield layers significantly increased the life time of the containment vessel. A representative increase from 12,000 to 100,000 seconds in the time to rupture for the undeformed model was indicated.
5. Deformation of the reactor with a W/LiH/ UO_2 shield shortened the time to failure significantly from 100,000 to 10,000 seconds. Similar results are expected for the W/water/ UO_2 shield, W/water, and W/LiH shields.

6. Preventing the core from "dropping" onto the containment vessel significantly increased the life time of the containment vessel as indicated by the 112,000 second time to failure calculated for the deformed model filled with a composite shield (HTM-8) having the capacitance of LiH and not displaced by the core.
7. Partial earth burials of 33 percent and 50 percent for the undeformed model indicated a negligible effect (about 6000 seconds) on the containment vessel temperature response and the time to failure.
8. The containment vessel temperature response was very sensitive to the deposition of fission products on it. Consideration of fission product deposition on LiH and UO_2 adjacent to the containment vessel should extend the calculated time to failure.
9. Sodium heat pipe operation occurs at a temperature such that rupture of the containment vessel can still occur; however, the time to failure was increased through the use of heat pipes by about 75,000 seconds.
10. The presence of 5 percent of the moderator water (160 lbm (72.6 kgm)) is sufficient to increase the internal pressure by 50 (34.5) to 160 psi (110 n/cm^2) by hydrogen release from metal-water reactions. This release occurs within the first 200 seconds of the transient.
11. Bulk soil fusion did not occur based on relative large soil node sizes. Local soil fusion is anticipated with a deformed system.

6.0 RECOMMENDATIONS FOR FUTURE WORK

Evaluation of the calculation models and the results obtained in the analyses of the HTM's suggested several possible refinements in the calculational procedures. The following code improvements are recommended:

1. Modify the fission product redistribution scheme to include the option to specify as part of input those shield layers capable of receiving fission products.
2. Update data on fission product decay, escape, and deposition based on a more comprehensive survey.
3. Include the degree of containment vessel deformation and LiH layer thickness in the deformed model as part of the input data.
4. Increase the number of nodes representing the soil.
5. Develop a three-dimensional nodal representation of the in-pile test model.
6. Develop a subroutine to treat dissociation of LiH.
7. Develop a generalized shield model permitting the program user to specify as part of input the material representation of each shield layer.
8. Include a program restart capability at any printout time in the afterheat decay-transient.

Analysis and comparison of the HTM's indicated several items that should be considered in more detail with additional computer runs. Listed below are recommendations for more analysis:

1. Analyze additional composite shield materials.

2. Reanalyze cases with the updated fission product redistribution scheme recommended above and, if available, more representative data.
3. Evaluate alternate initial internal pressure levels and percent of moderator water remaining in the core.
4. Evaluate the deformed model with updated deformation characteristics obtained from the Rocket Sled Test Programs.
5. Evaluate LiH and water filled shields without UO_2 .
6. Consider alternate shielding materials.
7. Evaluate heat pipes with an alternate fluid for lower temperature operation.
8. Consider more effective insulation such as "supported" Min-K adjacent to the containment vessel.
9. Consider greater burial depths than 50 percent.

APPENDIX A

HTM GENERATION SUBROUTINES

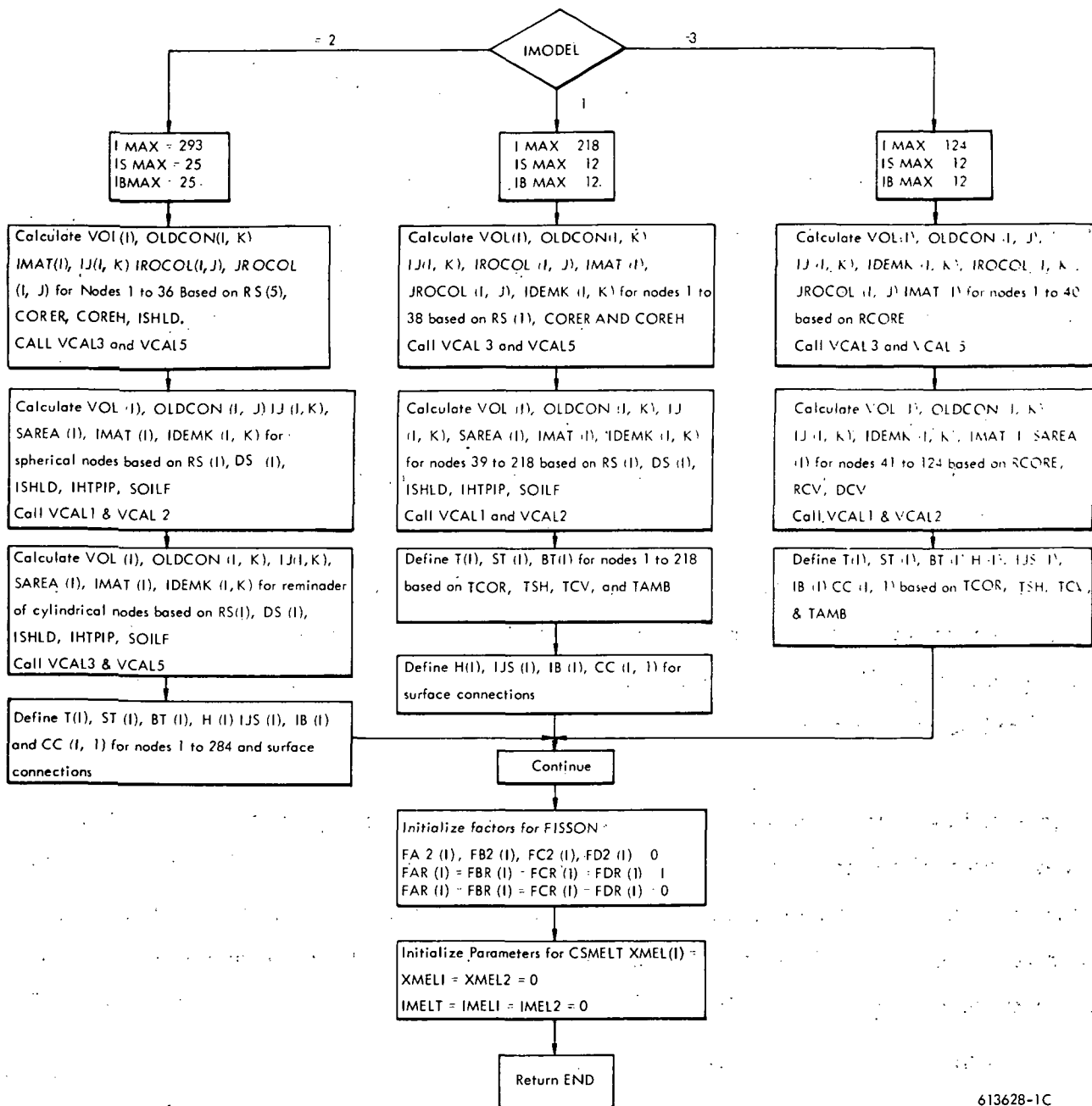
A total of ten subroutines are used to define the nodal structures for the undeformed, deformed, and in-pile test models. The main subroutine for defining these models, HTMGEN, was divided into six subroutines (HTMGEN, HTMGN1, HTMGN2, HTMGN3, HTMGN4, and HTMGN5) to meet storage limitations for the IBM-7094. These subroutines perform the following functions:

- HTMGN1 - defines undeformed model
- HTMGN2, HTMGN4, HTMGN5 - defines deformed model
- HTMGN3 - defines the in-pile test model

Four subroutines (VCAL1, VCAL2, VCAL3, and VCAL5) are used in the above subroutines for performing repetitive type calculations. Another subroutine, FIXPAM, is used to set up variables for calling these subroutines. The remainder of this discussion will consider HTMGEN as one subroutine.

A general flow diagram of HTMGEN (plus HTMGN1 through 5) is shown in Figure A-1 with a description of nomenclature presented in Table A-1. Figures A-2, A-3, and A-4 are the node structures for the undeformed reactor model, the deformed reactor model, and the in-pile test model respectively. This subroutine sets up the following arrays which define the basic model, and are used in VARK, POWER, CONDO, and other subroutines in ESATA.

VOL (i)	volume on node i
IJ (i, k)	index of node connected to node i by connection number k
IMAT (i)	material number of node i
OLDCON (i, k)	the length to area ratio for node i and connection number k
IDEMK (i, j)	define use of primary or secondary conductivity
	= 0, use primary or secondary conductivity
	= 1, use secondary conductivity which is a fixed value



613628-1C

Figure A-1. Summary Flow Diagram HTMGEN Subroutine

TABLE A-1
HTMGEN NOMENCLATURE

Symbol	
BT (i)	Temperature for boundary node i
CC (i, j)	Emittance for surface node i and connection j
COREH	Core height
CORER	Core radius
DS (i)	Thickness of shield layers and containment vessel i = 1, 5 for 4 shield layers and the vessel
H (i, j)	Heat transfer coefficient for surface node i and connection j
IB (i)	Boundary coefficient table number for surface node i.
IBMAX	Maximum boundary node index
IDEMK (i, j)	Trigger to define choice of conductivity for node i and connection j
	IDEMK = 0 primary conductivity
	IDEMK = 1 secondary conductivity
IHTPIP	Trigger for heat pipe operation
	IHTPIP = 1 Zero operation
	IHTPIP = 2 50 percent operation
	IHTPIP = 3 100 percent operation
IJ (i, j)	Index to denote node connected to node i by connection number j
IJS (i, j)	Index to denote boundary node connected to surface node i by connection j
IMAT (i)	Material index for node i
IMODEL	Trigger to denote model selection
	IMODEL = 1 undeformed model
	IMODEL = 2 deformed model
	IMODEL = 3 in-pile test model

TABLE A-1 (Continued)

<u>Symbol</u>	<u>Definition</u>
IROCOL (k, l)	Array to define node number in column k and row l
ISHLD	Trigger to denote shield selection
ISHLD = 1	heavy metal shield - LiH
ISHLD = 2	heavy metal shield-water
ISHLD = 3	heavy metal shield-water-heavy insulation
ISHLD = 4	composite shield
ISHLD = 5	heavy metal shield-LiH-heavy insulation
ISMAX	Maximum surface node index
JROCOL (k, l)	Trigger to denote presence of core or shield in column k and row l
JROCOL = 1	core
JROCOL = 2	shield
OLDCON (i, j)	Length to area ratio of node i for connection number j
RS (i)	Inner radius of shield layers and containment vessel i = 1, 5
SAREA (i)	Surface area of surface node i
SOILF	Fraction of soil burial
ST (i)	Temperature of surface node i
T (i)	Temperature of internal node i
TAMB	Ambient temperature
TCV	Containment vessel temperature
TSH	Shield temperature
TCOR	Core temperature
VOL (i)	Volume of node i

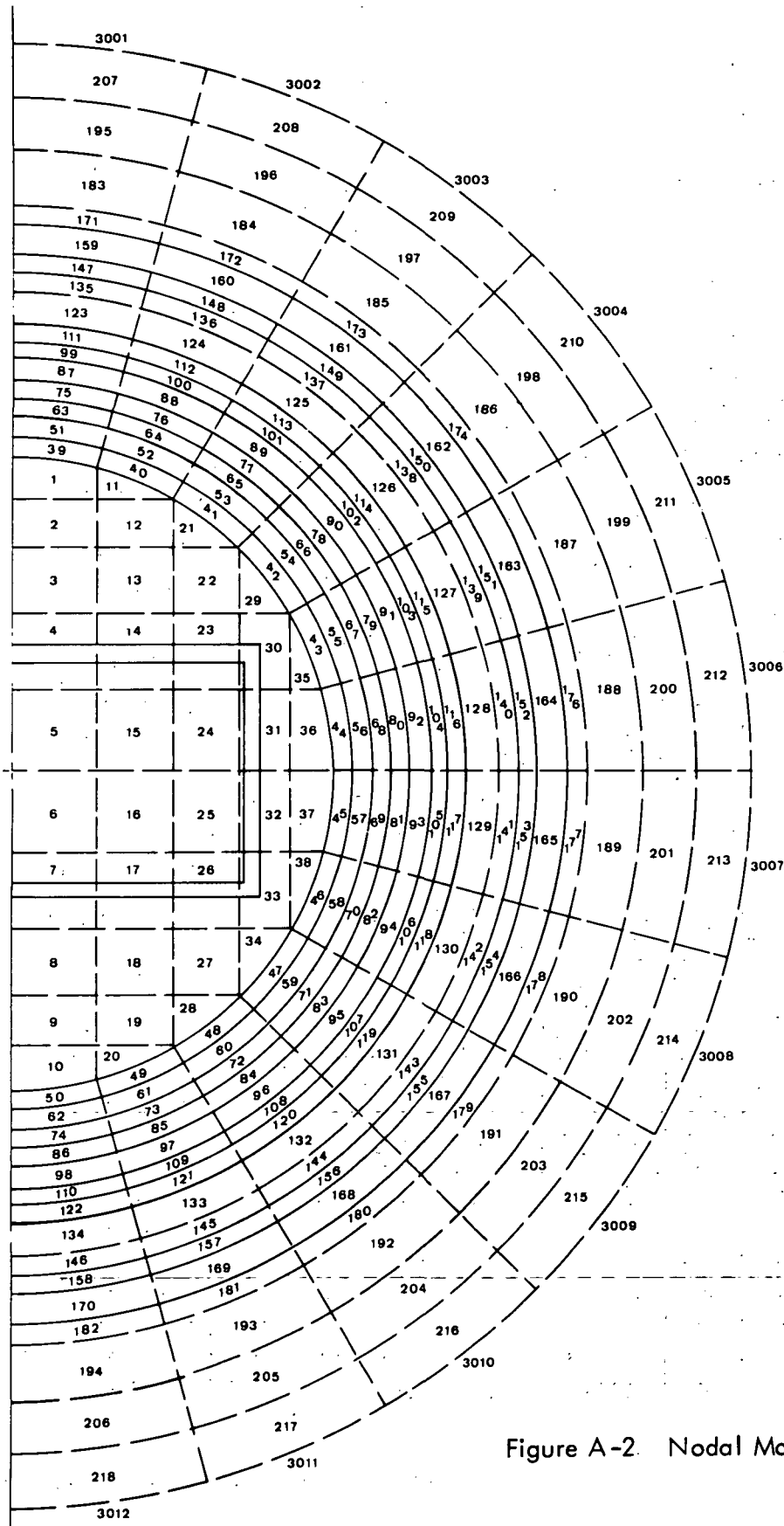


Figure A-2. Nodal Model for Undeformed HTM

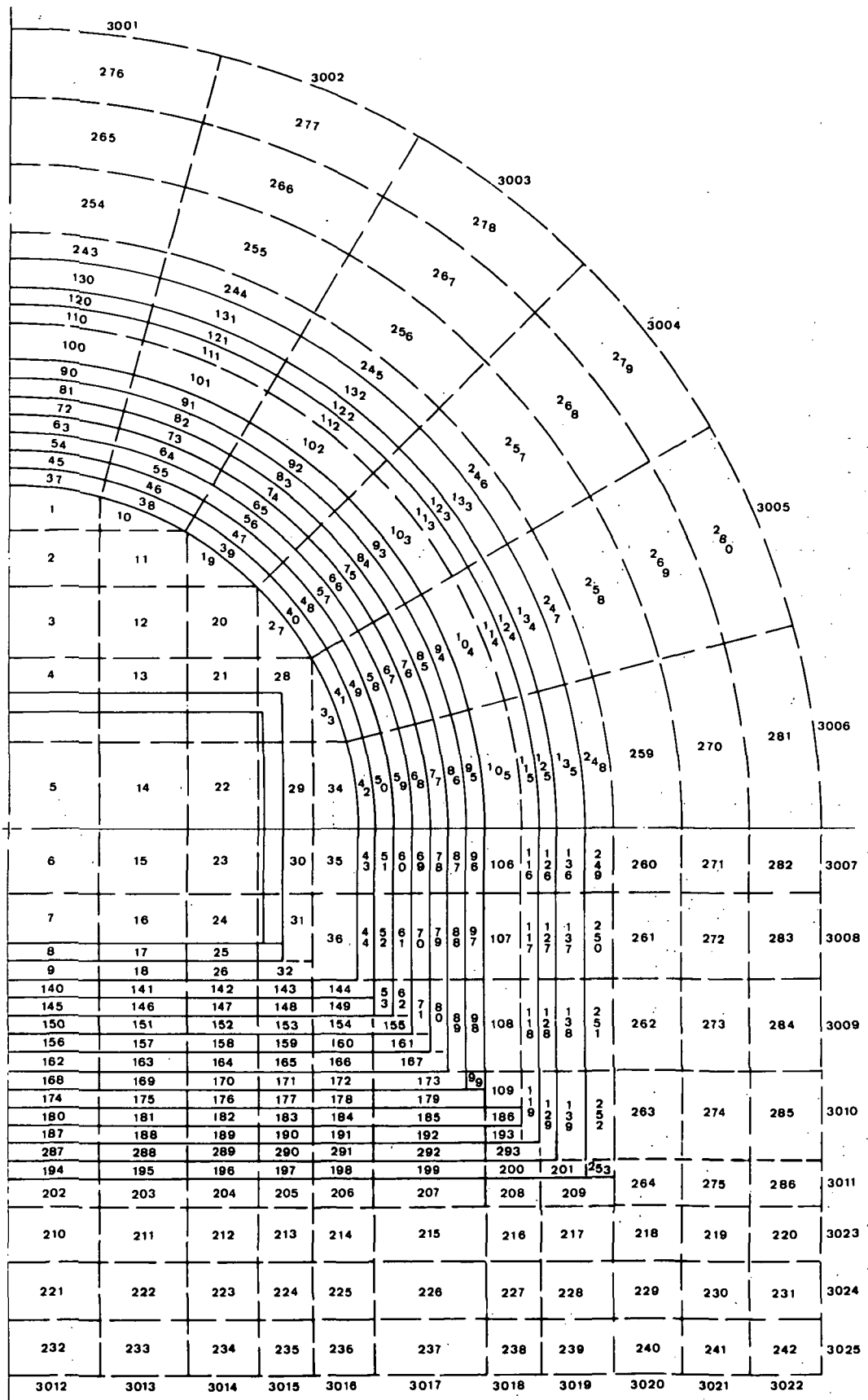


Figure A-3. Nodal Model for Deformed HTM

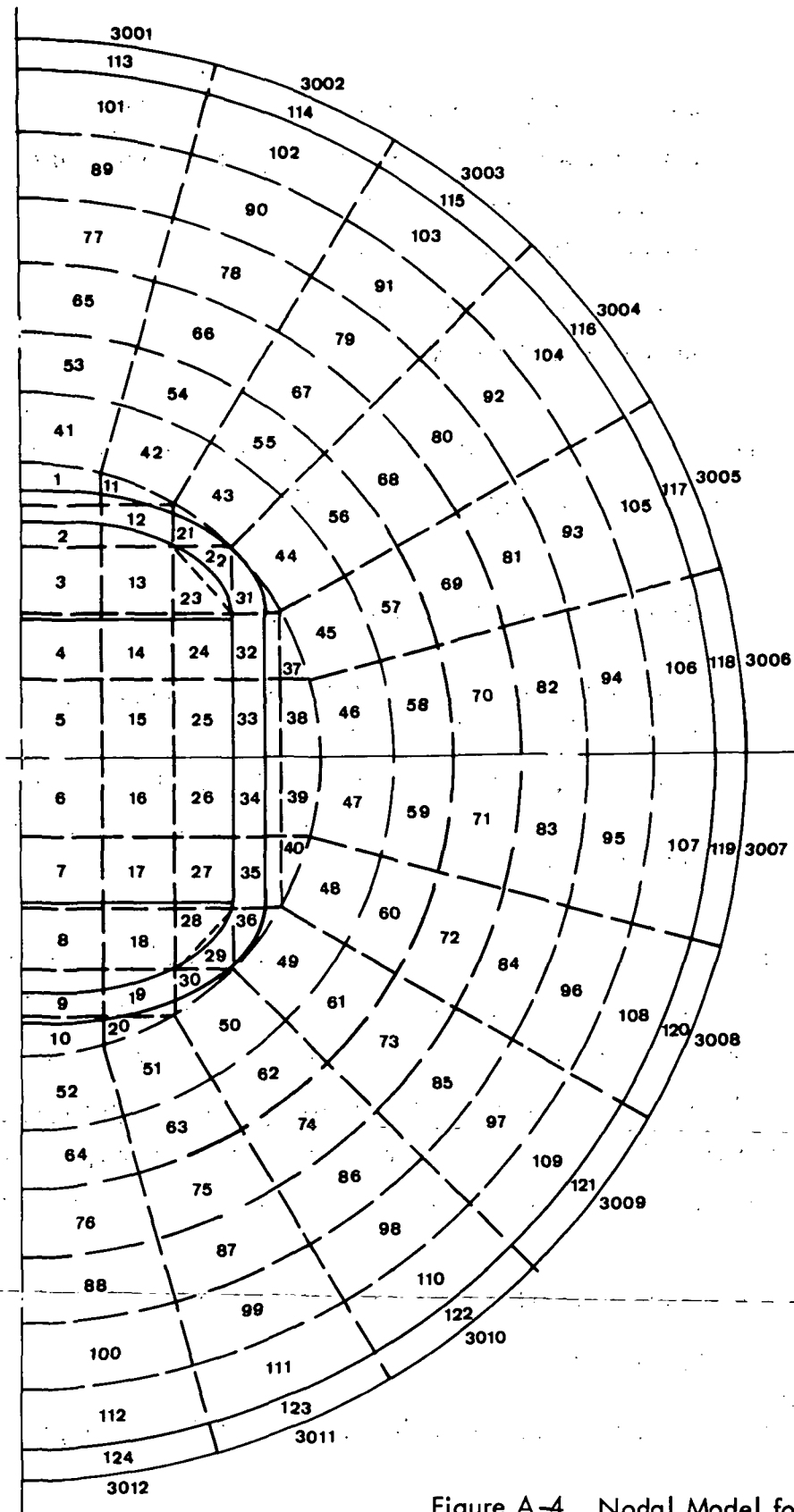


Figure A-4. Nodal Model for In-Pile Test Model

SAREA (i)	Surface area for surface to boundary connections
IJS (i)	Node index for internal or boundary node connected to node i
H (i)	Surface heat transfer coefficients
ST (i)	Surface node temperature
BT (i)	Boundary node temperature
T (i)	Internal node temperature

The following four subroutines were defined which store repetitive type calculations used to define the above described arrays. Figures A-5 to A-8 contains flow charts of these subroutines.

VCAL1	Calculates the volume, l/A 's, and material number for a row of spherical nodes
VCAL2	Calculates the volume and l/A 's for an individual spherical node. It is called from VCAL1.
VCAL3	Calculates the volume and l/A 's for a cylindrical node
VCAL5	Calculates the volume and l/A for three sided cylindrical to spherical interface nodes

The three nodal models are defined internally in HTMGEN based on key radii and material thicknesses which are read in as part of the input. This is accomplished by defining equations for each node to calculate the volume and length-to-area ratios. In addition the material numbers are assigned to each node. Based on the material number used, the properties are assigned to each node by table look up of permanently stored material properties, calculated parameters defined in the SHIELD subroutine, and fixed parameters stored in HTMGEN.

For the undeformed and deformed models the dimensions read in include:

- Core radius and height
- Inner radius and thickness of each heavy metal (W) shield layer

CALCULATE VOL(i), OLDCON(i, j), IMAT(i), IDEMK(i, j) FOR A ROW OF SPHERICAL NODES

$$R = (R_o + R_i) / 2$$

$$AE = 2 \pi R^2 (R_o - R_i)$$

$$Z4 = \left(\frac{R_i}{R} \right) \left(\frac{R - R_i}{2 \pi R_i^2} \right)$$

$$Z5 = \left(\frac{R_o}{R} \right) \left(\frac{R_o - R}{2 \pi R_o^2} \right)$$

$$Z6 = \left(\frac{R}{24} \right) (R_o^2 - R_i^2)$$

R_o OUTER RADIUS
 R_i INNER RADIUS
 K6 INITIAL NODE NUMBER IN A ROW
 K7 FINAL NODE NUMBER IN A ROW
 K8 SUBTRACTOR INDEX TO INNER ROW NUMBERS
 K9 ADDER INDEX TO OUTER ROW NUMBERS

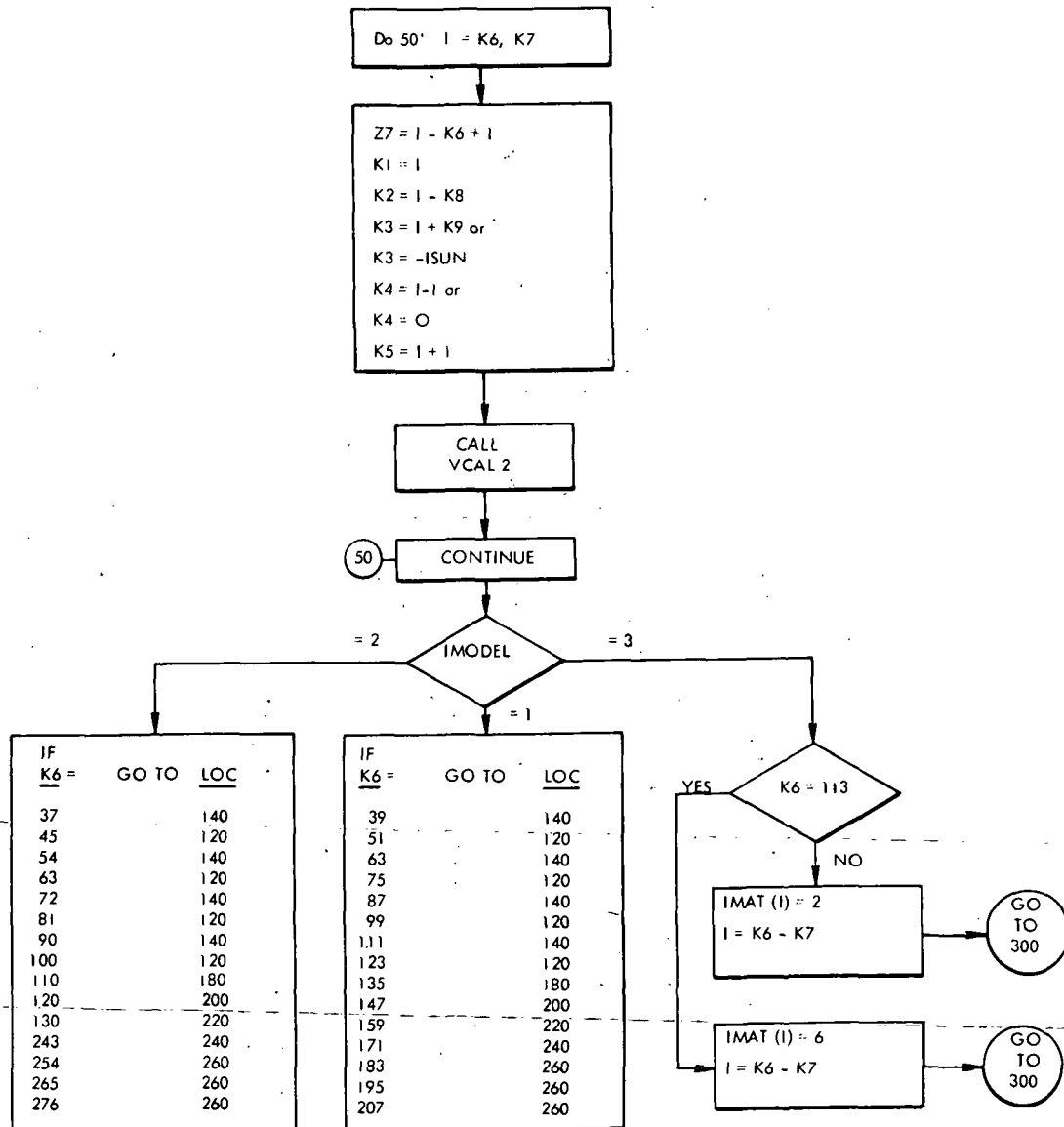
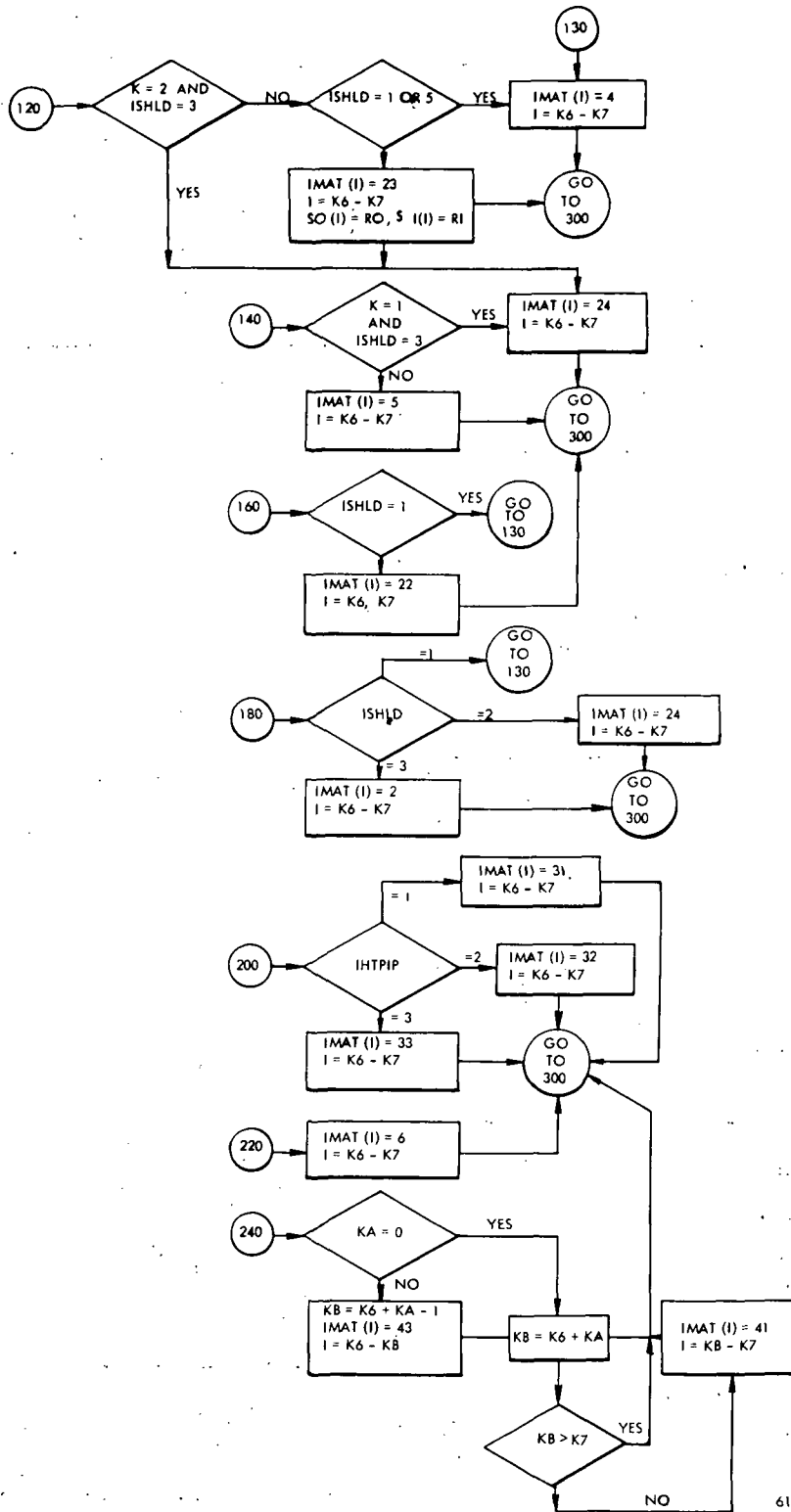


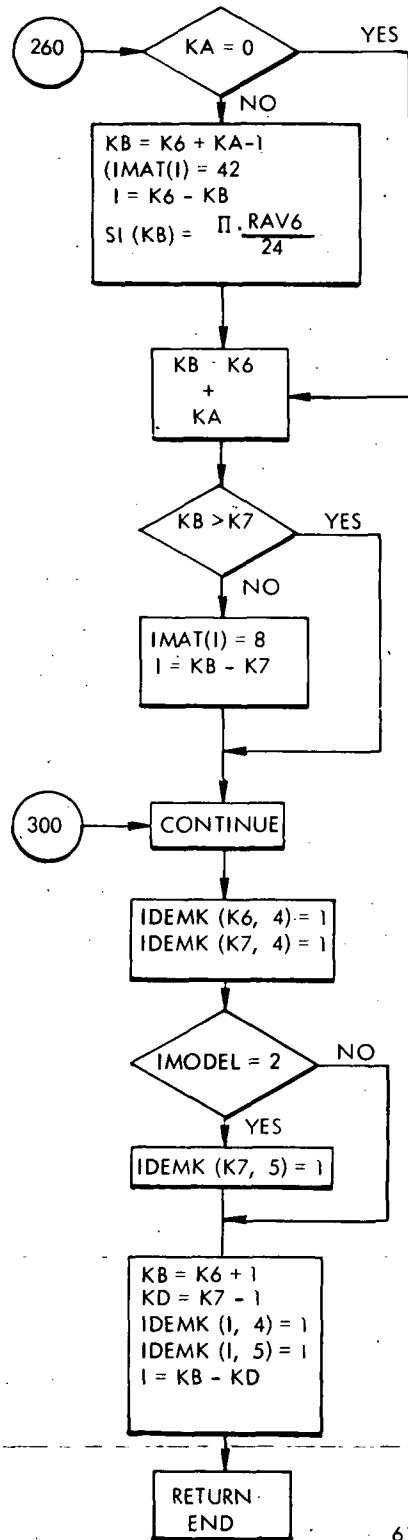
Figure A-5. VCAL1 Subroutine

613628-28



613628-3B

Figure A-5. (Continued)

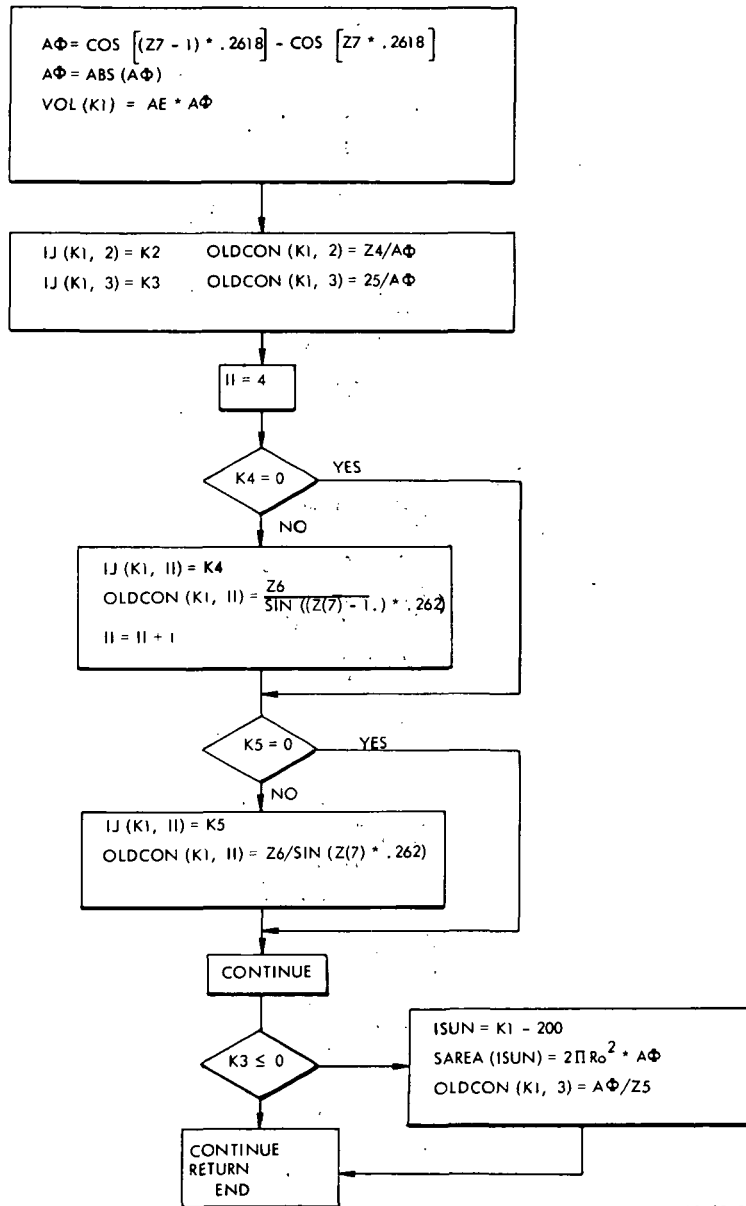


613628-4B

Figure A-5. (Continued)

CALCULATES VOL(i) IJ(i, k), OLDCON(i, k) FOR A SPHERICAL NODE

- K1 NODE BEING CALCULATED
- K2 NODE INSIDE K1
- K3 NODE OUTSIDE K1
- K4 NODE COUNTERCLOCKWISE AND ADJACENT
- K5 NODE CLOCKWISE ADJACENT
- Z4 LENGTHS DEFINED IN VCAL1
- Z5 LENGTHS DEFINED IN VCAL1
- Z6 LENGTHS DEFINED IN VCAL1
- Z7 NUMBER OF NODE CLOCKWISE FROM CENTERLINE
- AE AREA DEFINED IN VCAL1

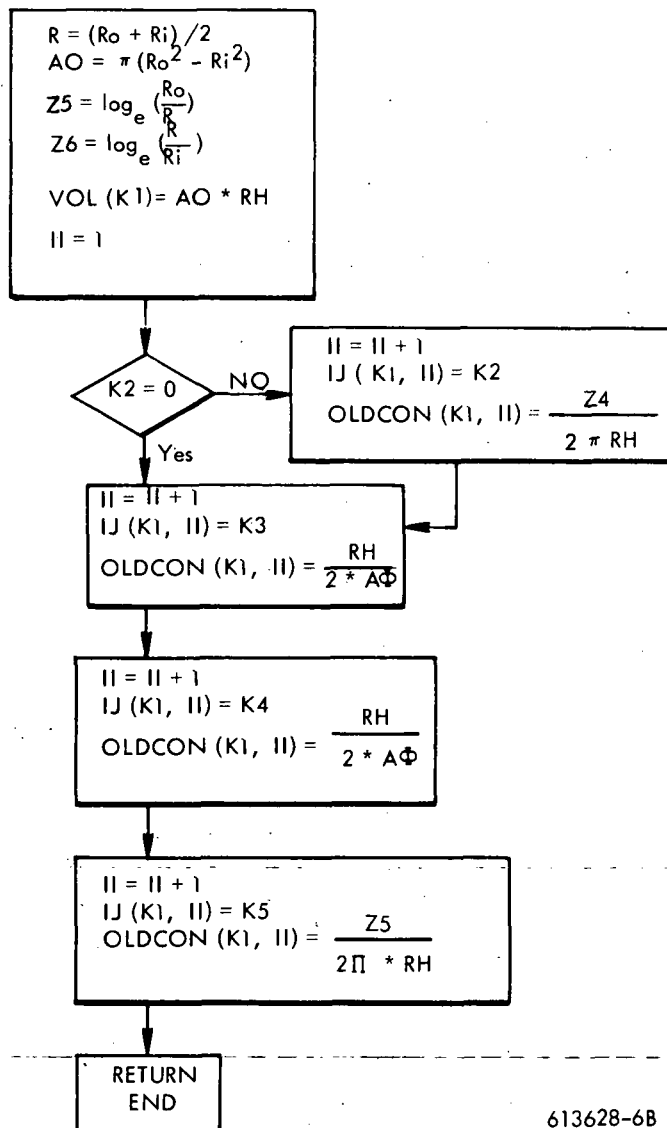


613628-5B

Figure A-6. VCAL2 Subroutine

CALCULATES VOL (i), IJ (i, k), OLDCON (i, k) FOR ANY CYLINDRICAL NODE

Ri INNER RADIUS
 Ro OUTER RADIUS
 RH THICKNESS
 K1 NODE NUMBER
 K2 ADJACENT NODE SAME ROW LEFT COLUMN
 K3 ADJACENT NODE UPPER ROW SAME COLUMN
 K4 ADJACENT NODE LOWER ROW SAME COLUMN
 K5 ADJACENT NODE SAME ROW RIGHT COLUMN



613628-6B

Figure A-7. VCAL3 Subroutine

Calculates VOL (i), OLDCON (i, k) for any 3 sided cylindrical to spherical interface node

- R_i inner radius
- R_o outer radius
- RHO Largest distance from horizontal reference line
- RHI Smallest distance from horizontal reference line
- K1 Node number
- K2 Adjacent node same row inner column
- K3 Adjacent node same column inner row
- K4 Adjacent node radially outward
- Z7 Node Position

RH	=	RHO - RHI
R	=	(R _o + R _i)/2
AO	=	$\pi (R_o^2 - R_i^2)$
Z5	=	$\log_e (R_o/R)$
Z6	=	$\log_e (R/R_i)$
RDR	=	$\frac{R_o - R_i}{2}$
RDX	=	RS (1) * .2618
RSS	=	.5 * (RH + RDR + RDX)
RR	=	$\sqrt{\frac{(RSS - RH) (RSS - RDR) (RSS - RDX)}{RSS}}$
RADR	=	$\left(\frac{AO}{2}\right) \left(1 + \frac{RH - RR}{RDR}\right)$
RAH	=	$\pi * R_i * RH * \left(1 + \frac{RDR - RR}{RDR}\right)$
Z8	=	(Z7-1) * .2618
Z9	=	(Z7-.5) * .2618
Z10	=	Z7 * .2618
RADX	=	$2\pi * RS (1)^2 \left[\cos (Z8) - \cos (Z10) \right] \left[1 + \frac{RDR * \sin (Z4) - RRR}{RDR * \sin (Z9)} \right]$
VOL (K1)	=	$\left[\frac{\pi/3}{\left[\frac{\cos (1.579 - Z9)}{\sin (1.579 - Z9)} \right]} \right] \left[\left(RS (1) * \sin (Z10) \right)^3 - \left(RS (1) * \sin (Z8) \right)^3 \right]$
	=	$3 * \left(RS (1) * \sin (Z8) \right)^2 * RH$
RADX	=	ABS (RADX)

IJ (K1, 2) = K2	OLDCON (K1, 2) = RR/RAH
IJ (K1, 3) = K3	OLDCON (K1, 3) = RR/RADR
IJ (K1, 4) = K4	OLDCON (K1, 4) = RR/RADX

613628-7B

RETURN
END

Figure A-8. VCAL5 Subroutine

- Inner radius and thickness of containment vessel
- Thickness of UO_2 insulation

For the in-pile test model the following dimensions are read in

- Inner radius and thickness of containment vessel
- Radius of minimum sphere that encloses core

Typical equations are shown below for representative nodes in the undeformed model (Figure A-9).

- a. Cylindrical node 13 (dimensions defined in Figure 5)

R_{s1} is the inner radius of the inner shield layer

δ_{s1} is the thickness of the inner shield layer

$$R_o = R_{s1} \sin 30^\circ$$

$$R_i = R_{s1} \sin 15^\circ$$

$$L_o = R_s \cos 45^\circ$$

$$L_i = R_s \cos 60^\circ$$

$$H = L_o - L_i$$

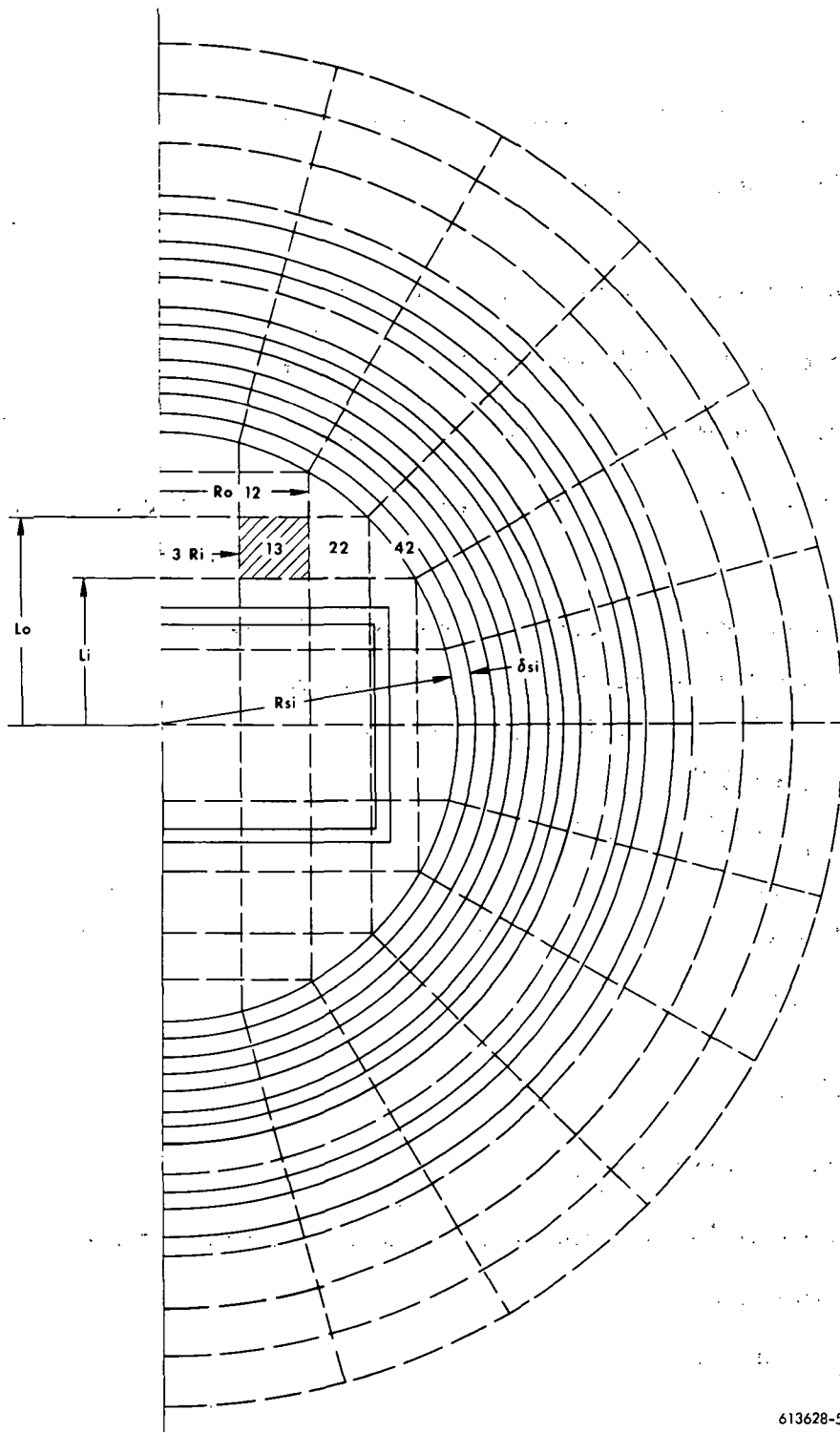
$$R = \frac{R_o + R_i}{2}$$

$$\text{VOL (13)} = \pi(R_o^2 - R_i^2) H$$

Equivalent $\frac{1}{A}$ in node 13 for the convecting node 13 to surrounding nodes are

Node 13 to Node 3

$$\frac{1}{A} = \frac{1}{2\pi H} \ln \frac{R}{R_i}$$



613628-52B

Figure A-9. Dimensions for Representative Nodes in an Undeformed HTM

Node 13 to Node 12

$$\frac{l}{A} = \frac{H}{\pi(R_o^2 - R_i^2)} = \frac{H^2}{2 \text{ VOL (13)}}$$

Node 13 to Node 14

$$\frac{l}{A} = \frac{H^2}{2 \text{ VOL (13)}}$$

Node 13 to Node 22

$$\frac{l}{A} = \frac{l}{2 \pi H} \ln \frac{R_o}{R}$$

These length to area ratios are in the node 13 only. To obtain the total conductance between 2 nodes (say 13 and 22 for example) the following relation exists:

$$Y(13, 22) = \frac{1}{\left(\frac{l}{K(13)}\right) \left(\frac{l}{2 \pi H}\right) \left(\ln \frac{R_o}{R_{13}}\right) + \left(\frac{l}{K(22)}\right) \left(\frac{l}{2 \pi H}\right) \left(\ln \frac{R_{22}}{R_o}\right)}$$

This is calculated in VARK.

b. Spherical Node 42

$$R_o = R_{s1} + \delta_{s1}$$

$$R_i = R_s$$

$$R = \frac{R_o + R_{s1}}{2}$$

$$\text{VOL (42)} = 2 \pi R^2 (\cos 45^\circ - \cos 60) \delta_{s1}$$

Equivalent $\frac{1}{A}$'s for connecting node 42 to surrounding nodes are

Node 42 to 29

$$\frac{1}{A} = \frac{\frac{R}{R_i} (R - R_i)}{2 \pi R^2 (\cos 45^\circ - \cos 60^\circ)}$$

Node 42 to node 43

$$\frac{1}{A} = \frac{\left(\frac{\pi}{24}\right)R}{\pi(R_o^2 - R_i^2)} = \frac{R}{24(R_o^2 - R_i^2)} \left(\frac{1}{\sin 60^\circ}\right)$$

Node 42 to node 41

$$\frac{1}{A} = \frac{R}{24(R_o^2 - R_i^2)} \left(\frac{1}{\sin 45^\circ}\right)$$

Node 42 to 54

$$\frac{1}{A} = \frac{\frac{R}{R_o} (R_o - R)}{2 \pi R_o^2 (\cos 45 - \cos 60)}$$

Similar type equations are defined for each of the nodes in the undeformed model for nodes representing the interface between cylindrical and spherical nodes. These nodes are represented approximately by a cylinder cut by an inclined plane perpendicular to the radius through the center of the spherical segment enclosing the node.

The deformed model contains spherical and cylindrical nodes which can be similarly defined by the radii and thicknesses that are input. Similar treatment is accorded to the in-pile test model.

APPENDIX B

HEAT GENERATION SUBROUTINES

B.1 FISSION PRODUCTS RELEASE AND DEPOSITION SURVEY

In the event of clad rupture or gross melting of the core, the fission products in the fuel will escape from the reactor core into the containment space, thereby tending to reduce heat generation in the molten fuel. This could conceivably relieve the melt-through problem. The effect of the release of fission products on afterheat distribution is therefore evaluated. The computer program developed takes into consideration such a heat source redistribution due to fission products release. By treating fission products in several groups according to their volatility, the transport of these products can be reasonably represented. The release rates of each group as a function of the time after shutdown and the temperature in the core are required to estimate the amount of the product transported at various times. By means of the redistribution subroutine, the deposition of these products on relatively cool surfaces is computed and the heat generation rates for these locations is adjusted accordingly. Decay heat curves, corresponding to each group of fission products, are therefore required as input data to the computer program. Heat source contributions from non-condensable gaseous products are also considered, where significant, by assigning heating rates to surface nodal points exposed to the gas. For these and other required data for the heat source redistribution model, a literature survey was completed which covered the work performed at ORNL, BNL, and other institutions such as BMI, BNW, LASL, and Westinghouse. The pertinent information from the survey is summarized and data input to the program are given in the following sections.

B.1.1 Product Groups According to Volatility

A basic study was made by Hilliard, et al, to determine the effects of temperature, time of heating, atmosphere in which heated, irradiation level, and specimen size on release of key fission product elements from irradiated normal uranium⁽³⁾. Experimentally measured

fractional release of radioisotopes in air, steam, and helium provides a means for grouping the isotopes roughly in the order of their decreasing volatility, i. e., volatile, semi-volatile, and non-volatile. Fission-product gas pressure in uranium oxide fuel elements was calculated over the temperature range of 1800 (1000) to 4500°R (2500°K)⁽⁴⁾. In an expanded table, five groups were listed by ORNL for the important fission product isotopes⁽⁵⁾. Since a UO₂ fuel is assumed, the group involving Ru, Te, and Mo will form oxides and becomes as volatile as Cs and I, and these groupings can be reduced to four groups as shown in Table B-1 with their elements.

B.1.2 Release Rates and Deposition

A number of factors affect the fission product release rates, i. e., heating time, temperature, volume to area ratio, depth of the condensed phase, fission product solubility in the liquid phase, and gas phase mass transfer.^(3, 6) Other factors such as the effect of containment system size can also be significant.⁽⁷⁾ The release rates also depend on the type of fuel, the degree of meltdown, the duration of the molten condition, the accessibility of coolant to the melted fuel,⁽⁸⁾ and the fuel burnup (irradiation exposure).⁽⁹⁾ Very limited data have been reported, for instance, the effect of the liquid depth on the release of iodine from molten U was shown in Figure B-1.⁽⁸⁾ Although attempts have been made to analytically describe the release rate by the diffusion mechanism in the literature, the process involves so many variables that no correlation can be found.

In lieu of experimental data for the release rates under specific reactor conditions, use was made of the results of the laboratory study of natural uranium cylinders in air and steam⁽³⁾ and the measured fission product emission from UO₂.⁽¹⁰⁾ Table B-2 indicates the available data from these references. By averaging the available data, the effect of fuel temperature on the release rates of different fission groups was estimated as shown in Figure B-2. To be useful in the computation scheme, the effect of temperature on the release rate is expressed as a multiplier factor applied to the reference release rate measured at a specified temperature. In other words, the relative variation of release rates due to the temperature effect was assumed constant at all times and the multiplier factor was determined by the normalized values

TABLE B-1
YIELDS AND CHARACTERISTICS OF
IMPORTANT FISSION PRODUCT ELEMENTS

	Isotope	Normal Boiling, (°R)	Boiling, (°K)	Weight Percent of Yield after 1 year of Irradiation*	
A. High Volatility	Kr	216	120	1.4	} 17.5
	Xe	297	165	15.3	
	Br	598	332	0.1	
	I	821	456	0.7	
B. Intermediate Volatility	Cs	1724	958	10.2	} 29.5
	Te	2268	1260	1.6	
	Ru	8105	4503	5.5	
	Tc	8771	4873	2.8	
	Mo	9131	5073	9.4	
C. Low Volatility	Sr	2950	1639	4.0	} 8.0
	Ba	3434	1908	4.0	
	Sb	3443	1913	-	
D. Refractory	Sm	3375	1875	1.5	} 45.0
	Pr	5927	3293	3.4	
	Y	5501	3056	1.9	
	Nd	6053	3363	11.8	
	La	6557	3643	3.6	
	Ce	6737	3743	9.8	
	Zr	8276	4598	12.7	
	Nb	9365	5203	0.3	

*Assumed thermal neutron flux, 5×10^{12} neutrons/cm² sec

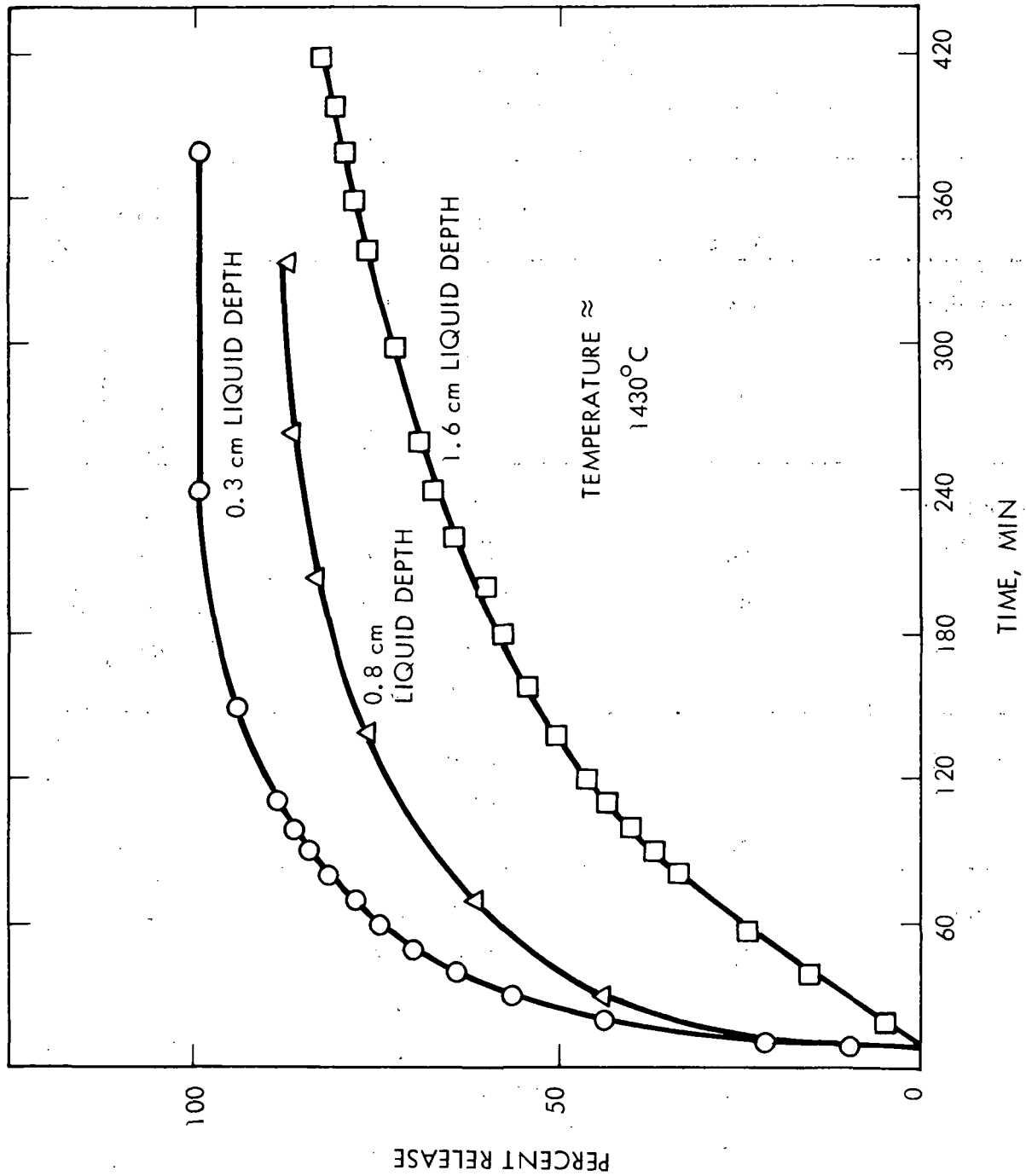


Figure B-1. The Effect of Liquid Depth on Iodine Release from Molten Uranium

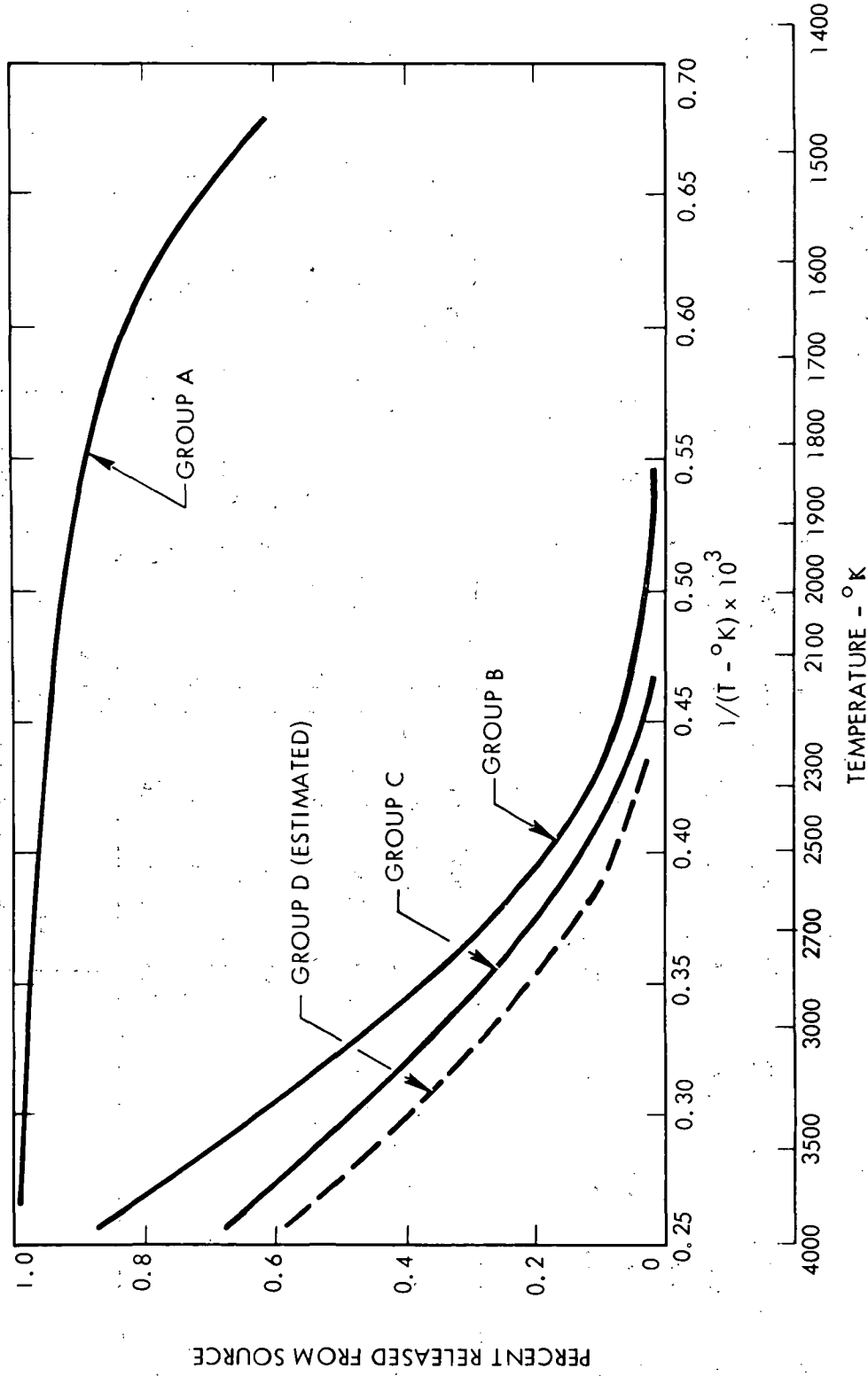


Figure B-2. Temperature Effect on Release of Fission Products (Time Range 20 Minutes Heating)

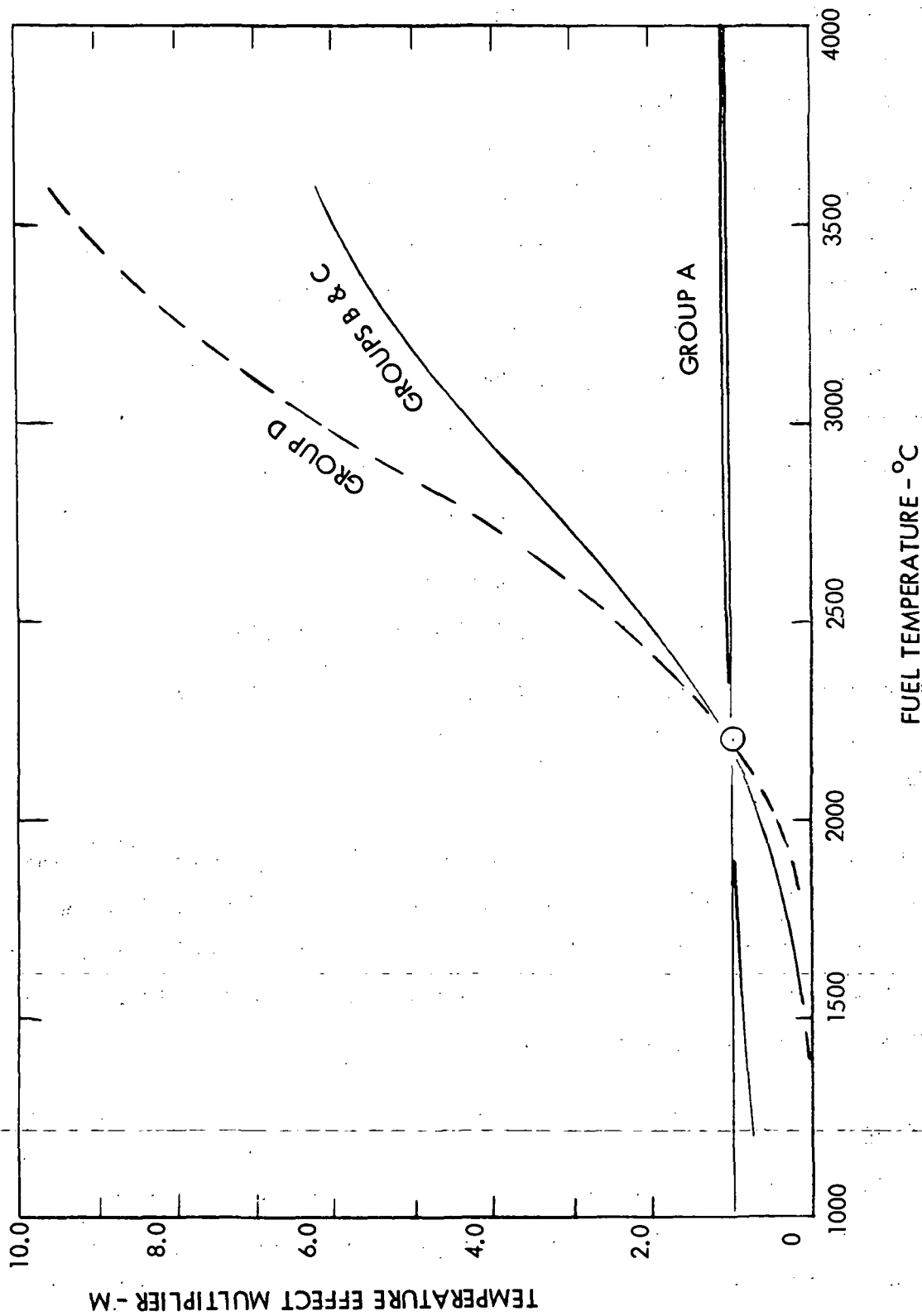


Figure B-3. Normalized Temperature Effect on Fission Product Release

for each group from Figure B-2. These multipliers are shown in Figure B-3. The reference fission product release versus time (at 2470°K) is shown in Figure B-4.⁽¹¹⁾ The deposition of fission products is assumed instantaneous upon hitting cold surfaces, since the latent heat of condensation of the fission products is considered negligible. Using thermochromatographic apparatus, Castleman and Tang studied the deposition of fission products from metallic uranium and U-Mo alloy released to the stream.⁽¹²⁾ They found at flow rates within the range of 5 to 250 cm³/minute, the deposition temperature of the iodine varied within 30°K. No significant difference was noted in the deposition results for experiments carried out over different periods (10 to 60 minutes). Likewise, experimental results showed that the deposition temperatures were independent of the distance from the heated fuel to the deposition region, as well as the temperature gradient. A typical fission product deposition pattern reported in Reference 12 was used as a basis for deposition temperature ranges of various groups (Table B-3).

TABLE B-3
DEPOSITION PATTERNS IN THERMAL GRADIENT TUBE

Temperature Range	470 to 870°K	870 to 1070°K	1070 to 1670°K
Deposition Fission Product Group	A	B	C, D

Other studies of fission-product deposition in out-of-pile loops were reported⁽¹³⁾ using mildly irradiated UC₂ fuel elements. The behavior of individual fission products, except iodine, was somewhat analogous to that of the gross mixture. Behavior of the fission products in the group, comprised of Ce, Ba-La, Zr-Nb, and Ru was comparable. These findings support the division of fission products by groups.

B.1.2 Decay Heat Curves

The effect of fission product redistribution on the afterheat distribution study lies in the fact that the fission product carries the decay heating out of the core with it, thus reducing the heat generation in the core. It is important, therefore, to determine the decay

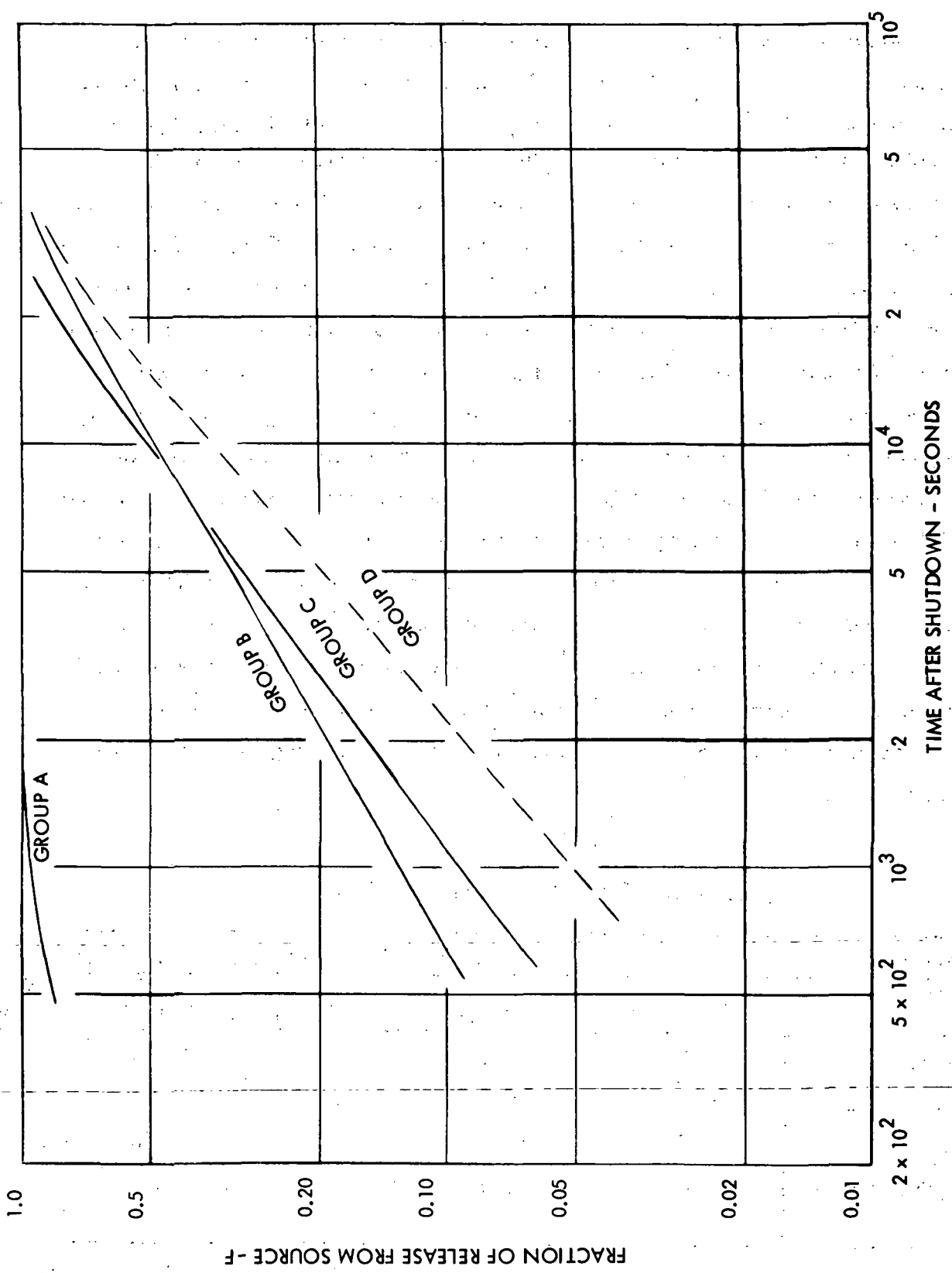


Figure B-4. Estimated Fission Product Release from UO_2 Fuel Reference Temperature = $2200^\circ C$

heat from individual fission product groups. From computations made by Bolles and Ballou, the percentage contributions of activity of chemical groups to total fission product activity after fission are obtained.⁽¹⁴⁾ These chemical groups are very close to the groupings used in the present computer program. For instance, the halogens and rare gases belong to Group A; alkali metals, noble metals and oxygenated anions to Group B; alkaline earths and miscellaneous groups to Group C; and rare earths and Nb and Zr belong to Group D. Figure B-5 shows the various contributions to the fission power expressed in percent of operating power versus time after reactor shutdown. Since the total energy distribution among each fission product group consists of beta and gamma rays,⁽¹⁵⁾ it may be desirable to separate these two sources of decay heat. An attempt was made to evaluate the contributions of gamma energy to the decay heat in various product groups. The relative gamma ray spectral distribution as a function of cooling time was reported in Shure's review.⁽¹⁵⁾ The decay energy for several gamma energy groups which were divided according to energy range were shown. To convert this information to the desirable decay curves for fission product groups according to volatility, the following procedure was used. The data on energy range and yield for important gamma-emitting fission products from the standard handbook⁽¹⁶⁾ were used to evaluate the relative spectral distribution for each important isotope in the fission product group. The sum of these distributions represents the normalized yield fraction in each energy range from the entire group, as shown in Table B-4.

TABLE B-4
NORMALIZED GAMMA ENERGY YIELD

Fission Product Group	Normalized Yield Fraction in Energy Range				
	0.1-0.4 Mev	0.4-0.9 Mev.	0.9-1.35 Mev.	1.35-1.8 Mev	1.8-2.2 Mev
A (Kr, Xe, I, Br)	1.15	0.22	0.29	0.54	1.0
B (Cs, Te, Rn, Tc, Mo)	0.29	0.18	0.44	0	0
C (Sr, Ba, Sb)	0.275	0.12	0.27	0.03	0
D (Sm, Y, Zr, Nb, La, Ce, Pr, Nd)	0.285	0.48	0	0.43	0
Total fission products	1.0	1.0	1.0	1.0	1.0

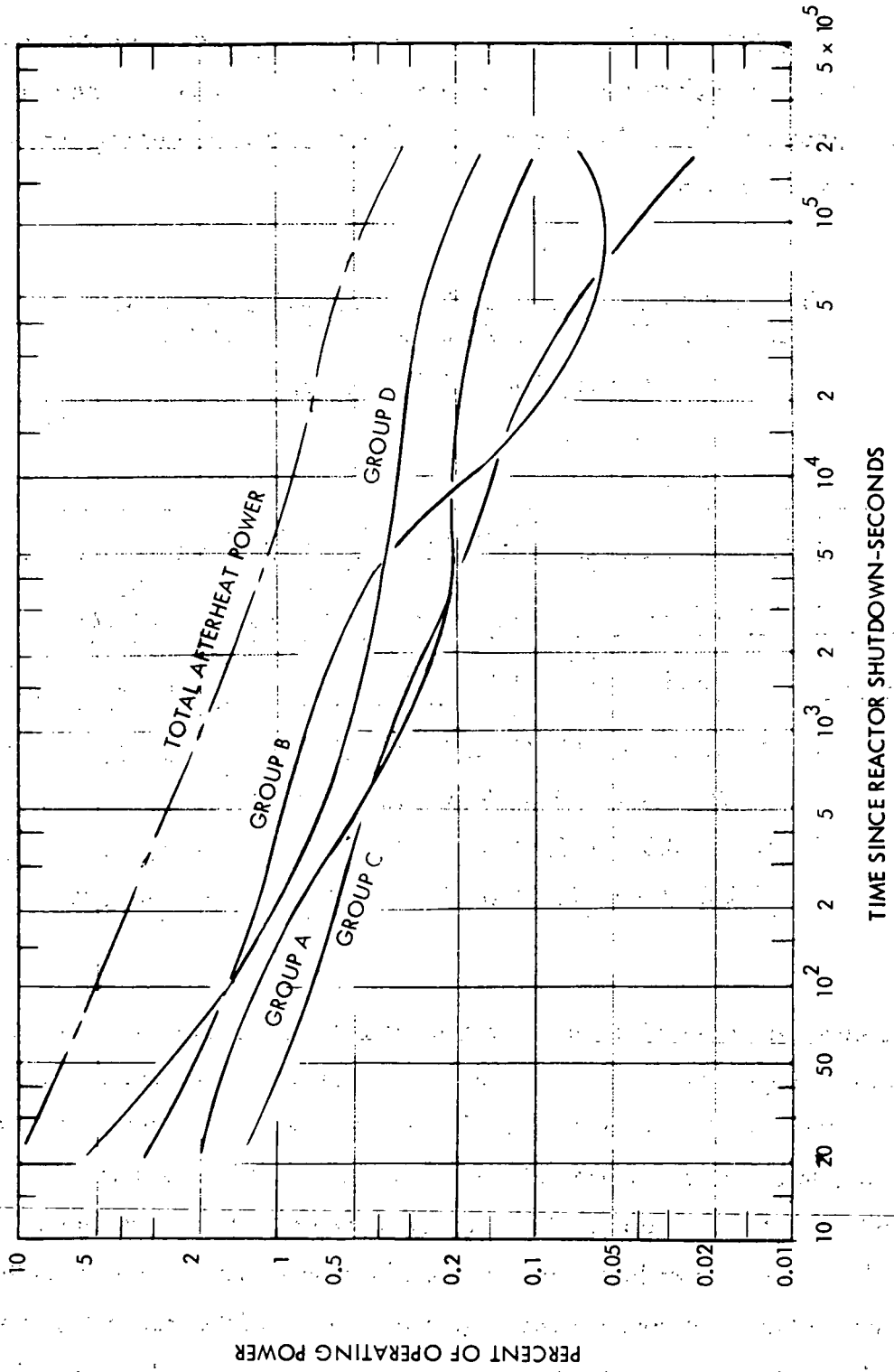


Figure B-5. Fission Product Decay Curves

Combining the normalized yield fraction in each gamma energy range with the reported decay energy for such energy range versus time resulted in a decay energy curve for the fission product group. Table B-5 illustrates the computation of fission decay gammas, after one year of reactor operations.

TABLE B-5
FISSION PRODUCT GROUP DECAY GAMMAS CALCULATION
BASIS: AFTER ONE YEAR REACTOR OPERATION
(Cooling Time = 10^2 Seconds)

Fission Product	Percent of Operating Power					Total Gamma
	0.1-0.4 Mev	0.4-0.9 Mev	0.9 - 1.35 Mev	1.35 - 1.8 Mev	1.8 - 2.2 Mev	
Total Fission Products	0.09	0.40	0.34	0.30	0.07	1.20
Group A	(0.15) (0.09)	(0.22) (0.4)	(0.29) (0.34)	(0.54) (0.3)	(0.07) (1)	0.43
Group B	(0.29) (0.09)	(0.18) (0.4)	(0.44) (0.34)	0	0	0.25
Group C	(0.28) (0.09)	(0.12) (0.4)	(0.27) (0.34)	(0.03) (0.3)	0	0.17
Group D	(0.285) (0.09)	(0.48) (0.4)	0	(0.43) (0.3)	0	0.35

The same procedure was repeated for different cooling times, and the resultant decay curves are shown in Figure B-6. By comparing the total decay heat curves of each fission product group with the gamma contribution in the same group, the beta ray contributions were calculated and are shown in Figure B-7. Because of the difference in the penetration to the shielding materials, this information may be used to differentiate the energy that will be readily absorbed at the surface of the node (beta energy) from that which attenuates in the nodal volume according to the density of the material (gamma energy). For simplicity, the gamma energy was assumed to be completely absorbed in the shield layer.

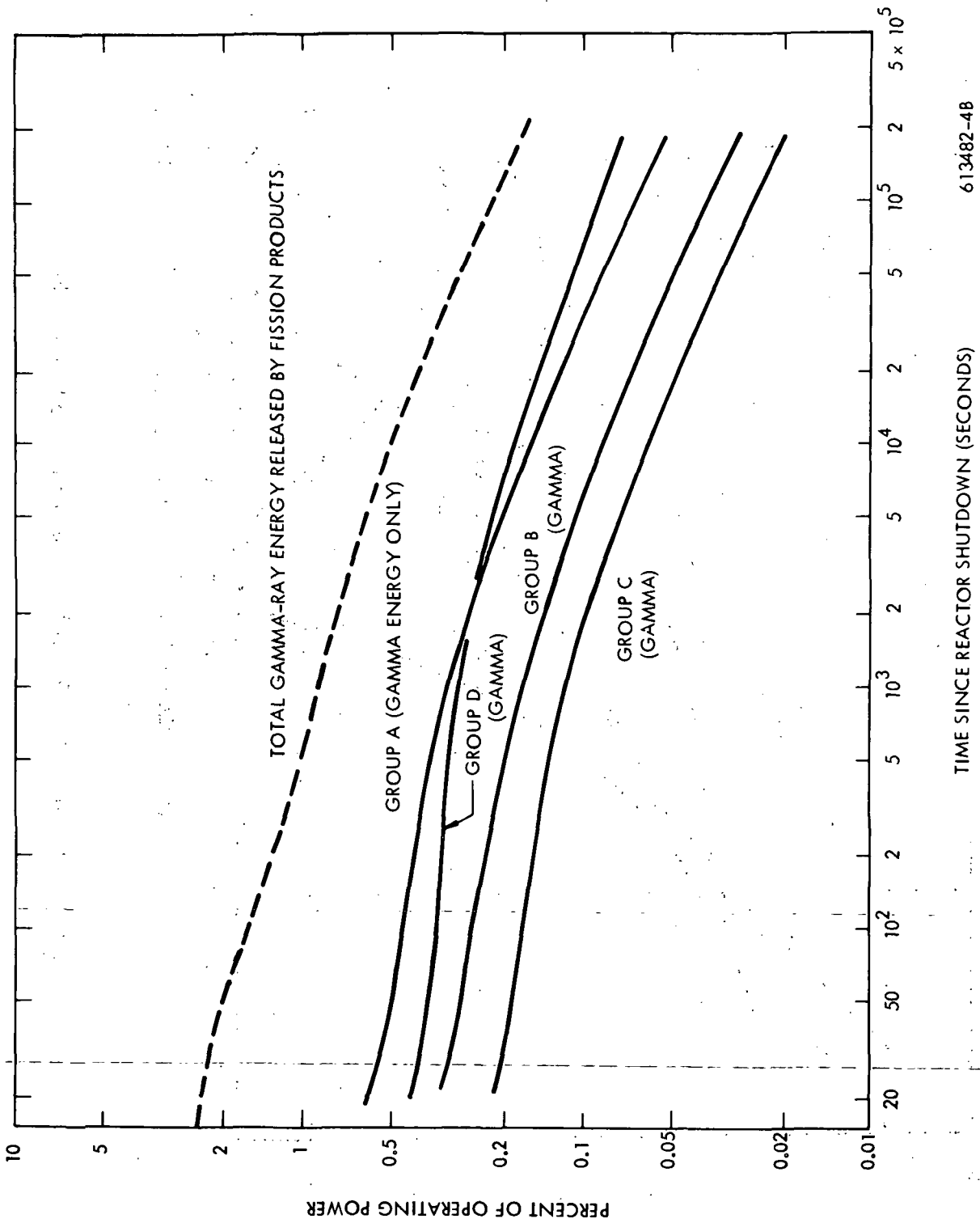
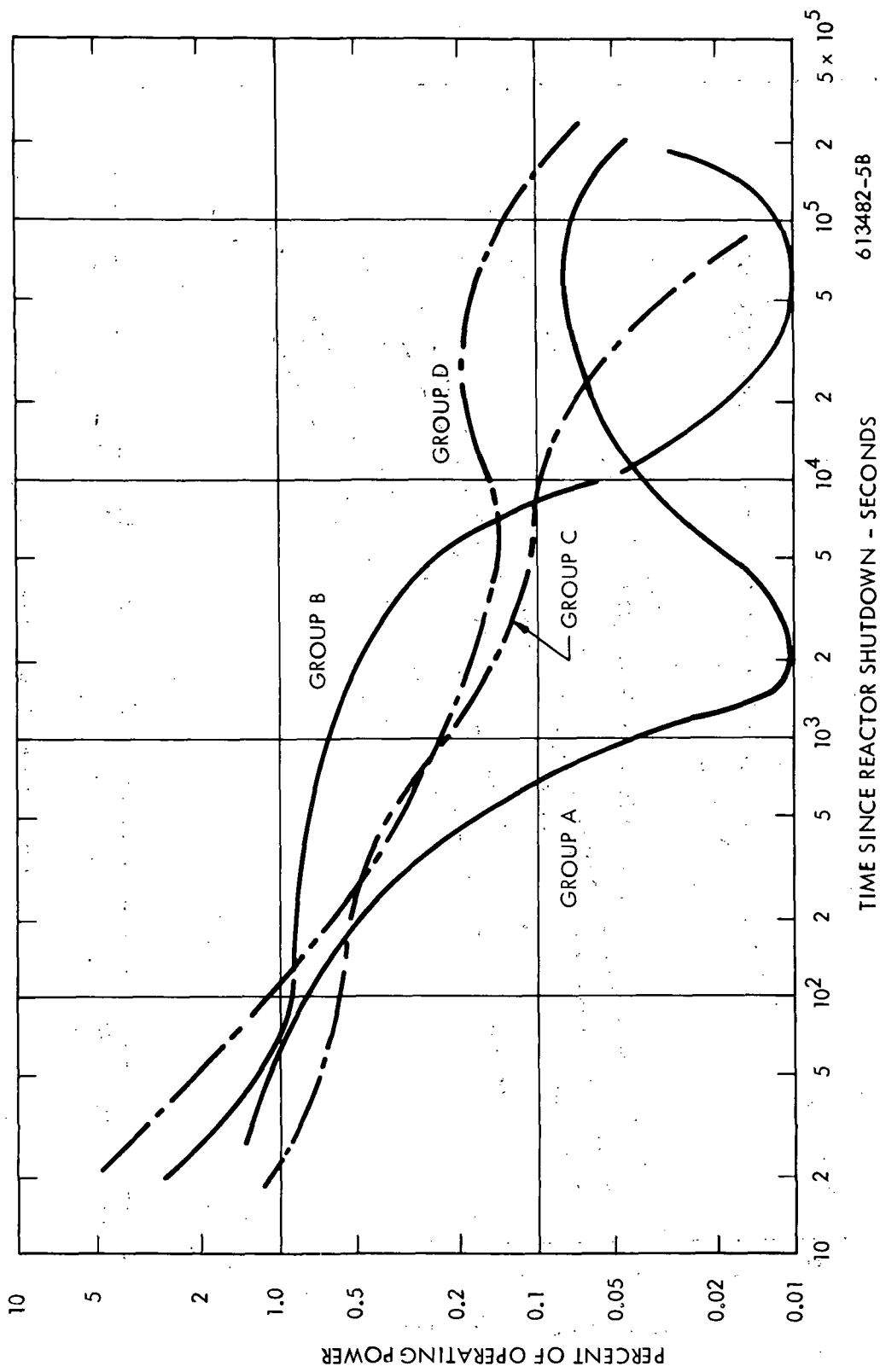


Figure B-6. Fission Product Decay Heat Curves Due to Gamma Emission After 1 Year Operation

613482-48



613482-5B

Figure B-7. Fission Product Decay Heat Curves Due to Beta Ray Emission

B.2 FISSON SUBROUTINE

In the FISSON subroutine the fission products were identified by four groups as listed in Table B-1 according to volatility. Each group was defined by a power decay rate Q_a , Q_b , Q_c , Q_d , which were calculated from the normal operating power level, Q_{tot} , and power decay factors, F_a , F_b , F_c , F_d as shown in Figure B-5.

Each fission product group is assigned a factor to determine the percent of fission vapor that escapes at the time (F_{a1} , F_{b1} , F_{c1} , F_{d1}). These factors were determined by the product of temperature dependent and time dependent factors represented by $F_{a1} = F_a(\tau) M_a(T)$ for group A. Values of $F(\tau)$ and $M(T)$ are shown in Figures B-3 and B-4, respectively. During the transient the F_{a1} , F_{b1} , F_{c1} , F_{d1} factors are not allowed to decrease with time nor exceed 1.0.

A second factor (F_{a2} , F_{b2} , F_{c2} , F_{d2}) is used to establish the fraction of escaped heat that gets to the nodes that qualify for receipt of heat.

To calculate these fractions, a temperature is assigned for each grouping to represent the maximum condensation temperature for that grouping. (T_a for group a, T_b for group b, etc.). Another set of fractions is used to define the percent of escape energy in each group that are deposited in each of the four shield layers and the vessel layer. ($F_{a1} - F_{a5}$ for group a, $F_{b1} - F_{b5}$ for group b etc.)

As energy is released from the core for any of the groupings at any time step, it is allowed to condense on all of the nodes on the innermost shield layer that are below the condensation temperature for that grouping. The heat of condensation or evaporation is considered as negligible compared to the fission decay power level. If there are no nodes below the condensation temperature, the amount of fission products released is transported on to the next layer. In a subsequent time step, if a node rises above the condensation temperature for any grouping, the fraction of that grouping that is deposited on that node is released to

the next radial layer. That fraction of fission products is condensed on any nodes in the next layer that are below the condensation temperature. The fractions of energy in each layer (Fas 1, Fas 2, etc) is adjusted to account for these transfers from layer to layer. If none of the nodes in the next shield layer is below the condensation temperature, then that fraction of fission products is passed to the next layer. By this process of condensation followed by evaporation, the energy factors is "walked out" from layer to layer to the vessel. Energy that has been deposited on the containment vessel and is driven off by evaporation is treated as a vapor and will contribute to the pressure buildup. The fraction of energy assigned to each layer for each group, (Far (i) Fdr(i), are used to calculate the fractions of the energy deposited in individual nodes on a volume weighted basis

$$Fa2 (j) = Far (i) \frac{V (j)}{V_{tot a}}$$

where j denotes the node number, i denotes the row number, V (j) is the volume of node j, $V_{tot a}$ is the total volume of eligible nodes in row i.

The equation for calculating the new temperature for any node is defined in CONDO as:

$$T' (i) = \frac{Q_{into}^{(i)} + Q_{inti}^{(i)} + eC_p VT (i)/\Delta\tau + \sum \lambda(i, j) T (j)}{\sum \lambda (i, j) + \frac{eC_p V}{\Delta\tau}}$$

where Q_{into} is the heat generated due to fission products and Q_{inti} is the heat generated due to the water metal reaction. The definition of Q_{into} takes different forms for core and shield nodes. Excluding consideration of water vapor transport, the equation of Q for a core node is:

$$Q_{into} = \left[Q_a (1-F_{a1}) + Q_b (1-F_{b1}) + Q_c (1-F_{c1}) + Q_d (1-F_{d1}) \right] Fv$$

where F_v is the fraction of the total energy deposited in each core node and is simply defined on a volume weighted basis. For shield and vessel nodes the equation for Q would be:

$$Q_{\text{into}}(i) = Q_a F_{a2}(i) + Q_b F_{b2}(i) + Q_c F_{c2}(i) + Q_d F_{d2}(i)$$

Figure B-8 is a simplified flow chart illustrating the above described logic.

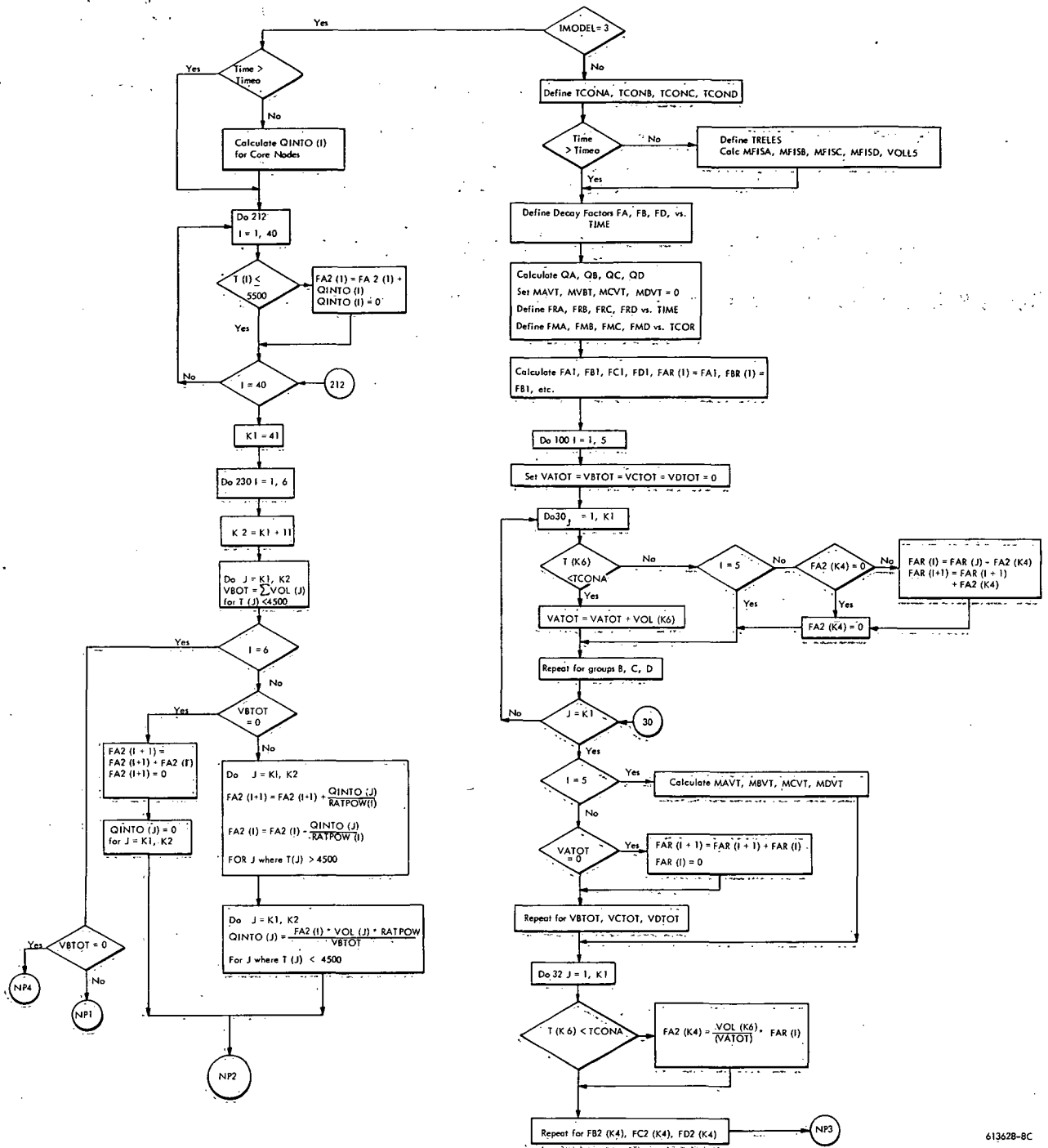
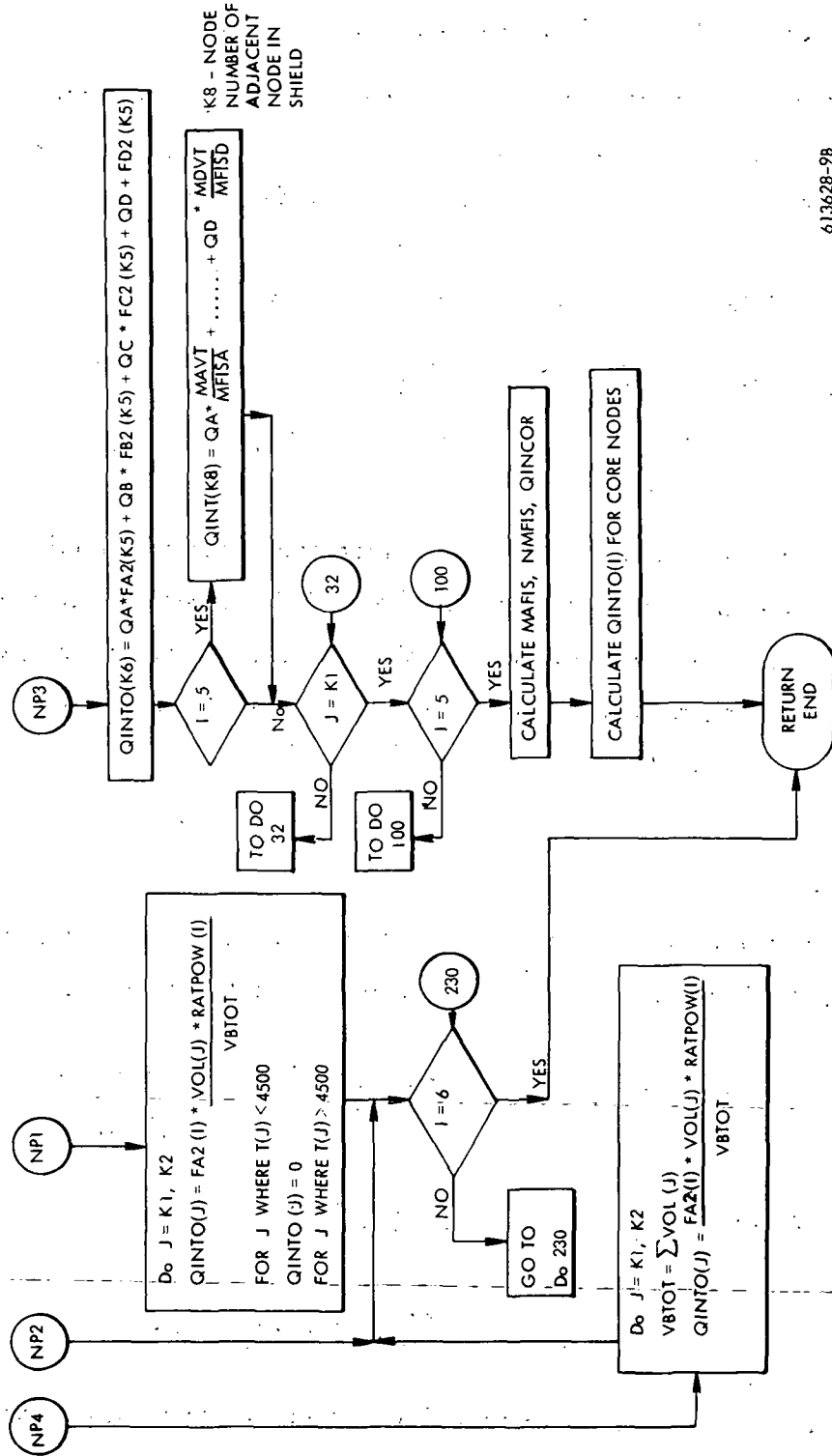


Figure B-8. FISSON Subroutine

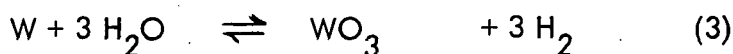
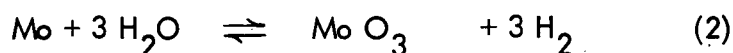
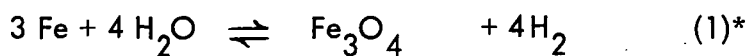


613628-98

Figure B-8. FISSON Subroutine (cont.)

B.3 WATER-METAL REACTIONS (REACT SUBROUTINE)

In order to evaluate the reaction rates as a function of temperature and the accompanying thermal effects, the materials in the reactor core that react with water, or steam are specified. These are stainless steel, molybdenum and tungsten. The principal reactions are:



Although the form of reaction is similar, the refractory materials show a behavior different from that of steels or aluminum. The oxidation of steel or aluminum forms a protective oxide layer, but the refractory metals do not. For instance, the oxides of Mo and W are volatile at reactor temperatures. This fact causes higher reaction rates than that for aluminum and steels.

Reaction Rates

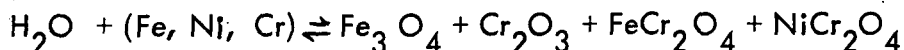
The rate data for the steam oxidation of Mo and W between 1370°K and 1970°K are shown in Figures B-9 and B-10. (17) The corresponding Arrhenius equations are:

$$(k)_{\text{rctn 2}} = (6.58 \pm 1.54) \times 10^2 \exp\left(\frac{-54400 \pm 700}{RT}\right) \frac{\text{g-atom metal}}{(\text{cm}^2) (\text{Min})}$$

$$(k)_{\text{rctn 3}} = (1.69 \pm 0.59) \times 10^2 \exp\left(\frac{-48900 \pm 1000}{RT}\right); 1323^\circ\text{K} < T < 1723^\circ\text{K}$$

$$(0.28 \pm 0.18) \times 10^2 \exp\left(\frac{-22700 \pm 2200}{RT}\right); 1723^\circ\text{K} < T < 1973^\circ\text{K}$$

* A more detailed reaction between stainless steel and steam may be expressed as:



The number of atoms for metals to react with oxygen is essentially same for each component in the steel.

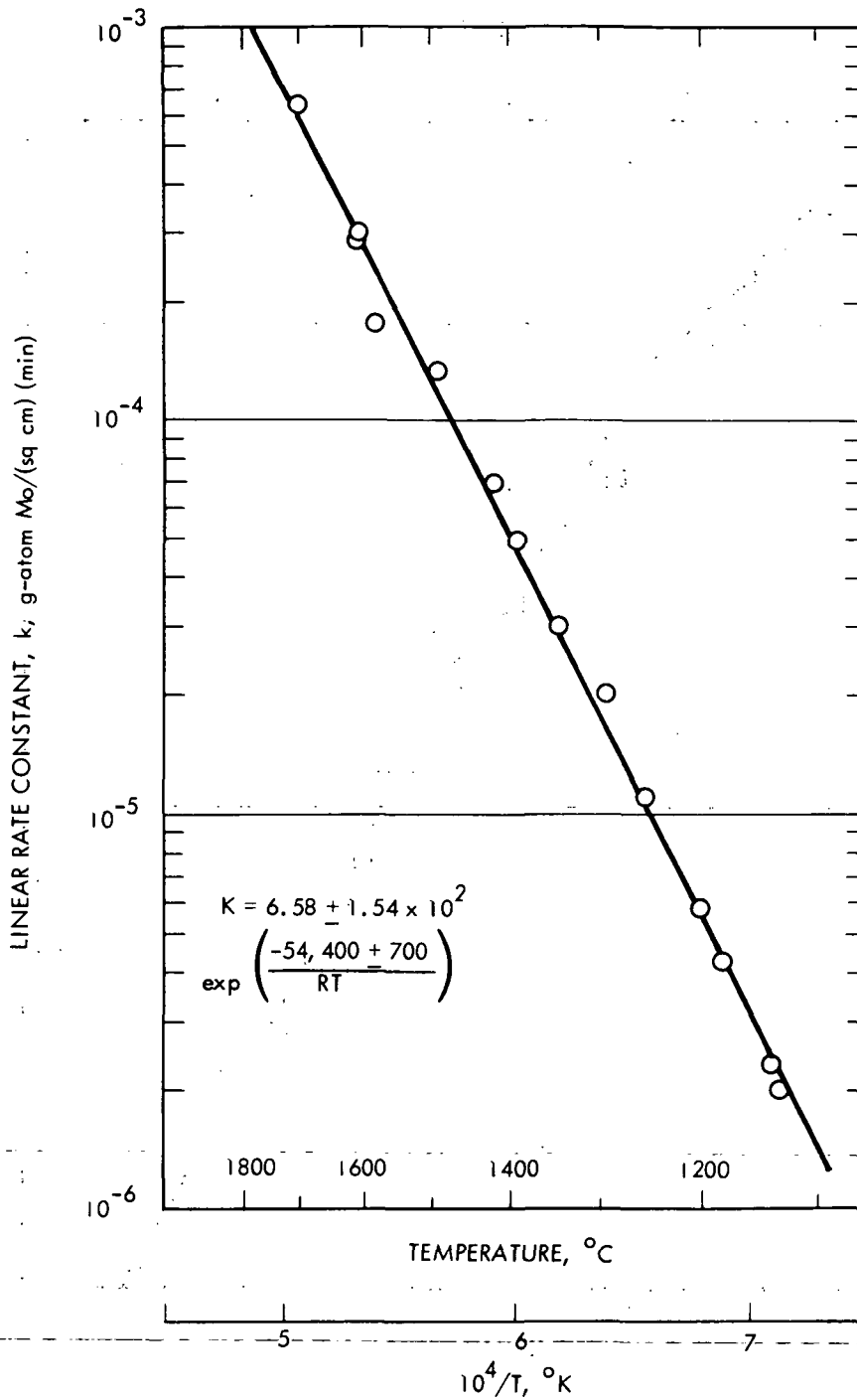


Figure B-9. Linear Rate Constants for the Molybdenum-Steam Reaction (1100-1700°C)

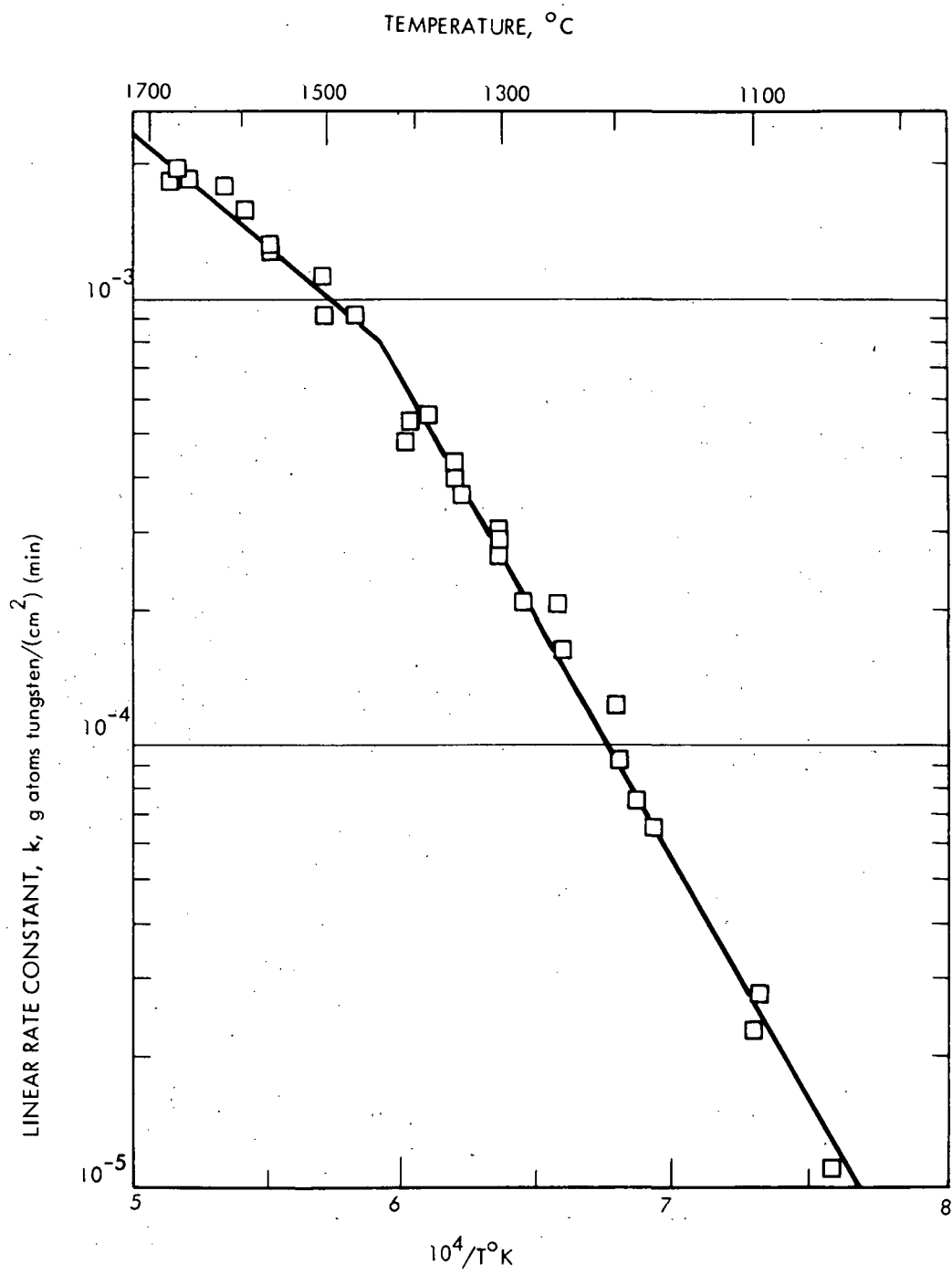


Figure B-10. Arrhenius Plot for the Tungsten-Steam Reaction

where k is linear rate constant, R = universal gas constant and T is absolute temperature, $^{\circ}\text{K}$.

The rate of oxidation of stainless steel is estimated from the experimental data ⁽¹⁹⁾ in terms of the linear rate constants as,

$$(k)_{\text{rctn 1}} = 2.58 \times 10^5 \exp(-21060/RT) \frac{\text{ml H}_2 \text{ evolved}}{(\text{g-metal}) (\text{Min})}$$

or, using the geometry of the reactor (pressure tube surface area to weight ratio = $2.21 \frac{\text{gm}}{\text{cm}^2}$) the rate constant becomes,

$$(k)_{\text{rctn 1}} = 5.68 \times 10^2 \exp(-21060/RT) \frac{\text{ml H}_2 \text{ evolved}}{(\text{cm}^2) (\text{min})}$$

or

$$19.2 \exp(-21060/RT) \text{ g-atom metal}/(\text{cm})^2 (\text{min})$$

Before the melting of pressure tubes in the reactor, only steam-stainless reaction prevails. As the stainless steel melts, the contact of Mo and steam results in the Mo-H₂O reaction.

$$\begin{aligned} \text{Total stainless steel surfaces } A_1 &= (279) (3.3") (\pi) (42") = 120,000 \text{ in}^2 \\ \text{(before melting)} &= 7 \times 10^5 \text{ cm}^2 \end{aligned}$$

The extent of the reaction depends on the amount of water available in the system. It is, therefore, more convenient to express the reaction rate in terms of steam consumption rate:

For $k = 0.031 \text{ g - atom Fe/cm}^2 \text{ min at } 1670^{\circ}\text{K}$,

Rate of Steam Consumption

$$\begin{aligned} &= (0.031) (7 \times 10^5) \left(\frac{4}{3}\right) (18) \quad \text{gm/min} \\ &= 5.2 \times 10^5 \text{ gm/min or } 1150 \text{ lb/min} \end{aligned}$$

Since the time required to use up all steam in the reactor is about the same order of magnitude as the time to melt the pressure tubes, the reaction between Mo and H₂O should be considered. The surface available for reaction in this case becomes increased because the number of fuel pins are 19 times the number of pressure tubes.

Thus,

$$A_2 = (259) (19) (0.47") (42") (\pi) = 3.05 \times 10^5 \text{ cm}^2$$

Rate of Steam Consumption at 1770°K

$$= (10^{-4}) (3 \times 10^5) (3) (18) = 1600 \text{ gm/min or } 3.3 \text{ lb/min}$$

Rate of Steam Consumption at 2070°K

$$= (10^{-3}) (3 \times 10^5) (3) (18) = 16,000 \text{ gm/min (33 lb/min)}$$

Heats of Reaction

Thermodynamic data of these reactions are compiled by Elliot and Gleiser⁽²⁰⁾ which are presented in Tables B-6 and B-7.

The heats of reaction for stainless steel and for Mo are calculated at two temperatures:

$$\Delta H_1 = -12 \frac{\text{kcal}}{\text{g-atom Fe}} \quad \text{or} \quad -900 \frac{\text{Btu}}{\text{lb-steam}} \quad \text{at } 1670^\circ\text{K}$$

$$\Delta H_1 = -6 \frac{\text{kcal}}{\text{g-atom Fe}} \quad \text{or} \quad -450 \frac{\text{Btu}}{\text{lb-steam}} \quad \text{at } 2070^\circ\text{K}$$

$$\Delta H_2 = 53 \frac{\text{kcal}}{\text{g-atom Mo}} \quad \text{or} \quad 1800 \frac{\text{Btu}}{\text{lb-steam}} \quad \text{at } 1670^\circ\text{K}$$

$$\Delta H_2 = 50 \frac{\text{kcal}}{\text{g-atom Mo}} \quad \text{or} \quad 1700 \frac{\text{Btu}}{\text{lb-steam}} \quad \text{at } 2070^\circ\text{K}$$

TABLE B-6
HEAT AND FREE ENERGY OF FORMATION OF MoO₃

MoO₃ (c, l, g)
Mol. wt. 143.95

<i>T</i> , °K	ΔH_f° , cal/mole	ΔF_f° , cal/mole	<i>T</i> , °K	ΔH_f° , cal/mole	ΔF_f° , cal/mole
298.15	-178,100 (±100)	-159,700 (±200)	1,600	-113,800	-93,200
			1,700	-113,800	-91,900
400	-177,800	-153,400	1,800	-113,800	-90,600
500	-177,400	-147,400	1,900	-113,800	-89,300
600	-177,000	-141,400	2,000	-113,800	-88,100
700	-176,500	-135,600	2,100	-113,800	-86,800
800	-175,900	-129,700	2,200	-113,800	-85,500
900	-175,400	-123,900	2,300	-113,800	-84,200
1,000	-174,700	-118,300	2,400	-113,800	-82,900
1,068	-174,300	-114,300	2,500	-113,800	-81,600
1,068	-162,400	-114,300	2,600	-113,800	-80,300
1,100	-161,800	-112,900	2,700	-113,800	-79,100
1,200	-160,300	-108,500	2,800	-113,800	-77,800
1,300	-159,300	-104,200	2,880	-113,800	-76,700
1,400	-158,200	-100,100	2,880	-120,400	-76,700
1,500	-157,000	-95,900	2,900	-120,400	-76,400
1,553	-156,500	-93,800	3,000	-120,400	-74,900
1,553	-113,800	-93,800			

Phase changes

METAL

M.P., 2,880°K; $\Delta H_m = 6,600$ cal/gin-atom

OXIDE

M.P., 1,068°K; $\Delta H_m = 11,910$ cal/mole

B.P., 1,553°K; $\Delta H_v = 42,700$ cal/mole

SOURCES OF DATA

Heat of formation: A. D. Mah, *J. Phys. Chem.*, **61**, 1572 (1957). High-temperature heat contents of crystalline and liquid oxide: L. A. Cosgrove, and P. E. Snyder, *J. Am. Chem. Soc.*, **75**, 1227 (1953). Melting point of oxide: L. Brewer, *Chem. Reviews*, **52**, 1 (1953). Heat of fusion of oxide derived from L. A. Cosgrove, and P. E. Snyder, *J. Am. Chem. Soc.*, **75**, 1227 (1953), assuming a *C_p* of 32.0 cal/degree/mole for the liquid oxide. Entropy of MoO₃ at 298.15°K: D. F. Smith, D. Brown, A. S. Dworkin, D. J. Sasnor, and E. R. Van Artsdalen, *J. Am. Chem. Soc.*, **78**, 1533 (1956).

TABLE B-7
HEAT AND FREE ENERGY OF FORMATION OF Fe₃O₄

Fe₃O₄ (magnetite, β, l)
Mol. wt. 231.55

<i>T</i> , °K	ΔH_f° , cal/mole	ΔF_f° , cal/mole	<i>T</i> , °K	ΔH_f° , cal/mole	ΔF_f° , cal/mole
298.15	-266,800 (±2,000)	-242,200 (±2,200)	1,700	-259,600	-139,000
400	-266,100	-233,900	1,800	-259,500	-131,900
500	-265,300	-225,900	1,809	-259,500	-131,300
600	-264,300	-218,100	1,809	-270,600	-131,300
700	-262,900	-210,500	1,870	-270,600	-126,600
800	-261,200	-203,100	1,870	-237,600	-126,600
900	-259,500	-196,000	1,900	-237,700	-124,800
1,000	-259,700	-188,900	2,000	-237,800	-118,900
1,100	-260,500	-181,800	2,100	-238,000	-112,900
1,184	-260,500	-175,700	2,200	-238,300	-107,000
1,184	-261,200	-175,700	2,300	-238,500	-101,000
1,200	-261,100	-174,600	2,400	-238,800	-95,000
1,300	-260,600	-167,400	2,500	-239,000	-89,000
1,400	-260,100	-160,300	2,600	-239,300	-83,000
1,500	-259,600	-153,200	2,700	-239,700	-77,000
1,600	-259,100	-146,100	2,800	-240,000	-71,000
1,665	-258,800	-141,500	2,900	-240,400	-64,900
1,665	-259,600	-141,500	3,000	-240,800	-58,900

Phase changes

METAL

T.P.(Curie point), 1,042°K; $\Delta H_t = 0$
T.P. ($\alpha \rightarrow \gamma$), 1,184°K; $\Delta H_t = 215$ cal/gm-atom
T.P. ($\gamma \rightarrow \delta$), 1,665°K; $\Delta H_t = 270$ cal/gm-atom
M.P. ($\delta \rightarrow l$), 1,809°K; $\Delta H_m = 3,700$ cal/gm-atom

OXIDE

T.P.(Curie point), 900°K; $\Delta H_t = 0$
M.P., 1,870°K; $\Delta H_m = 33,000$ cal/mole

SOURCES OF DATA

Heat of formation at 298.15°K: W. A. Roth and F. Weinert, *Arch. Eisenhüttenwesen*, **7**, 460 (1934), in moderately good agreement with L. S. Darken and R. W. Gurry, *J. Am. Chem. Soc.*, **67**, 1398 (1945). High-temperature heat content of crystalline oxide: J. P. Coughlin, E. G. King, and K. R. Bonnickson, *J. Am. Chem. Soc.*, **73**, 3891 (1951). Heat of fusion of oxide: L. S. Darken and R. W. Gurry, *J. Am. Chem. Soc.*, **68**, 799 (1946).

While the reaction with stainless steel is slightly exothermic, the net thermal effect including the latent heat of vaporization of water would be in the range of 100 Btu/lb H₂O(l) (232 joules/gram) to 550 Btu/lb H₂O (1278 joules/gram) (1) heat absorbed from the liquid state. In the case of molybdenum-water reaction, the net thermal effect would be in the range of 2700 to 2800 Btu/lb H₂O (1) (6275 to 6507 joules/gram). The computational procedure can, therefore, be recommended as follows:

Computational Procedure

The computational procedure for the steam - metal reaction is programmed in the REACT subroutine. This subroutine requires the input of the total surface area of the pressure tubes in the reactor, A_{PT}, and the total surface area of the fuel pins, A_{MO}. In core temperatures below 1770°K (3191°R) the reaction rate is calculated for a stainless steel - steam reaction by the equation

$$R = (.1092) (A_{PT}) e^{(-19080/TCOR)} \frac{\text{lbm water}}{\text{sec}}$$

$$(.00767) (A_{PT}) e^{(-10600/TCOR)} \frac{\text{kgm water}}{\text{sec}}$$

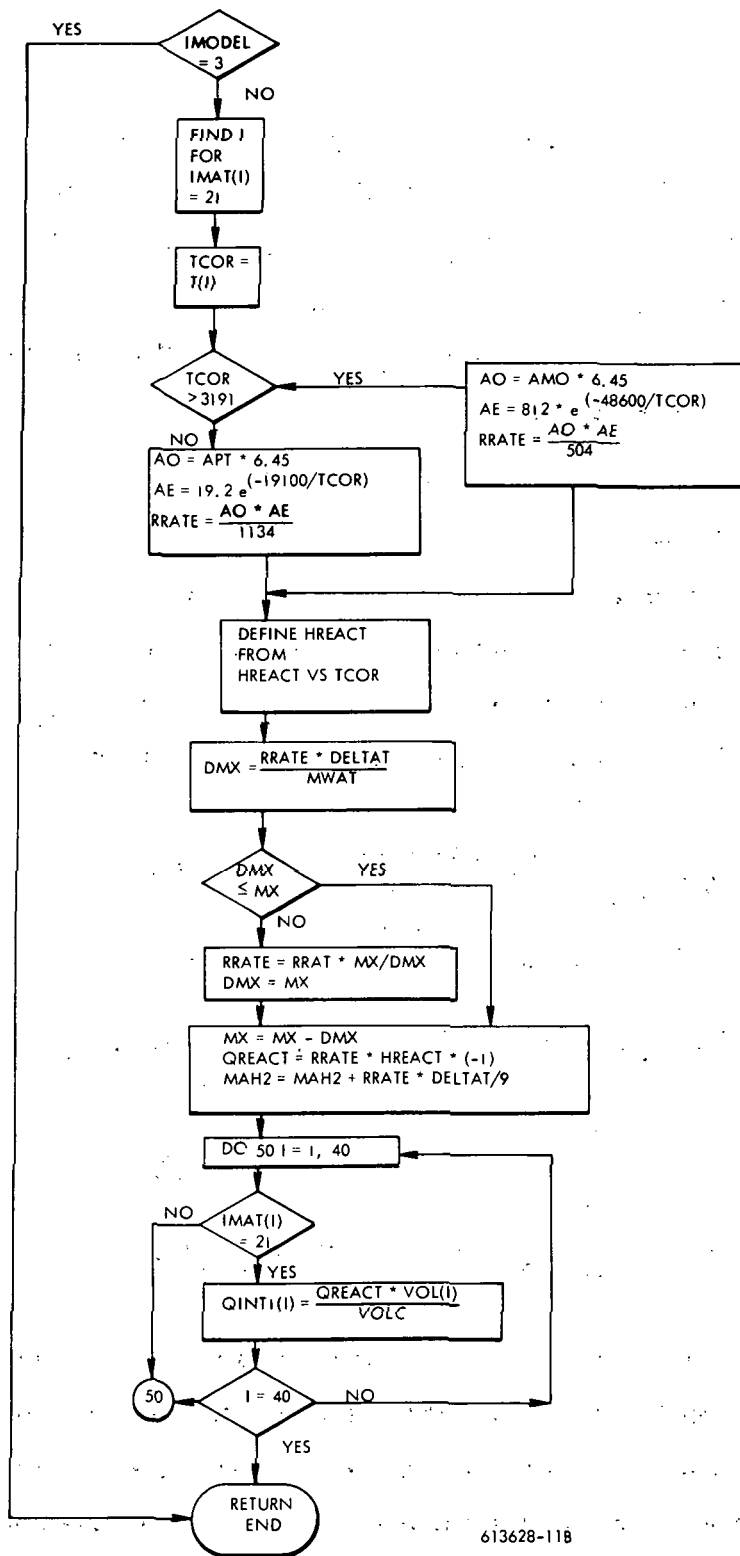
For core temperatures above 1500°C the reaction rate is calculated for a molybdenum - steam reaction by

$$R = (10.38) (A_{MO}) e^{(-48646/TCOR)} \frac{\text{lbm water}}{\text{sec}}$$

$$(.731) (A_{MO}) e^{(-27026/TCOR)} \frac{\text{kgm water}}{\text{sec}}$$

The mass of water that is reacted is summed and compared to the initial mass of water in the system which is an input value. The heats of reaction for both reactions are stored in data statements versus temperature in this subroutine. The total heat release or absorption for the core is calculated for each time step based on the reaction rate and the corresponding heat of reaction. This total heat is distributed among the core nodes by a volume weighted basis.

Figure B-11 is a flow chart of this subroutine.



613628-11B

Figure B-11.

APPENDIX C

PROPERTY DATA SUBROUTINES

C.1 SUBROUTINE VARK

The VARK subroutine defines the thermal conductivity for each node and calculates the thermal conductance between each node in the model. It calls the SHELDK and PROTK subroutines described below. VARK contains logic to calculate the effective conductivity to simulate heat pipe operation and to simulate vessel to air and vessel to soil interfaces. Figure C-1 shows in general the flow of this subroutine.

C.1.1 Heat Pipe Calculation

VARK calculates the effective thermal conductivity of the nodes representing the heat pipe for the three modes of operation - zero, 50 percent, and 100 percent heat pipe operation. Figure C-1 contains the flow chart for this logic, and Table C-1 contains its nomenclature.

For zero operation (MAHT = 31) the thermal conductivity is based on the thermal conductivity of stainless steel and the void fraction. An additional correction factor, CFHTPP, is shown in Figure C-1 to account for nodal area compared to the area enclosing a 1 inch thick matrix of heat pipes. This factor is applied to all equations. (MAHT = 33 and 32, respectively).

For full and 50 percent operation the thermal conductivity for operation is defined within temperature limits of 500°C (1390°R) and 1000 °C (2290°R). A curve has been defined for a maximum heat flux versus temperature representative of 100 percent sodium heat pipe operation as shown in Figure C-2. In VARK maximum allowable heat fluxes are calculated from analytical expressions in the operating range consistent with Figure C-2. These equations are:

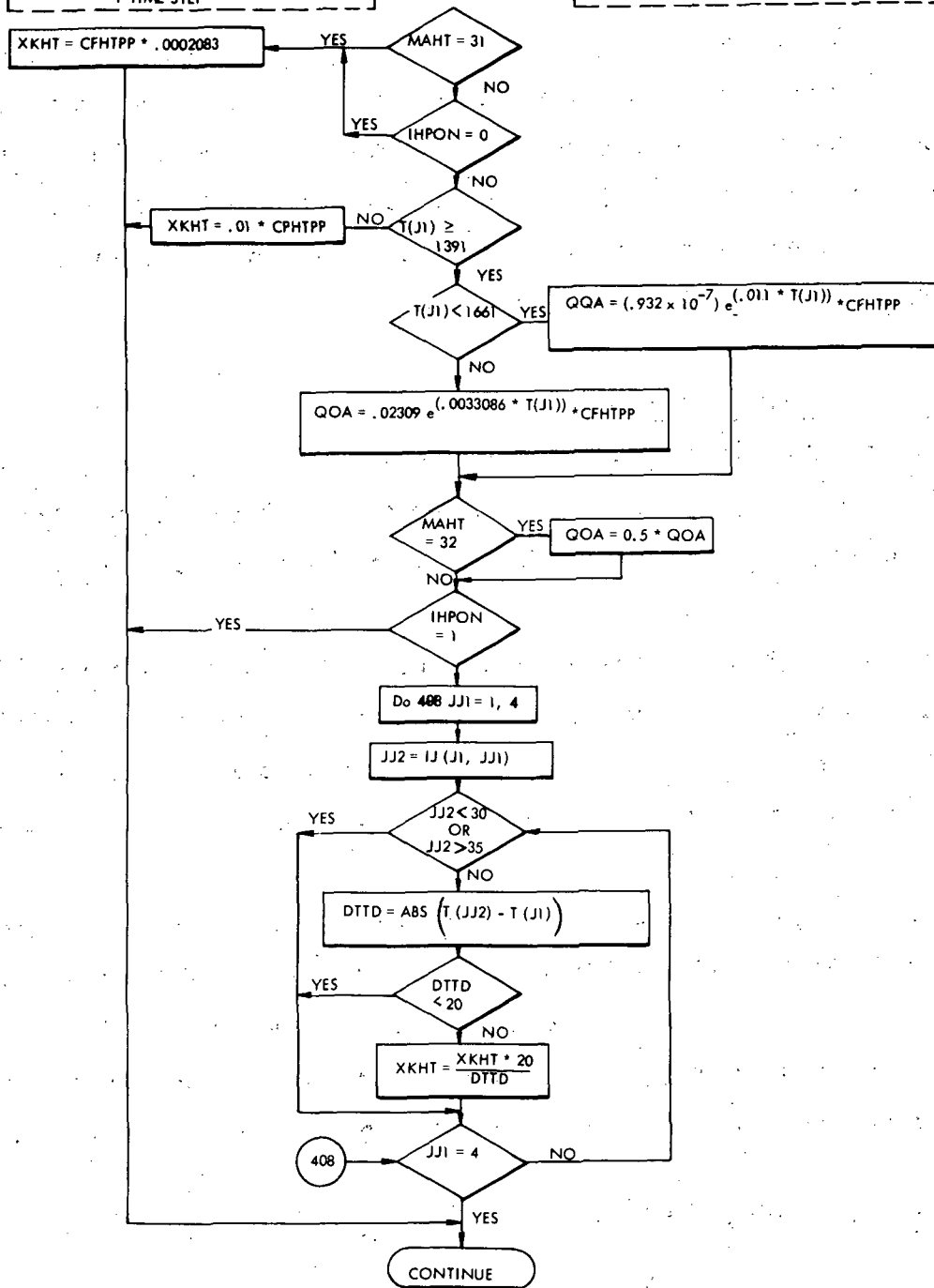
$$\begin{aligned}
 Q/A &= 0.023 e^{(.0033T)} \text{ Btu/sec/in}^2 \text{ for } 1660^\circ\text{R} < T < 2290^\circ\text{R} \\
 &= 3.76 e^{(.0059 T)} \text{ watts/cm}^2 \text{ for } 920^\circ\text{K} < T < 1270^\circ\text{K}
 \end{aligned}$$

IHPON = 0 - NO HEAT PIPES ON
 IHPON = 1 - HEAT PIPES ALL ON FOR FIRST TIME
 IHPON > 1 - HEAT PIPES ON FOR MORE THAN 1 TIME STEP

AREA CORRECTIONS DEFINED IN HTMGEN

$$CPHTPP = \frac{\sqrt{(RS(5) + 1)^2 - RS(5)^2}}{AHTPIP}$$

$$AHTPIP = \sqrt{RS(5)^2 - (RS(5) - 0.1)^2}$$



613628-12B

Figure C-1. Logic for Heat Pipe Simulation

TABLE C-1
HEAT PIPE NOMENCLATURE

MAHT	Material Number
K1	Node Number
K2	Connection Number
K3	Index of Adjacent Node Connected to Node K1, by Connection Number K3
XKHT	Thermal Conductivity
CFHTPP	Correction Factor for Using Nodal Area to Simulate Actual Heat Pipe Annular Area
AHTPIP	Annular Area of Node Used in HTMGEN
QOAMAX	Maximum Allowable Heat Flux
QOA	Heat Flux

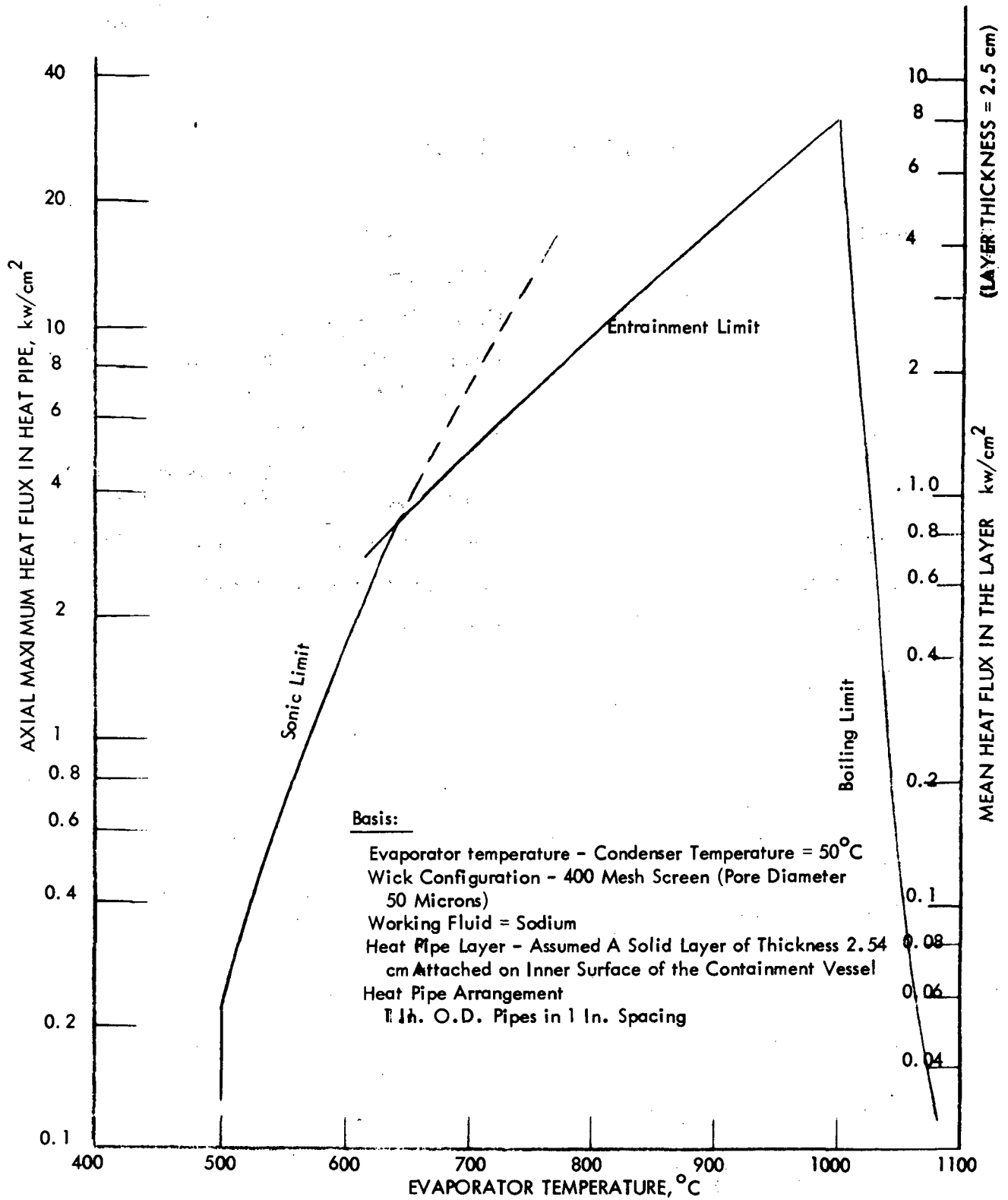


Figure C-2. Maximum Heat Flux vs Heat Pipe Evaporator Temperature

$$Q/A = 0.93 \times 10^{-7} e^{(.011T)} \text{ Btu/sec/in}^2 \text{ for } 1390^{\circ}\text{R} < T < 1660^{\circ}\text{R}$$

$$= 1.52 \times 10^{-5} e^{(.020T)} \text{ watts/cm}^2 \text{ for } 770^{\circ}\text{K} < T < 920^{\circ}\text{K}$$

Based on a predefined ΔT of 20°F between adjacent heat pipe nodes, thermal conductivities are calculated from the heat flux at the calculated heat pipe node temperature. If adjacent heat pipe nodes exceed a temperature drop of 20°F (11°K), then the thermal conductivity is adjusted to prevent the heat flux from exceeding its maximum value. For 50 percent operation the heat flux and thus thermal conductivity are divided by two.

A thermal conductivity of 2.1×10^{-4} Btu/sec/in $^{\circ}\text{R}$ (0.157 watts/cm $^{\circ}\text{K}$) representation of stainless steel with a 0.25 void fraction is used for zero percent operation or in the case that all the heat pipe nodes are below 1390°R (770°K) or above 2295°R (1270°K). If any heat pipe node is in the 1390°R (770°K) to 2290°R (1270°K) operating range then all the heat pipe nodes are considered to be operating. In this case those nodes below 1390°R (770°K) are assigned a thermal conductivity of 0.01 Btu/sec/in $^{\circ}\text{R}$ (7.47 watts/cm $^{\circ}\text{K}$).

C.1.2 Ambient Effective Thermal Conductivity

The following three ambient material representations are calculated to represent the ambient conditions. The soil thermal conductivity is stored in PROTK.

Material
Number

Description and equations

41

Defines contact coefficient for vessel to soil interface

$$H = 1000 \text{ Btu/hours ft}^2 \text{ }^{\circ}\text{R}$$

$$= .00193 \text{ Btu/sec in}^2 \text{ }^{\circ}\text{R}$$

$$= .567 \text{ watts/cm}^2 \text{ }^{\circ}\text{K}$$

$$K = H \times F_t$$

$$F_t = \left(\frac{R}{R_i} \right) (R - R_i) + \left(\frac{R}{R_o} \right) (R_o - R) \quad \text{radially in sphere}$$

$$F_t = R \left(\ln \frac{R}{R_i} + \ln \frac{R_o}{R} \right) \quad \text{radially in cylinder}$$

$$F_t = \delta \quad \text{axially in cylinder}$$

42

Large thermal conductivity for air to air connection

$$K = 10. \text{ Btu}/(\text{sec inch}^{\circ}\text{R})$$

$$= .75 \times 10^5 \text{ watts}/\text{cm}^{\circ}\text{K}$$

43

Effective conductivity representative of radiation plus convection across interface from vessel to ambient

 T_1 = adjacent vessel node temperature

 T_2 = ambient temperature

$$\epsilon = 0.5$$

$$F = 1.0$$

$$H_r = \epsilon F \sigma \left(T_1^3 + T_1^2 T_2 + T_1 T_2^2 + T_2^3 \right)$$

$$H_c = 0.19 \left(T_1 - T_2 \right)^{.333} \text{ Btu}/\text{hour ft}^2 \text{ }^{\circ}\text{R}$$

$$H = H_c + H_r$$

$$K = H \times F_t$$

 F_t is same as for material 41

C.2 FUNCTION SHELDK

This function calculates the effective thermal conductivity to simulate radiation from core to shield and between shield layers. It assigns high or low thermal conductivities for one dimensional heat transfer paths through materials or across interfaces. It also assigns a large thermal conductivity for the homogenized core representation. Presented below are descriptions and defining equations for each shield material.

Material
Number

Description and defining equations and assumptions

21

Core node (high conductivity)

$$K = 1.0 \text{ Btu/ (sec inch - R)}$$

$$K = .75 \times 10^3 \text{ watts/cm}^{\circ}\text{K}$$

22

Effective conductivity to represent radiation at interface
between core and shield

$T(i)$ = interface node temperature

T_2 = cold shield temperature

$$T_1 = T_2 + 2(T(i) - T_2)$$

$$F_{t1} = T_1^3 + T_1^2 T_2 + T_1 T_2^2 + T_2^3$$

$$F_{t2} = 4 * T(i)^3$$

$$F_t = (F_{t1} + F_{t2})/2$$

$$\epsilon_1 = .5$$

$$\epsilon_2 = .25$$

$$\epsilon = \frac{1}{\frac{1}{\epsilon_1} + \frac{1}{\epsilon_2}} - 1$$

$$F = 1.0$$

$$H = \epsilon F \sigma F_t$$

$$K = H \delta \quad \text{axial-radiation}$$

$$K = H * R \left(\ln \frac{R}{R_i} + \ln \frac{R_o}{R} \right) \quad \text{Radial radiation}$$

$$K = 0.01 K_i \quad \text{in direction perpendicular to direction of
of radiation connection}$$

23

Effective conductivity to represent radiation between shield layers

$$\epsilon_1 = .25$$

$$\epsilon_2 = .25$$

Material
Number

Description and defining equations and assumptions

$$\epsilon = \frac{1}{\frac{1}{\epsilon_1} + \frac{R_o}{R_i} \left(\frac{1}{\epsilon_2} - 1 \right)}$$

23 (cont'd)

$$Y = \frac{\pi}{12}$$

$$X = \frac{R_o}{R_i}$$

$$A = Y^2 + X^2 - 1$$

$$B = Y^2 + 1 - X^2$$

$$F = \frac{1}{X} - \frac{X}{\pi} \left(\cos^{-1} \left(\frac{B}{A} \right) - \frac{1}{2Y} \sqrt{(A+2)^2 - 2X^2} \cos^{-1} \left(\frac{B}{XA} \right) + B \sin^{-1} \left(\frac{1}{X} \right) - \frac{\pi}{2A} \right)$$

$$FS = \frac{1-F}{2}$$

T_2 = representative cold side temperature

$$2(T(i) - T_2)$$

$$T_1 = T_2 + 2(T_2 - T(i))$$

$$F_{t1} = T_1^3 + T_1^2 T_2 + T_1 T_2^2 + T_2^3$$

$$F_{t2} = 4(T(i))^3$$

$$F_t = (F_{t1} + F_{t2})/2$$

$$H = \epsilon F \sigma F_t$$

$$K = H \frac{R}{R_i} (R - R_i) + \frac{R}{R_o} (R_o - R) \quad \text{radially}$$

$$K = FS * K/F \quad \text{circumferentially}$$

24

High thermal conductivity in shield in radial direction

IF IDEMK = 1	K = 1.0	Btu/sec. inch °R	(.75 x 10 ³ watts/cm °K)
IF IDEMK = 0	K = .0001	Btu/sec. inch °R	(.075 watts/cm °K)

<u>Material Number</u>	<u>Description and defining equations and assumptions</u>
25	High thermal conductivity in shield in axial direction IF IDEMK = 1 K = .0001 Btu/sec inch ^{°R} (.075 watts/cm ^{°K}) IF IDEMK = 0 K = 1.0 Btu/sec inch ^{°R} (.75 x 10 ³ watts/cm ^{°K})
26	High thermal conductivity in shield in both directions K = 1.0 Btu/sec inch ^{°R} (.75 x 10 ³ watts/cm ^{°K})

C.3 FUNCTION PROTK

This subroutine stores thermal conductivity data versus temperature for 9 materials used in the gas cooled reactor concept. It does a linear interpolation of this data to define a thermal conductivity for a prescribed material and temperature. The following data is contained in this function:

<u>Material Number</u>	<u>Material</u>	<u>Temperature</u>		<u>Thermal Conductivity</u>	
		<u>°R</u>	<u>°K</u>	<u>Btu/(sec in. R)</u>	<u>(watts/cm ^{°K})</u>
1	Moly ⁽²¹⁾	720	(1513)	.001792	(1.338)
		1440	(800)	.001585	(1.184)
		2160	(1200)	.001417	(1.058)
		2880	(1600)	.001288	(.962)
		3600	(2000)	.001204	(.899)
		4320	(2400)	.001148	(.850)
		5040	(2800)	.001120	(.837)
2	UO ₂ ⁽²²⁾	855	(473)	.700 x 10 ⁻⁴	(.0523)
		1391	(773)	.526 x 10 ⁻⁴	(.0393)
		1640	(913)	.465 x 10 ⁻⁴	(.0347)
		2291	(1275)	.364 x 10 ⁻⁴	(.0272)
		2474	(1373)	.318 x 10 ⁻⁴	(.0238)
		3019	(1673)	.265 x 10 ⁻⁴	(.0198)
		3494	(1943)	.258 x 10 ⁻⁴	(.0193)

Material Number	Material	Temperature		Thermal Conductivity	
		$^{\circ}\text{R}$	$^{\circ}\text{K}$	Btu/(sec in. R)	(watts/cm $^{\circ}\text{K}$)
3	AM 355 ⁽²⁴⁾	540	(300)	1.96×10^{-4}	(.146)
		900	(500)	2.32×10^{-4}	(.173)
		1080	(600)	2.49×10^{-4}	(.186)
		1440	(800)	2.37×10^{-4}	(.177)
		1800	(1000)	3.22×10^{-4}	(.241)
		2169	(1200)	3.53×10^{-4}	(.264)
		2520	(1400)	3.78×10^{-4}	(.282)
		2880	(1600)	4.03×10^{-4}	(.301)
4	LiH ⁽²³⁾	720	(400)	1.37×10^{-4}	(.102)
		900	(500)	1.04×10^{-4}	(.0777)
		1080	(600)	0.84×10^{-4}	(.0627)
		1260	(700)	0.73×10^{-4}	(.0545)
		1440	(800)	0.67×10^{-4}	(.0500)
5	Tungsten ⁽²¹⁾	540	(300)	.00269	(2.00)
		720	(400)	.0021	(1.57)
		1440	(800)	.00174	(1.30)
		2160	(1200)	.00154	(1.15)
		2880	(1600)	.00143	(1.07)
		3600	(2000)	.00132	(.986)
		4320	(2400)	.00129	(.964)
		5580	(3100)	.00120	(.896)
6	Stainless Steel ⁽²³⁾ 316	540	(300)	1.344×10^{-4}	(.100)
		720	(400)	1.568×10^{-4}	(.117)
		1080	(600)	2.072×10^{-4}	(.155)
		1440	(800)	2.548×10^{-4}	(.190)
		1800	(1000)	3.052×10^{-4}	(.228)
		2160	(1200)	3.70×10^{-4}	(.276)
7	Coastal Plains ⁽²⁵⁾ Soil	671	(373)	3.75×10^{-6}	(2.80×10^{-3})
		851	(474)	4.01×10^{-6}	(3.0×10^{-3})
		1211	(673)	4.55×10^{-6}	(3.4×10^{-3})
		1571	(873)	5.35×10^{-6}	(4.0×10^{-3})
		1931	(1073)	6.29×10^{-6}	(4.7×10^{-3})
		2291	(1273)	7.49×10^{-6}	(5.59×10^{-3})
		2651	(1473)	10.0×10^{-6}	(7.5×10^{-3})
		2831	(1573)	12.8×10^{-6}	(9.56×10^{-3})
		3011	(1673)	18.5×10^{-6}	(13.8×10^{-3})
		3191	(1773)	29.4×10^{-6}	(22.0×10^{-3})
		3371	(1873)	49.5×10^{-6}	(37.0×10^{-3})
		3461	(1923)	64.2×10^{-6}	(47.9×10^{-3})

Material Number	Material	Temperature		Thermal Conductivity	
		$^{\circ}\text{R}$	$^{\circ}\text{K}$	Btu/(sec in. R)	
8	Water	492	(273)	7.38×10^{-6}	(5.51×10^{-3})
		564	(313)	8.4×10^{-6}	(6.27×10^{-3})
		636	(353)	8.94×10^{-6}	(6.68×10^{-3})
		708	(393)	9.17×10^{-6}	(6.85×10^{-3})
		816	(453)	9.03×10^{-6}	(6.74×10^{-3})
		888	(493)	8.73×10^{-6}	(6.52×10^{-3})
		960	(533)	8.17×10^{-6}	(6.10×10^{-3})
		1032	(573)	7.22×10^{-6}	(5.34×10^{-3})
		1460	(813)	6.94×10^{-6}	(5.18×10^{-3})
9	Composite Material (UO_2 , LiH)	855	(473)	$.700 \times 10^{-4}$	(.0523)
		1391	(773)	$.526 \times 10^{-4}$	(.0393)
		1640	(913)	$.465 \times 10^{-4}$	(.0347)
		2291	(1273)	$.364 \times 10^{-4}$	(.0272)
		2474	(1373)	$.318 \times 10^{-4}$	(.0238)
		3019	(1673)	$.265 \times 10^{-4}$	(.0198)
		3494	(1943)	$.258 \times 10^{-4}$	(.0193)

C.4 BLOCK DATA

This block stores density, melting point temperature, and the effective specific heat to simulate the heat of fusion for nine basic materials indicated below. The effective specific heat is defined for a temperature differential of 50°F by the equation

$$C_p' = \frac{H_{fg}}{50}$$

Material Number	Material	Density		Melt. Temp.		$H_{fg}/-50$	
		lbm/in ³	(gm/cm ³)	$^{\circ}\text{R}$	$^{\circ}\text{K}$	Btu/(lbm-R)	(joules/gm $^{\circ}\text{K}$)
1	Moly	.370	(10.24)	5200	(2889)	2.52	(10.54)
2	UO_2	.379	(10.49)	5040	(2800)	1.	(4.18)
3	AM-355	.282	(7.81)	2950	(1639)	2.5	(10.46)
4	LiH	.0245	(.678)	1700	(944)	31.6	(13.22)
5	Tungsten	.697	(19.29)	6550	(3639)	1.49	(6.23)
6	SS-316	.294	(8.14)	2800	(1555)	--	---
7	Soil	.0482	(1.334)	3460	(1922)	--	---
8	Water	.0361	(.999)	----	----	--	---
9	Composite	.379	(10.49)	1700	(944)	31.6	(13.22)

C.5 FUNCTION PROCP

This subroutine stores specific heat data versus temperature for nine materials used in the gas cooled reactor. It does a linear interpolation of this data to define a specific heat for a prescribed material and temperature. The following data are stored in this subroutine.

<u>Material Number</u>	<u>Material</u>	<u>Temperature</u>		<u>Specific Heat</u>	
		<u>°R</u>	<u>°K</u>	<u>Btu/(lb-R)</u>	<u>(joules/gm°K)</u>
1	Moly ⁽²¹⁾	360	(200)	.054	(.226)
		720	(400)	.062	(.259)
		1440	(800)	.068	(.284)
		2160	(1200)	.074	(.310)
		2880	(1800)	.081	(.339)
		3600	(2000)	.088	(.368)
		4320	(2400)	.097	(.406)
		5040	(2800)	.101	(.422)
		5199	(2888)	.101	(.422)
		5200	(2889)	2.52	(10.54)
		5250	(2917)	2.52	(10.54)
		5251	(2918)	.101	(.422)
		2	UO ₂ ⁽²²⁾	671	(373)
855	(473)			.067	(.280)
1391	(773)			.074	(.310)
1640	(913)			.076	(.318)
2291	(1273)			.078	(.326)
2479	(1373)			.079	(.330)
3019	(1673)			.081	(.339)
3494	(1943)			.083	(.347)
5400	(3000)			.084	(.351)
3	AM-355 ⁽²⁴⁾	540	(300)	.140	(.586)
		900	(500)	.142	(.594)
		1080	(600)	.149	(.623)
		1440	(800)	.162	(.678)
		1870	(1050)	.175	(.732)
		2160	(1200)	.110	(.460)
		2520	(1400)	.148	(.619)
		2880	(1600)	.170	(.711)
		2949	(1638)	.170	(.711)
		2950	(1639)	2.5	(10.5)
		3000	(1666)	2.5	(10.5)
3001	(1667)	.17	(.71)		

<u>Material Number</u>	<u>Material</u>	<u>Temperature</u>		<u>Specific Heat</u>	
		<u>°R</u>	<u>(°K)</u>	<u>Btu/(lb-R)</u>	<u>(joules/gm °K)</u>
4	LiH ⁽²³⁾	540	(300)	.84	(3.5)
		720	(400)	1.04	(4.35)
		900	(500)	1.19	(4.98)
		1080	(600)	1.33	(5.56)
		1260	(700)	1.48	(6.19)
		1440	(800)	1.62	(6.78)
		1620	(900)	1.76	(7.36)
		1699	(944)	1.76	(7.36)
		1700	(945)	31.6	(132.2)
		1750	(972)	31.6	(132.2)
		1751	(973)	1.76	(7.36)
5	Tungsten ⁽²¹⁾	540	(300)	.0315	(.132)
		720	(400)	.032	(.134)
		1440	(800)	.034	(.142)
		2160	(1200)	.036	(.151)
		2880	(1600)	.0375	(.157)
		3600	(2000)	.039	(.163)
		4320	(2400)	.041	(.172)
		5580	(3100)	.044	(.184)
		6549	(3638)	.044	(.184)
		6550	(3639)	1.49	(6.23)
		6600	(3667)	1.49	(6.23)
		6601	(3668)	.044	(.184)
6	Stainless Steel 316 ⁽²³⁾	540	(300)	.11	(.46)
		720	(400)	.115	(.48)
		1080	(600)	.12	(.50)
		1440	(800)	.13	(.54)
		1800	(1000)	.15	(.63)
		2160	(1200)	.18	(.75)
7	Coastal Plains ⁽²⁵⁾	671	(373)	.2	(.84)
		2290	(1273)	.2	(.84)
		3500	(1944)	.2	(.84)

<u>Material Number</u>	<u>Material</u>	<u>Temperature</u>		<u>Specific Heat</u>	
		<u>°R</u>	<u>(°K)</u>	<u>Btu/(lb-R)</u>	<u>(joules/gm°K)</u>
8	Water	492	(273)	1.0074	(4.21)
		564	(313)	.998	(4.17)
		816	(453)	1.055	(4.41)
		1032	(573)	1.368	(5.72)
9	Composite (UO ₂ , LiH)	540	(300)	.84	(3.5)
		720	(400)	1.04	(4.35)
		900	(500)	1.19	(4.98)
		1080	(600)	1.33	(5.56)
		1260	(700)	1.48	(6.19)
		1440	(800)	1.62	(6.78)
		1620	(900)	1.76	(7.36)
		1699	(944)	1.76	(7.36)
		1700	(945)	31.6	(132.2)
		1750	(972)	31.6	(132.2)
	1751	(973)	1.76	(7.36)	

C.6 SUBROUTINE CPCAL

This subroutine defines the specific heat and density for all materials not defined by basic material properties; for example, effective properties for the homogenized gas cooled thermal reactor core. The following calculations are performed in this subroutine.

<u>Material Number</u>	<u>Description and defining equations and assumptions</u>
------------------------	---

21	Core node
----	-----------

$$\rho = \frac{M_{\text{moly}} + M_{\text{UO}_2} + M_{\text{AM-355}} + M_{\text{H}_2\text{O}}}{\text{VOLC}}$$

$$\text{VOLC} = \sum_i \text{VØL}(i) \quad \text{for } i\text{'s where } \text{IMAT}(i) = 21$$

$$C_P = \frac{M_{\text{moly}} C_{P \text{ moly}} + M_{\text{UO}_2} C_{\text{PU02}} + M_{\text{AM-355}} C_{\text{PAM-355}} + M_{\text{H}_2\text{O}} C_P}{M_{\text{moly}} + M_{\text{UO}_2} + M_{\text{AM-355}} + M_{\text{H}_2\text{O}}}$$

<u>Material Number</u>	<u>Description and defining equations and assumptions</u>
22, 23, 24, 25, 26	Shield nodes representing radiation or high conductivity $C_p = 1.242$ (helium) $\rho = \frac{M_{\text{Hel}}}{\text{VOLS}}$ $\text{VOLS} = \sum_i \text{V}\emptyset\text{L} (i)$ where IMAT (i) = 22, 23, 24, 25, 26
31, 32, 33	Heat pipe $C_p = C_p \text{ AM-355}$ $\rho = \rho_{\text{AM-355}} * (1 - F_{\text{void}})$ F_{void} is void fraction and equals .75
41, 42	Air and air to vessel interface $\rho = .0230 * T_{\text{ambient}}$ $C_p = 0.24$
43	Soil interface $C_p = C_p \text{ soil}$ $\rho = \rho_{\text{soil}}$

C.7 ALTERNATE SOIL PROPERTIES

Reference 25 presents the detailed results of an experimental program by the NBS to measure the thermal conductivity of nine soils for SANDIA. These data and WANL test data were used for the soil property selection for the ESATA program usage. Table C-2 lists the nine soils used for the thermal conductivity measurements and their density. Table C-3 lists the derived thermal conductivity as a function of temperature for the soil. Because of its commonness and low thermal conductivity the coastal plains clay soil is being used in the ESATA cases.

TABLE C-2
SOIL SAMPLES

	Symbol	Average Density (gm/cm ³)
1. Calcareous Soil (natural weathered limestone)	C	2.0
2. Granitic Detrital Soil (weathered decomposed granite soil)	GD	1.92
3. Dune Sand (windblown sand)	DS	1.57
4. Magnesian Soil (magnesium aluminum silicate)	M	1.79
5. Podzol Soil (leached organic timberland soil)	P	1.75
6. Coastal Plains Clay (coastal flood plain soil)	CP	1.34
7. Laterite Soil (tropical rain forest soil)	L	1.49
8. Estancia Playa (Dog Lake) Soil (highly saline playa soil)	EP	1.53
9. Ottawa Sand (silica-artificial soil)	OS ₁	1.76
	OS ₂	1.57

TABLE C-3

THE DERIVED THERMAL CONDUCTIVITY, $\gamma(T_D)$,
(EXPRESSED IN $Wm^{-1} \text{ } ^\circ C^{-1}$) OF THE NINE TYPES OF SOIL

Type of Soil	Temperature, $^\circ K$											
	370	470	670	870	1070	1270	1470	1570	1670	1770	1870	1920
Calcareous	.78	.74	.68	.63	.58	.54	.54	.62	.82	1.32	2.4	3.4
Granitic Detrital	.88	.83	.77	.74	.75	.82	1.05	1.44	2.5	5.2*	---	---
Dune Sand	.30	.34	.40	.44	.51	.70	1.25	1.77	2.5	3.7	5.2*	---
Magnesian	.66	.65	.64	.65	.67	.73	.93	1.17	1.6	---	---	---
Podzol	.52	.53	.51	.52	.64	.98	1.63	2.1	2.7	3.4	4.2*	---
Coastal Plains	.28	.30	.34	.40	.47	.56	.75	.96	1.38	2.2	3.7	4.8
Laterite	.32	.27	.19	.13	.13	.30	.85	1.38	2.2	3.3	4.9	5.9
Estancia Playa	.38	.40	.42	.41	.35	.28	.38	.76	1.8	4.4	---	---
Ottawa Sand ^{a/}	.43	.51	.68	.85	1.04	1.24	1.45	1.56	1.68	1.80	---	---
Ottawa Sand ^{b/}	.30	.34	.45	.57	.75	.98	1.29	1.48	1.70	---	---	---

*Extrapolated value

^{a/} 1760 kg m⁻³ density^{b/} 1570 kg m⁻³ density

Specific heat data for these soils were not presented. Data presented in standard references (26-28) were surveyed. Table C-4 presents specific heat data of materials that comprise a part of the nine soils or are similar to these. Until better data are defined a specific heat of 0.2 Btu/lb^{°R} (.84 joules/gm^{°K}), was assumed for use in ESATA.

TABLE C-4
SPECIFIC HEATS OF VARIOUS SUBSTANCES

	<u>C_p-Btu/lb^{°F} (joules/gm^{°K})</u>	
Limestone	.22	(.92)
Granite	.20	(.84)
Sand	.20	(.84)
Quartz	.17-.28	(.71 - 1.17)
SiO ₂	.19	(.79)
Magnesia	.22	(.92)
Gypson	.26	(1.09)
Earth (gravelly)	.44	(1.84)
Clay	.21	(.88)
Concrete	.21	(.88)
Sandstone	.17	(.71)
Diatomoceous earth	.21	(.88)
Marble	.19	(.79)

APPENDIX D

CORE AND SHIELD MELT AND DISPLACEMENT SUBROUTINES

D.1 SUBROUTINE TMPCAL

A separate subroutine was developed and programmed for correcting temperatures in the shield and core to account for the heat of fusion during phase changes of the various materials. In the PROCP function and the DATA block are defined effective specific heats simulating the heat of fusion spread over a prescribed (δT) of 50°R (27.8°K). Namely

$$\text{CPP} = \frac{H_{fg}}{\text{DELTT}} \quad \text{where: DELTT} = 50^{\circ}\text{R} \quad (27.8^{\circ}\text{K})$$

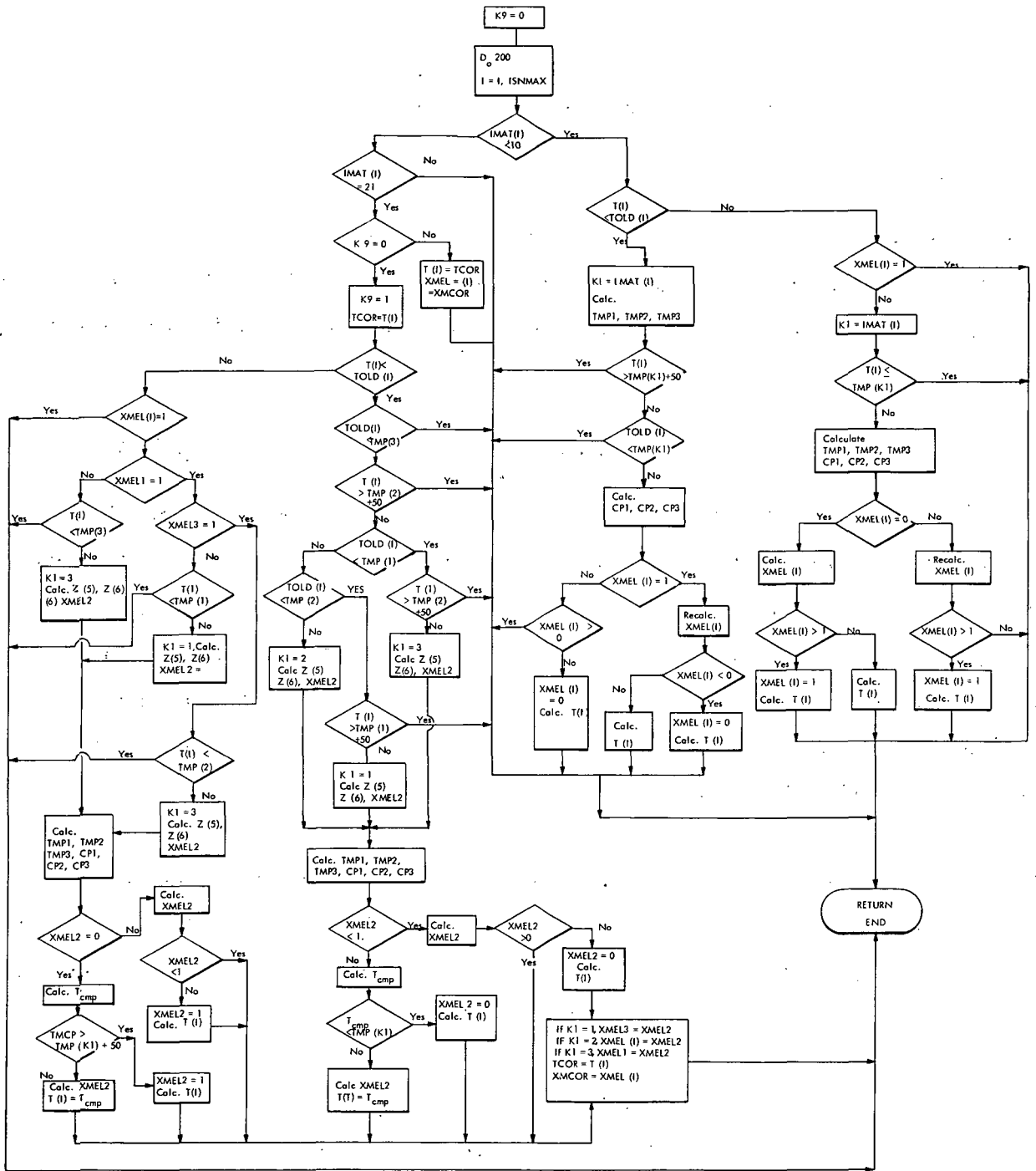
Presently this data is defined for 6 materials used in the core and shield - molybdenum, UO_2 , tungsten, AM-355, lithium hydrid and a composite of LiH and UO_2 . TMPCAL was written to simulate phase changes for these five materials as separate components and to simulate the effect of phase changes of three materials in the component core (IMAT = 21) consisting of molybdenum, UO_2 and AM-355. Figure D-1 presents the flow chart for this subroutine with a list of nomenclature in Table D-1. The method for modeling a single component phase change is described below.

After a temperature convergence is obtained in CONDO for a particular time step, the temperature of all nodes assigned one of the above materials and compared to their melting point temperature, TMP. When the calculated temperature exceeds TMP for a node, the fraction of melting in that node is calculated by the equation

$$X = \frac{C_{ps} (T - \text{TMP})}{\text{CPP} \cdot \text{DELTT}}$$

where C_{ps} is the specific heat of the material at the previously calculated temperature

T is the temperature calculated by CONDO.



613628-13C

Figure D-1. Subroutine TMPCAL

TABLE D-1

NOMENCLATURE FOR THE TMPICAL SUBROUTINE

CP (I, T)	Represents specific heat of material I at temperature T
CPP (I)	Effective specific heat - $(H_{fg}/50)$
CP1	Solid phase specific heat prior to melting
CP2	= CPP (I)
CP3	Liquid phase specific heat just after melting
IMAT (I)	Material number of node I
ISNMAX	Maximum shield node index
K1	= IMAT (I)
K9	Trigger used to denote if core temperature has been for this line step
MMOLY	Mass of molybdenum
MPV	Mass core pressure vessel and structure
MUO2	Mass of UO_2
T (I)	Temperature of node I an end of time step
TMP (I)	Melting point temperature of material I
TMP1	Temperature at beginning of melting (= TMP (I))
TMP2	Temperature at end of melting
TMP3	Temperature of liquid phase
TOLD (I)	Temperature of node I at previous time step
XMEL (I)	Fraction of melting in node I (for core nodes it represents UO_2)

TABLE D-1 (Continued)

XMEL1	Fraction of melting of structure in core
XMEL2	Fraction of melting of particular component in core
XMEL3	Fraction of melting of moly in core
Z (5)	Capacitance of components in core not going through melting process at time step in question
Z (6)	Mass of component that is melting

TMP is the melting point temperature

CPP is the effective specific heat simulating the heat of fusion

DELTT is the prescribed temperature increment over which melting is simulated.

If X is calculated to be less than 1 indicating that melting is not completed for this node during the time step in question, then the temperature is corrected to a new temperature

$$T' = TMP + X \cdot DELTT$$

If X exceeds 1 indicating that all the material is melted for that node, then the temperature correction takes the form

$$T' = TMP2 + \frac{C_{P3}(T - TMP2) - C_{P1} \cdot DELTT}{C_{P2}}$$

where $TMP2 = TMP + DELTT$ is the temperature at the end of the melting process

For nodes with incomplete melting, or $T' < TMP2$, the calculation of the fraction of melting will be continued during the next time step,

$$X' = X + \frac{T - TOLD}{DELTT}$$

where T OLD is the calculated temperature from the previous time step

If the fraction X' is still less than 1 indicating that melting is not completed, then no temperature correction is needed. If X' exceeds 1 then it is set equal to 1 and the temperature is corrected by the equation

$$T' = TMP2 + \frac{C_{P1}}{C_{P2}} (T - TMP2)$$

For the three component core simulation a similar set of equations are defined; however, the capacitance of the two non-melting components must be included. For example, the core equation for melting of moly which compares to the preceding equation would be

$$T' = \text{TMP2} + \left[\frac{(M C_p)_{\text{UO}_2} + (M C_p)_{\text{am}} + \text{CP1}}{(M C_p)_{\text{UO}_2} + (M C_p)_{\text{am}} + \text{CP2}} \right] (T - \text{TMP2})$$

where TMP2, CP1, and CP2 are set up for moly melting.

If the melting of AM-355 is taking place the equation would be

$$T' = \text{TMP2} + \left[\frac{(M C_p)_{\text{UO}_2} + (M C_p)_{\text{Mo}} + \text{CP1}}{(M C_p)_{\text{UO}_2} + (M C_p)_{\text{Mo}} + \text{CP2}} \right] (T - \text{TMP2})$$

where TMP2, CP1, and CP2 are defined for AM-355 melting.

The detailed procedure for setting these equations are shown in the flow chart.

D.2 SUBROUTINE CSMELT

This subroutine redefines the IMAT array to simulate the effects of melting on displacing the core and/or shield. Figure D-2 presents a general flow diagram of the subroutine. Included in this subroutine is logic for handling an all UO₂ shield defined by ISHLD = 4.

This subroutine allows the core to displace LiH (lighter than UO₂ material) or drop onto the inner shield layer when the core structure melts. It also allows the core to fill the base of the inner shield layer during the time step after the core reaches the bottom.

Displacement or movement of the core within the inner shield layer (first layer of spherical nodes) is accomplished by changing the nodes that represent the core (IMAT = 21). Once the core is resting at the inner shield base no further changes are made in the core location. Everytime the core material is reassigned the total core volume and density will be recalculated at each step to maintain the same total core mass and its proper capacitance, and to provide for proper distribution of the core heat generation terms.

In the shield the core will not displace tungsten heavier than UO₂ material or UO₂. When the nodes of the tungsten shield melt the phase change will be calculated as described in TPCAL subroutine and molten material remain in the same location. However, the

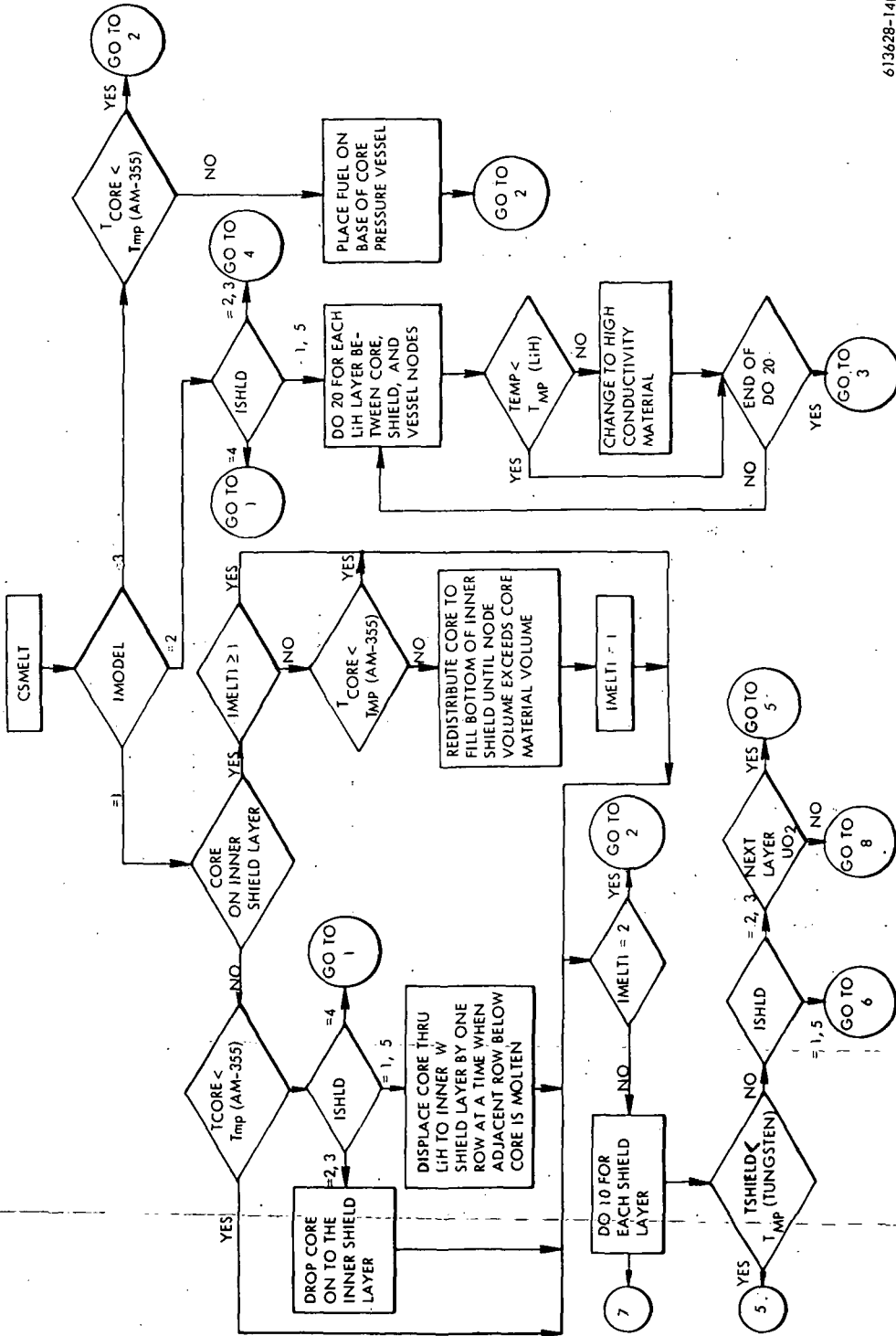
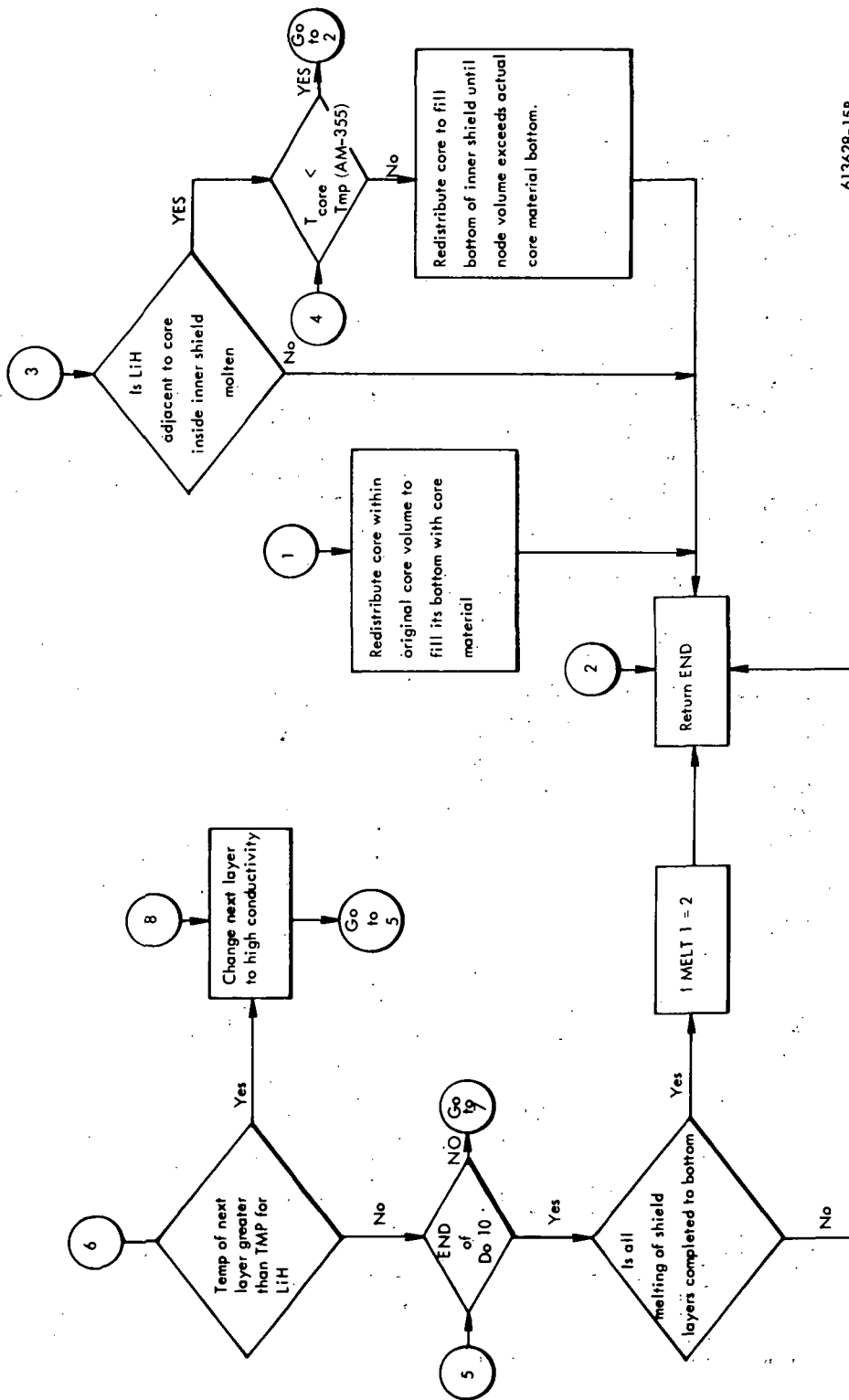


Figure D-2. Subroutine CSMELT



613628-15B

Figure D-2. Subroutine CSMELT (Continued)

node adjacent to it will be checked. If it is a void, which is represented by a radiation gap, it will be redefined as a high K material. Thus, the molten tungsten (heavy metal) effectively fill the void. If LiH is present in the adjacent node, no change will be made unless the LiH is molten in which case that node will be changed also to a high K. In this manner the melting process of the core and shield layers are simulated by reducing the heat transfer resistance. This procedure was adopted because it is most feasible for the program logic, and yet compatible with other subroutines such as FISSON.

APPENDIX E

PRESSURE AND STRESS SUBROUTINE

E.1 PRESSURE CALCULATION PROCEDURE

A procedure for calculating the pressure build up in the shield is based on an ideal mixture of three perfect gases. The three components considered will include:

- helium
- hydrogen (released from water/metal reactions)
- non condensed fission products

The mixture temperature is the average of the heavy metal (W) shield node temperatures. Heat transfer from the gas to the shield is not considered. Initial parameters that are defined include the total pressure, P_o , temperature, T_o , and the volume of the gas mixture, V . From the REACT subroutine the mass of hydrogen released by water-metal reaction of the shield is defined at each time step. The FISSION subroutine defines the number of moles of fission products that are in a vapor state at each time step.

The total pressure is the sum of the partial pressure of the three constituents

$$P_{tot} = P_{he} + P_{h_2} + P_{fp}$$

The partial pressure is calculated from the perfect gas laws

$$P_i = \frac{n_i RT}{V}$$

where n_i is the number of moles of each component in the mixture. The number of moles is defined simply as

$$n_i = \frac{m_i}{M_i}$$

where m_i is the mass of components in the gas state and M_i is the molecular weight. The molecular weights for the four fission product groupings was estimated from the constituents

of each grouping as defined below and is stored in the FISSON subroutine.

<u>Group</u>	<u>Effective Molecular Weight</u>
A	125
B	108
C	107
D	120

Initially, the mass of helium will be calculated based on the initial total pressure, and temperature and is held constant for subsequent time steps.

Stress Calculation

A cursory procedure for computing the rupture life of the containment vessel (assumed to be 316 stainless steel) for the HTM's has been formulated and programmed as part of the computational sequence in the PRESUR subroutine of the ESATA program. The procedure consists of the following for each time increment in the transient analysis:

- The containment vessel stress is computed for the applied pressure based on thin spherical shell theory. The containment vessel deformations, areas of stress concentrations, and support provided by the soil for those cases when the vessel is buried are neglected.
- The computed stress, once established, permits determination of the value of the Larson-Miller parameter using the following equation.

$$(60 - LM)^{0.496} - (\log_{10} \alpha)^{1.2} + 1.2 = 0$$

where LM = Larson-Miller parameter

α = Computed stress level

The above equation is based on creep rupture data for 316 stainless steel from Reference²⁹. The Larson-Miller curve from which the equation was derived is shown in Figure E-1. This curve was developed from the creep rupture data using operating life times of 10 hours and 1000 hours for temperatures ranging from 1200°F to 2000°F to be representative of the entire data spectrum.

- The time to failure is computed from the Standard Larson Miller equation

$$LM = (T + 460) (a + \log_{10} t) 10^{-3}$$

where T = temperature of the vessel in °F

a = empirical constant having a value of 20 for the 316 stainless steel material

t = time to failure at the applied stress level

For ESATA calculations, the maximum containment vessel temperature at the end of the time increment is used for computational purposes.

- The percent of life used during the time increment is computed by dividing the time increment by the time to failure (t).
- The percent of life used is summed for each time increment during the transient analysis. When the sum is equal to 1, the containment vessel is considered to be ruptured. The ESATA program outputs a statement indicating that rupture has occurred. Pertinent data such as pressure, stress, temperature, and time are also printed out. In the subsequent time period, rather than ceasing the computations, the ESATA program continues computing thermal and pressure data but bypasses the stress calculation.

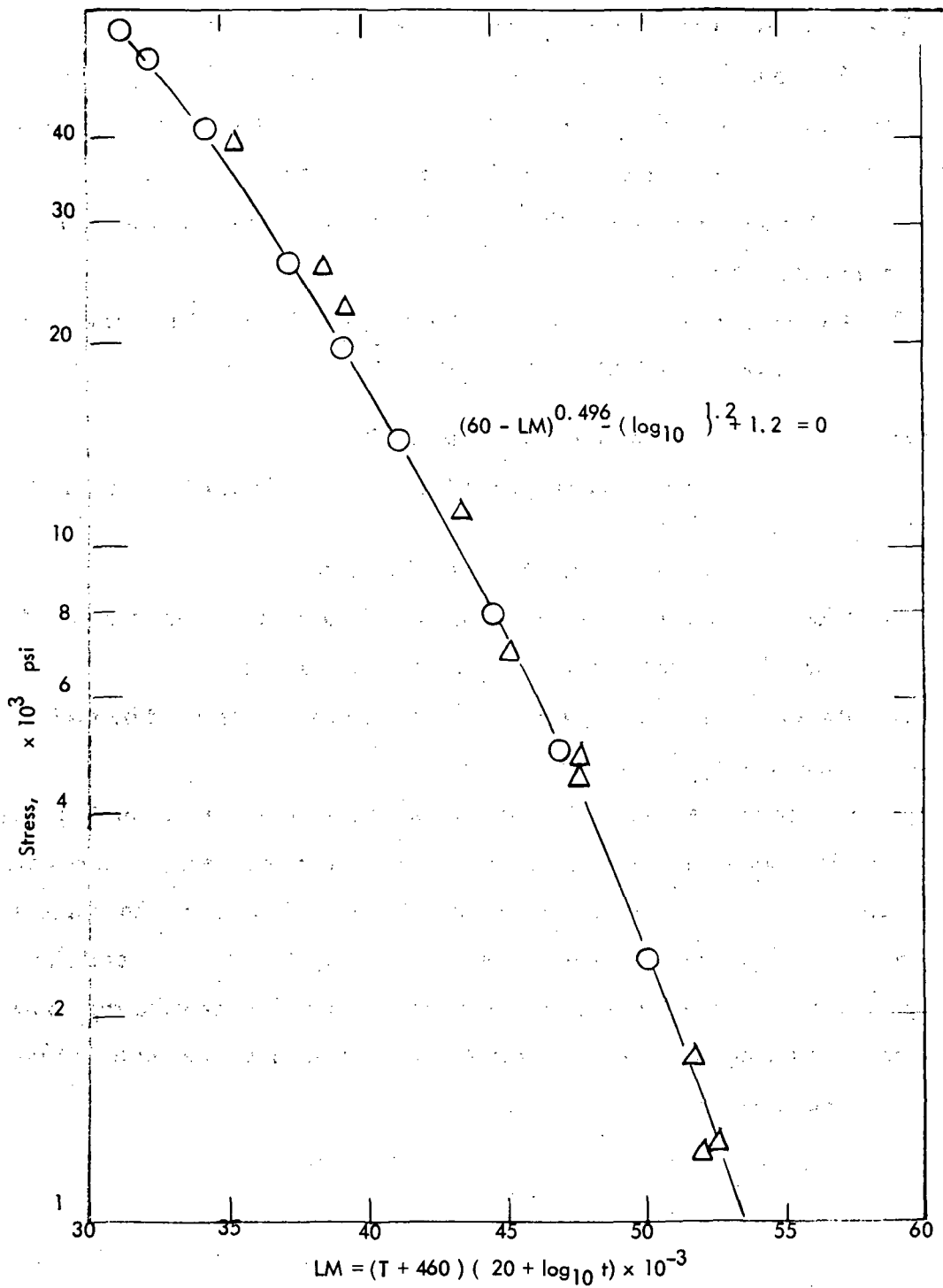


Figure E-1. Larson-Miller Curve for SS 316

APPENDIX F

SYMBOLS

a	Experimental constant for Larsen Miller equation
A_{mo}	Clad surface area
A_{pt}	Pressure tube area
C_p	Specific heat
C_p'	Effective specific heat to simulate the heat of fusion divided by δT
H_{fg}	Heat of fusion
LM	Larsen Miller parameter
Q_{gen}	Heat generation rate
T	Temperature
T_{mp}	Melting point temperature
V	Volume
X_{mel}	Fraction of melting for a component
δT	Prescribed temperature differential for simulation of heat of fusion
σ	Stress
τ	Time

APPENDIX G
REFERENCES

1. Parker, W. G., and Van Bibber, L. E., "Operations Manual for the ESATA Computer Program", Westinghouse Electric Corporation, Astronuclear Laboratory, NASA-CR- November 1971
2. Pierce, B. L., and Stumpf, H. J., "TAP-A Program For Computing Transients or Steady-State Temperature Distributions", WANL-TME-1872, December 1969.
3. Hilliard, R. K., Linderoth, C. E., Scott, A. J., "Fission Product Release from Overheated Uranium - A Laboratory Study," Health Physics, 7, 1 (1961).
4. Paulson, W. A., and Springborn, R. H., "Estimation of Fission-Product Gas Pressure in Uranium Dioxide Ceramic Fuel Elements," NASA TN D-4823 (1968).
5. Keilholtz, G. W., and Battle, Jr. G. C., "Fission Product Release and Transport in Liquid Metal," ORNL-NSIC-37 (March 1969).
6. Browning, Jr. W. E. et al., "Release of Fission Products During In-Pile Melting of UO_2 ," Nuclear Science and Engineering 18, 151 (1964).
7. Watson, G. M., Perez, R. B., Fontana, M. H., "Effect of Containment System Size on Fission Product Behavior," ORNL-4033 (1967).
8. Castleman, Jr. A., et al., "Fission Product Release Studies," Annular Report, Nuclear Engineering Department, BNL-50023 (S-69) (1966).
9. Morrison, D. L., Carbiener, W. A., Ritzman, R. L., "An Evaluation of the Applicability of Existing Data to the Analytical Description of a Nuclear Reactor Accident," Quarterly Progress Report, Oct. -Dec. 1968, BMI-1856 (1969).
10. Davies, D., Long, G., Stanaway, W. P., "The Emission of Volatile Fission Products from Uranium Dioxide," AERE-R-4342 (June 1963).
11. Miller, Jr. C. E., "The Light Bulb Model of Fission Product Release from Reactor Fuels," ORNL-4060 (1967).
12. Castleman, Jr. A. W., and Tang, I. N., "Vaporization of Fission Products from Irradiated Fuels - I. Experimental Method and General Fission-Product Behavior," Nuclear Science and Engineering 29, 159 (1967).

REFERENCES (Continued)

13. Raines, G. E., et al., "Studies of Fission Product Deposition in Out-of-Pile Loops," Symposium on Fission Product Release and Transport Under Accident Conditions, CONF-650407, Vol. 2, p. 655 (1965).
14. Bolles, R. C., Ballou, N. E., "Calculated Activities and Abundances of U-235 Fission Products," Nuclear Science and Engineering 5, 156 (1959).
15. Shure, K., "Fission Product Decay Energy," WAPD-BT-24, Westinghouse Bettis Laboratory (December 1961).
16. Etherington, H., ed., Nuclear Energy Handbook (st. ed. McGraw-Hill) (1958).
17. Vogel, R. C., Levenson, M. Masten, F. R. "Chemical Engineering Division Semiannual Report", V. Reactor Safety ANL-6925 (May 1965).
18. Furman, S. C., "Metal-Water Reactions V. The Kinetics of Metal-Water Reactions Low Pressure Studies", GEAP-3208 (July 1959).
19. Vogel, R. C., et al. "Chemical Engineering Division Semiannual Report", ANL-7325 (April 1967).
20. Elliot, J. F. and Gleiser, M., Thermochemistry for Steelmaking, Addison-Wesley Publishing Co., Inc. Reading, Mass. (1960).
21. Thermophysical Properties of High Temperature Solid Materials, Thermophysical Properties Research Center, Purdue University.
22. Belle, J., Uranium Dioxide: Properties and Nuclear Applications, USAEC (July 1961).
23. Material Properties Data Book, Report 2275, Aerojet Nuclear Systems Company, Revision of March 15, 1970.
24. Study of Thermal Gas-Cooled Reactor Technology, Aerojet General Nucleonics, NASA CR-72048 (October 1966).
25. Flynn, D. R., and Watson, T. W., "Measurements of the Thermal Conductivity of Soils to High Temperatures," Final Report, National Bureau of Standards for SANDIA (April 1969).

26. Marks, Mechanical Engineering Handbook, Sixth Edition, McGraw-Hill (1958).
27. Eckelt, E. R. G., and Drake, R. M., Heat and Mass Transfer, McGraw-Hill (1959).
28. McAdams, W. H., Heat Transmission, Third Edition, McGraw-Hill (1954).
29. Aerospace Structural Metals Handbook - Volume I, Ferrous Alloys, ASD-TDR-63-741, Air Force Materials Laboratory, Research & Technology Division, Air Force Systems Command, Wright-Patterson Air Force Base, Ohio.
30. Puthoff, R. L., "High Speed Impact Tests of a Model Nuclear Reactor Containment System," NASA-TMX-67856, June, 1971.